THE HONG KONG POLYTECHNIC UNIVERSITY
香港理工大學
Pao Yue-kong Library
包玉剛圖書館

Copyright Undertaking

This thesis is protected by copyright, with all rights reserved.

By reading and using the thesis, the reader understands and agrees to the following terms:

1. The reader will abide by the rules and legal ordinances governing copyright regarding the use of the thesis.
2. The reader will use the thesis for the purpose of research or private study only and not for distribution or further reproduction or any other purpose.
3. The reader agrees to indemnify and hold the University harmless from and against any loss, damage, cost, liability or expenses arising from copyright infringement or unauthorized usage.

IMPORTANT

If you have reasons to believe that any materials in this thesis are deemed not suitable to be distributed in this form, or a copyright owner having difficulty with the material being included in our database, please contact lbsys@polyu.edu.hk providing details. The Library will look into your claim and consider taking remedial action upon receipt of the written requests.

Pao Yue-kong Library, The Hong Kong Polytechnic University, Hung Hom, Kowloon, Hong Kong

http://www.lib.polyu.edu.hk

LOW-VOLTAGE AC SERIES ARC FAULT DETECTION AND PERFORMANCE ASSESSMENT

CHUANZHEN JIA

PhD

The Hong Kong Polytechnic University

2026

The Hong Kong Polytechnic University

Department of Building Environment and Energy Engineering

Low-Voltage AC Series Arc Fault Detection and Performance Assessment

Chuanzhen Jia

A thesis submitted in partial fulfilment of the requirements for the degree of Doctor of Philosophy

Nov 2025

CERTIFICATE OF ORIGINALITY

I hereby declare that this thesis is my work and that, to the best of my knowledge and belief, it reproduces no material previously published or written, nor material that has been accepted for the award of any other degree or diploma, except where due acknowledgment has been made in the text.

Signed:

Name of Student: Chuanzhen JIA

Abstract

Arc faults represent a major hidden risk in low-voltage AC systems, as they can generate persistent high-temperature plasma leading to insulation failure and fire hazards. Conventional protective devices often fail to detect these faults because arc signatures are transient, nonlinear, and strongly influenced by operating environments. Arc fault detection devices (AFDDs) are developed to prevent the electrical fires caused by arc faults. But, complex scenarios—such as various load conditions and line masking—further distort current signals, making detection highly unreliable. Existing standards address only limited arc-fault cases and lack comprehensive evaluation metrics, leaving a gap between laboratory testing and real-world residential environments. However, the circulation of these products in the market cannot effectively detect arc-fault events and prevent fires, thereby posing serious threats to human life and property safety.

To overcome the gaps, this thesis aims to systematically evaluate the performance of existing AFDDs, develop novel arc fault detection algorithms, and propose a unified explainable assessment scheme for improved reliability and applicability.

Standard tests cannot fully capture the complexity of real-life situations. To investigate the impact of diverse load types and line conditions on arc-fault signals, this thesis develops a sophisticated experimental platform and designs various additional tests to analyze the behavior of AFDDs under different complex real-world operating conditions. Based on the platform, existing AFDDs are systematically evaluated under both standard requirements and additional test scenarios to identify key weaknesses in practical implementations.

To address these challenges, two refined arc fault detection algorithms are proposed targeting complex load types and long cable lengths, thereby enhancing the accuracy, reliability, and real-world applicability of arc fault detection.

Existing arc fault detection methods struggle with low accuracy in complex load environments and lack adaptability to simultaneous or mixed load operations. Prior studies offer no clear guidance on optimal sampling parameters. To address the challenges, this thesis proposes a lightweight AC arc fault detection framework based on event-based load classification. The method first analyzes arc characteristics under different load conditions and performs load classification using transient events, categorizing loads into resistive, inductive, and switchable types.

For each category, sequential floating forward selection is employed to optimize feature subsets, and a KNN-based classifier is used to achieve efficient and accurate detection. The experimental results demonstrate that the proposed method performs effectively in practical arc fault detection under multi-load conditions and has stronger applicability in arc fault detection than other reported methods, including those using deep learning models. The proposed framework avoids the high computational cost of deep learning while maintaining strong detection performance.

AFDDs exhibit significant drops in detection accuracy when operating under long cable lengths. Regarding complex masking tests with line impedance, a novel approach to AC arc fault detection is introduced, combining multi-band feature fusion with Catboost. Due to the different attenuation degrees of high-frequency features under various load types in long-distance cables, the startup power variations are analyzed to capture their transient characteristics for classification. Recursive Feature Elimination and CatBoost classifiers are used to extract optimal features and detect arc-fault events, improving detection performance without requiring deep learning models. The proposed method achieves 97% accuracy in arc fault detection, even when models are trained only under ideal (0m) conditions, demonstrating excellent generalization under long-cable conditions. An ablation study and model comparison are conducted to validate the effectiveness of the proposed method.

The high accuracy does not guarantee true feature extraction. Existing arc fault diagnosis models often lack trustworthiness and interpretability, relying too heavily on accuracy while ignoring whether true features are captured. The study introduces a unified explainable assessment scheme that defines ground-truth fault features and integrates explainable artificial intelligence (XAI) to assess model reliability. Two XAI methods, Occlusion Sensitivity and SHAP, are used to assess how models identify key fault features for feature pool-based methods and deep learning methods. Several traditional machine learning methods and deep learning methods across two arc fault datasets with different sample times and noise levels are utilized to test the effectiveness of the proposed assessment scheme. Through this approach, the arc fault diagnosis models are easy to understand and trust, allowing practitioners to make informed and trustworthy decisions. Based on the results, a lightweight balanced neural network is developed to guarantee competitive accuracy and soft feature extraction score. The proposed method enhances model transparency, supports real-world deployment with low computational cost, and guides model selection and ensemble strategies.

In conclusion, this thesis presents a comprehensive framework that integrates a newly designed testing platform, two advanced arc fault detection algorithms, and a robust explainable assessment scheme. Building upon existing standards and arc fault detection algorithms, this thesis systematically addresses their limitations and introduces novel methods to enhance detection performance. The proposed framework enables reliable identification of arc-fault signals in real-world environments characterized by diverse loads and complex disturbances. In addition to improving detection accuracy and robustness, this work provides practical insights into standardized test requirements and algorithm evaluation. These contributions support manufacturers in developing safer and more reliable arc fault detection products and contribute to reducing the incidence of electrical fires.

Publications Arising from the Thesis

I. Papers in Journals

- **Chuanzhen Jia**, et al. "Serial arc-fault restriction survey with standard-listed products in the Chinese market." IEEE Transactions on Industry Applications 59.6 (2023): 7453-7461.
- Yang Zhang, Hong Cai Chen, Zhe Li, **Chuanzhen Jia**, Yaping Du, Kanjian Zhang, and Haikun Wei. "Lightweight AC arc fault detection method by integration of event-based load classification." *IEEE Transactions on Industrial Electronics* 71, no. 4 (2023): 4130-4140.
- **Jia, Chuanzhen**, et al. " Masking Cable-Oriented Series AC Arc Fault Detection Based on Multi-band Feature Fusion and Catboost." IEEE Transactions on Industrial Informatics, **Under Review.**
- Qianchao Wang, **Chuanzhen Jia**, Yuxuan Ding, Zhe Li, and Yaping Du. "Lightweight Ac Arc Fault Diagnosis via Fourier Transform Inspired Multi-frequency Neural Network." IEEE Transactions on Industrial Electronics, **Under Review.**
- Qianchao Wang, Yuxuan Ding, **Chuanzhen Jia**, Zhe Li, and Yaping Du. "Explainable Artificial Intelligence based Soft Evaluation Indicator for Arc Fault Diagnosis." IEEE Transactions on Industrial Informatics, **Under Review.**
- Qianchao Wang, Nan Feng, **Chuanzhen Jia**, Yuxuan Ding, and Yaping Du. "Super-expressive Activation Function Enhanced Lightweight Decomposition Network for Arc Fault Diagnosis." IEEE Transactions on Industrial Informatics, **Under Review.**
- Chakhung Yeung, Jianguo Wang, Yaping Du, Jinxin Cao, Quan Zhou, Yuxuan Ding, Mingli Chen, Weihan Zhao, and **Chuanzhen Jia**. "Comprehensive Analysis of Solar Irradiance and Photovoltaic Power Generation: Case Studies in Wuhan and Zhangbei, China." *IEEE Transactions on Industry Applications* (2025).
- Zhe Li, Jinxin Cao, Yaping Du, Yuxuan Ding, Yang Zhang, **Chuanzhen Jia**, Fangchi Qiu, Zhentao Du, and Mingli Chen. "Ground potential distribution and human-body touch voltage in old residential communities." *IEEE Transactions on Industry Applications* 59, no. 4 (2023): 4980-4989.
- Jinxin Cao, Yuxuan Ding, Zhe Li, Yaping Du, Jianguo Wang, **Chuanzhen Jia**, Chakhung Yeung, and Yang Zhang. "Analysis of Fault Potential Assessment under Typical Line Faults in a Real Urban Old Community." *IEEE Transactions on Industry Applications* (2025).

II. Papers in Conferences

- Zhaoming Wu, **Chuanzhen Jia**, Fengshu Ye, Junjie Tan, Zhaohe Huang, and Qingsha S. Cheng. "Arc Fault Detection Model Based on Semi-supervised Learning." In *Annual Conference of China Electrotechnical Society*, pp. 643-653. Singapore: Springer Nature Singapore, 2024.
- Nan Ma, **Chuanzhen Jia**, Jinxin Cao, Xiangen Zhao, Hongcai Chen, Fangchi Qiu, Yang Zhang, and Yaping Du. "Detection performance of arc fault detection devices according to the chinese standard GB31143." In *2022 IEEE/IAS 58th Industrial and Commercial Power Systems Technical Conference (I&CPS)*, pp. 1-6. IEEE, 2022.
- Zhanhua Huang, **Chuanzhen Jia**, Zhe Li, Yaping Du, Qingsha S. Cheng, Hao Du, and Xiao Li. "Detection performance of arcing fault detectors in the Chinese market according to the Chinese Standard GB/T 31143." In *Journal of Physics: Conference Series*, vol. 2703, no. 1, p. 012097. IOP Publishing, 2024.
- Nan Ma, **Chuanzhen Jia**, Zhe Li, Yaping Du, Qingsha S. Cheng, Zhaoming Wu, and Lu Pei. "Arc-Fault Unwanted Tripping Survey of Hair Dryers with GB31143-Listed Products." In *Annual Conference of China Electrotechnical Society*, pp. 192-199. Singapore: Springer Nature Singapore, 2023.
- Zhe Li, Yuxuan Ding, Jinxin Cao, Yaping Du, **Chuanzhen Jia**, and Xiangen Zhao. "The Distribution of Ground Potential around Grounding grids under a Direct Lightning Strike." In *2022 36th International Conference on Lightning Protection (ICLP)*, pp. 272-275. IEEE, 2022.
- Chakhung Yeung, Jianguo Wang, Yaping Du, Jinxin Cao, Yuxuan Ding, Mingli Chen, Weihan Zhao, and **Chuanzhen Jia**. "Research on solar irradiance distribution and correlation with photovoltaic generated output: A case study of wuhan and zhangbei, china." In *2024 IEEE/IAS 60th Industrial and Commercial Power Systems Technical Conference (I&CPS)*, pp. 1-6. IEEE, 2024.

Acknowledgements

To all the people who have crossed paths with mine — thank you for the quiet moments, the laughter, and the unwavering presence.
These past four years have been woven with your light.
Each of you, in your own way, has shaped this journey into something meaningful.
You are the quiet strength behind every page of this thesis.

Grateful beyond words.

Table of Contents

List of Figures

List of Tables

1 Introduction

1.1 Background

An electrical fire is a fire that originates from an electrical fault, such as faulty wiring, overloaded circuits, or malfunctioning appliances. Unlike other fires caused by open flames or combustible materials, electrical fires often smolder within walls or appliances before becoming visible. According to the U.S. Fire Administration, electrical fires in residential settings resulted in approximately 305 deaths and 800 injuries in 2023. Property losses associated with these fires were estimated at $1.5 billion in the United States [1]. In the European Union, the total number of fires of electrical origin is estimated at 273,000 per year. Electrical hazards account for approximately 25–30% of all fires in the EU, resulting in over 1,200 deaths and causing property damage exceeding €10 billion, as reported by the European Fire Safety Alliance [2]. Figure 1.1 shows the fire caused by arc faults in China. The consequences of these fires are severe, not only in terms of economic losses to society but also fatalities and injuries.

Figure 1.1 Fire caused by arc faults.

Electrical fires are generally attributed to multiple factors within electrical systems. The most prevalent causes include circuit overloading, short circuits, deteriorated wiring, defective equipment, and inadequate maintenance. These conditions often result in excessive heat generation or sparks that can ignite nearby combustible materials. Among these causes, arc faults represent a particularly significant hazard. U.S. Fire Administration pointed out that arc faults caused more than half of the casualties and losses in electrical fires.

An arc fault is defined as an unintended arcing situation in a circuit, accompanied by a luminous electrical discharge across an insulating medium [3]. Arcing, which results from long-term operation of cables, overload of electrical equipment, loose connections, external intrusions, or insulation damage, occurs frequently in residential buildings [4]. Figure 1.2 shows the arc fault generated in the laboratory by the damage to the cable insulation. Once an arc fault occurs, the temperature can reach as high as 2000–4000 °C, even when the arc current is only between 2–10 A. These arcs can release a tremendous amount of energy. If extreme heat readily ignites cable insulation or nearby combustible materials, it can give rise to serious fire hazards [5].

Figure 1.2 Arc faults caused by insulation damage.

According to the types of currents in the arc circuits, arc faults can be divided into DC arc faults and AC arc faults. The DC arc faults can bring hazards to the railway system [6-8], PV system [9-15], DC power grid [16-19] etc. The prevention of DC arc faults has become a hot topic as PV systems and other DC technologies have proliferated in recent years. Nevertheless, the problems caused by AC arc faults are always the most concerning problems and have been investigated for a long time. This is because the AC arc faults that happened in the low-voltage residential circuit pose a threat to property and human life in buildings.

According to the AC arc fault location, there are three main types of arc faults in Figure 1.3: series arc faults, parallel arc faults, and ground arc faults. The position of the series arc faults is connected in series with the load, and the arc current flows through the load. The current is small, only a few amperes in many cases, and not easily detected. A parallel arc fault is an arc connected in parallel with the load, which occurs between the phase lines, and the test current ranges from 75A to 500A. A ground arc fault is a particular type of parallel arc fault that occurs between the phase line and the ground line.

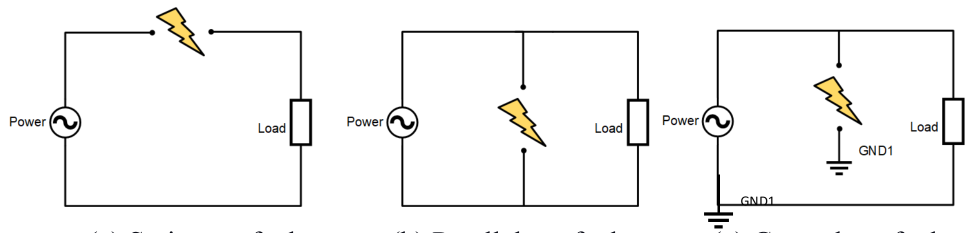

(a) Series arc fault (b) Parallel arc fault (c) Ground arc fault

Figure 1.3 Three types of arc fault.

Due to the appearance of arc resistance, the current generated by an arc fault is typically lower than the rated operating current of the load. As a result, conventional protective devices, such as Residual Current Devices (RCDs), are unable to detect or interrupt arc faults. To handle this problem, the Arc Fault Circuit Interrupter (AFCI) was invented in the US in 1993. As AFCIs became increasingly adopted for arc fault protection in residential buildings, the technical standard for AFCI has been released and revised by Underwriters Laboratories since 1999 [20]. The Electrotechnical Commission (IEC) and China Fire Institute promulgated IEC 62606-2013 and GB 31143-2014 to regulate the requirements of tests for Arc Fault Detection Devices (AFDDs) [21, 22]. Figure 1.4 shows the tested AFDD and AFCI.

Figure 1.4 Tested AFDD/AFCI.

The detection algorithms of AFDD or AFCI play an important role in arc protection. These algorithms have evolved significantly over time. Early time-domain approaches relied on basic electrical signal features but were prone to false tripping under complex load conditions. Later, frequency-domain and time-frequency-domain methods, such as wavelet transforms, enhanced the ability to capture arc signatures. More recently, machine learning methods and deep learning models have emerged as dominant approaches, offering data-driven classification and automated feature extraction that improve adaptability under dynamic load scenarios.

However, arc fault detection technologies still face significant limitations in practical applications. First, AFDDs are plagued by frequent missed detections and false alarms. The unstable and highly random characteristics of arc fault signals make these devices difficult to reliably distinguish from normal electrical disturbances. Moreover, many common household appliances, including various light systems (Figure 1.5), motor-driven devices, and switch-mode power supplies, generate high-frequency noise similar to arc signatures, which further increases the risk of misclassification. Additionally, AFDDs are further constrained by hardware limits, such as sampling rates and limited on-board computing power, which restrict complex algorithm deployment and real-time performance.

Figure 1.5 Light systems.

Existing arc fault detection algorithms demonstrate low recognition accuracy and limited applicability. Conventional approaches that rely on waveform distortion, harmonic content, or high-frequency features often lack robustness in complex working conditions. They are sensitive to noise, require high sampling rates, and struggle to balance real-time performance with accuracy. As a result, their reliability across diverse operating conditions remains insufficient, restricting large-scale deployment. Moreover, these methods often struggle to detect arc faults under complex operating conditions—such as the simultaneous operation of multiple appliances and the cable masking scenarios. In practical residential or commercial settings, long cable shielding layers can attenuate or distort arc fault signals, reducing the ability of existing algorithms to differentiate hazardous arcs from normal electrical noise. This discrepancy between performance observed in laboratory tests and real-world applicability further compromises the reliability of

AC fault arc detection solutions, particularly in the scenarios most critical for electrical fire prevention.

Additionally, the standardization of arc fault detection remains incomplete. Although standards have been established to regulate arc fault detection devices, the test configurations and evaluation results are often relatively limited and uniform. While arc fault detection algorithms typically achieve high accuracy on manufacturers' own datasets, the reliability of these results under diverse real-world conditions remains unclear. Without a unified framework, the effectiveness of arc fault detection algorithms varies considerably, leading to inconsistent performance and hindering user confidence.

To address the constraints of existing arc fault detection technologies, this thesis proposes to address a series of critical issues in the application of AFDDs: evaluating existing AFDDs, developing arc fault detection methods through event-based load classification and multi-band feature fusion with Catboost, and introducing an explainable artificial intelligence (AI) based assessment scheme, forming a comprehensive arc fault detection framework to improve accuracy, enhance applicability, and promote broader adoption in residential and industrial settings.

1.2 Objectives

The overall objective of this thesis is to address the critical limitations of existing AC fault arc detection technologies and to develop a comprehensive, reliable, and practical arc fault detection framework that enhances the accuracy and applicability of detection systems and further contributes to preventing electrical fires in residential, commercial, and industrial settings.

To achieve this goal, this thesis assesses the performance of AFDDs, proposes two novel arc fault detection algorithms, and an explainable AI-based assessment scheme for arc fault diagnosis. First, a systematic assessment of commercial AFDDs is conducted to examine their effectiveness according to the standard and additional tests, thereby identifying performance gaps and providing recommendations for improving standard test procedures. Then, based on these identified issues, two arc fault detection algorithms are developed for complex operating conditions and long-cable scenarios. To address the defect of single evaluation metrics, an explainable AI-based assessment scheme for arc fault diagnosis is proposed, providing credible assessments of model interpretability and reliability to comprehensively validate the arc fault detection algorithms and solidify the framework's overall trustworthiness.

1.2.1 Assessment of Arc Fault Detection Devices

In recent years, a wide variety of arc fault detection devices have emerged on the market. However, their actual performance under real-world residential conditions remains uncertain. Although most commercial devices claim compliance with standardized testing procedures, it is not clear whether they can reliably detect arc faults and provide effective protection against fire hazards in complex and dynamic household environments.

To address this gap, this thesis conducts a systematic assessment of commercial AFDDs, identifying performance differences through standard and additional tests, and proposes suggestions to standard tests to better bridge the gap between laboratory conditions and practical applications.

First, various commercial AFDDs are evaluated by a wide range of standard and additional tests using the arc-fault experimental platform, including standard tests and additional tests. Based on these performance results under standardized test conditions and in real-world operating environments, the testing configurations and load types that expose the weaknesses of AFDDs are identified.

Based on these insights, this thesis recommends improvements to existing standard tests. These enhancements are intended to capture the complexity of real-world operating conditions and provide a more rigorous framework for assessing AFDDs performance. This contributes directly to standardization work and helps bridge the gap between laboratory testing and real-world application scenarios.

1.2.2 A Lightweight AC Arc Fault Detection Method by Integration of Event-based Load Classification

To address the challenge of accurately detecting arc faults under complex electrical conditions, this thesis proposes an AC arc fault detection algorithm to extract dedicated discriminative features and enhance accuracy and computational efficiency in complex residential electrical environments. The algorithm is designed to overcome the limitations of traditional and AI-based methods, which often show high accuracy in laboratory settings but fail in real-world applications due to a lack of adaptability and masking effects.

In practical settings, multiple appliances often operate simultaneously, each exhibiting unique transient behaviors, start-up dynamics, and electrical characteristics. These overlapping signals can mask or distort the arc signature, leading to missed detections or false tripping. To address this challenge, classifying different loads is useful for identifying the characteristic features of fault arcs under complex conditions. Electrical loads are categorized into resistive, inductive, and switchable types based on their transient turn-on signatures. Different load categories interact differently with arc-fault signals. During runtime, the algorithm performs event recognition to determine the load type, after which the relevant feature set and classification model are deployed for arc fault detection.

The arc fault detection algorithm can adapt to unknown or evolving load conditions, while maintaining both high detection precision and computational efficiency, making it suitable for real-world deployment in residential systems.

1.2.3 A series AC arc fault detection with Line Impedance Based on Multi-band Feature Fusion and Catboost

To address the issue where algorithms fail to accurately identify long-distance arc faults, a series AC arc fault detection algorithm is proposed by mitigating the degradation in detection performance caused by signal attenuation in long-distance cables.

In long-distance residential wiring, the high-frequency components of current signals are heavily attenuated or distorted by cables. Although commercial AFDDs often achieve high accuracy in controlled laboratory environments, their performance significantly degrades in field applications, primarily due to this masking phenomenon. The attenuation characteristics of high-frequency signals during cable transmission are analyzed, and the attenuation of current signals under different load types is examined as the cable length increases.

An algorithm based on load classification and specific frequency band feature analysis is proposed to identify arc faults in long-distance cables, which can bridge the gap between laboratory validation and practical performance. By effectively addressing cable masking, this approach ensures that detection reliability is maintained across diverse wiring configurations and installation environments.

1.2.4 An Explainable Assessment Scheme for Arc Fault Diagnosis

While machine learning and deep learning algorithms have shown impressive accuracy in arc fault detection, a critical limitation remains: a lack of transparency and reliability regarding whether the models are genuinely learning from relevant arc fault features.

To address this gap, this thesis aims to establish a unified explainable assessment scheme for arc fault diagnosis to assess the consistency between model decisions and physical characteristics of arcs, addressing the limitations of traditional evaluation metrics.

The assessment scheme can assess whether a trained model's decision-making aligns with the physical characteristics of arc faults. This approach is essential to ensure that high-accuracy models do not simply overfit to noise or sample time, especially under varying conditions such as different sampling frequencies, noise levels, or load types. By comparing selected features with the ground truth features, the indicator quantitatively assesses how well the model's focus aligns with expected arc fault behavior. This indicator ultimately supports safer deployment of arc fault detection technology and encourages a standardized way to evaluate AI-based detection models.

1.3 Thesis Outline

This thesis presents a comprehensive study on the arc fault detection in AC low-voltage systems, focusing on the assessment of existing arc fault detection devices, proposing novel arc fault detection algorithms for complex scenarios and cable masking scenarios, and establishing a unified explainable assessment scheme for arc fault diagnosis to improve arc fault detection reliability and accuracy. Figure 1.6 shows the structure of the thesis.

Chapter 1 introduces the background and objectives of arc fault detection, outlines the structure of this research, including arc fault product assessment with recommendations, development of two arc fault detection algorithms, and the establishment of an explainable AI-based assessment scheme.

Chapter 2 reviews existing research on arc fault detection, outlining the field's detection algorithms, major challenges, and gaps. It begins with the mechanism and mathematical models of arcs, then introduces arc fault detection based on physical phenomena. Most arc fault detection methods focus on signal processing procedures and discuss data-driven detection based on feature extraction and artificial intelligence techniques. This chapter summarizes the requirements on operating characteristics for arc fault detection devices specified in existing standards.

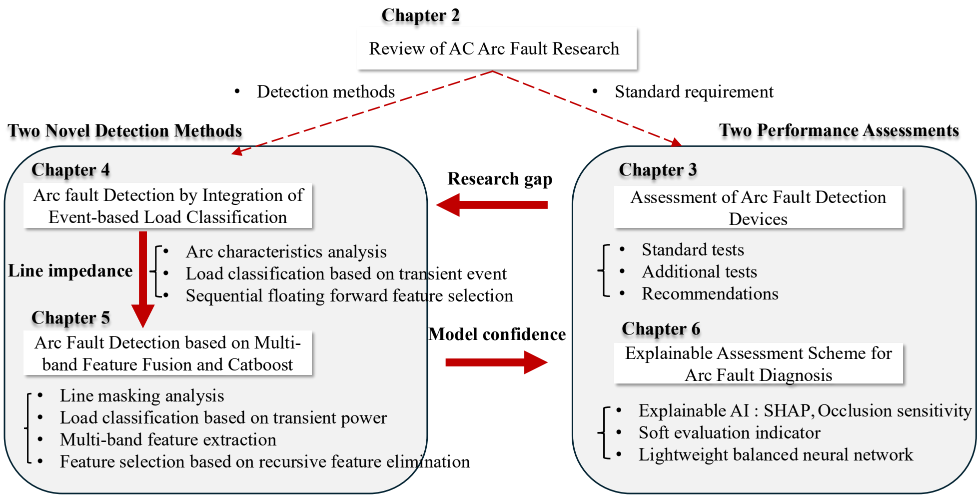

Figure 1.6 The structure of the thesis.

In Chapter 3, a thorough assessment of commercial AFDDs is performed according to the requirements of standards and additional tests, including masking tests with inhibition loads, masking tests with line impedance, and unwanted tripping tests. This chapter highlights the inadequacies of AFDDs in detecting complex arc faults. Based on the test results, enhancements to standard testing methods are proposed.

In Chapter 4, a new lightweight arc fault detection algorithm is introduced, which incorporates transient event-based load classification. The method uses sequential forward feature selection and is validated through real-world arc fault data. The chapter also includes sensitivity analysis and comparisons with AI and deep learning methods.

Chapter 5 presents an advanced arc fault detection method targeting line masking tests. This algorithm proposes a multi-band feature fusion framework and uses the CatBoost model for classification. Feature selection is performed using recursive feature elimination, and the method is rigorously tested through classification performance evaluations and ablation studies.

Recognizing the shortcomings of existing algorithm evaluation metrics, Chapter 6 introduces an assessment scheme using explainable AI techniques. It incorporates SHAP and occlusion sensitivity to define ground truth features and evaluate model transparency and performance. The chapter concludes with implementation results and a lightweight neural network design to support interpretability.

In Chapter 7, the conclusions and future work are summarized.

2 Review of AC Arc Fault Research

AC arc faults can cause electrical fire hazards and property loss. To detect arc faults, some standards and algorithms are proposed to solve the critical problems in electrical safety. However, in recent years, the increasing variability and complexity of electrical loads have posed significant challenges to accurate arc fault detection, such as dehumidifiers, air conditioners, and microwave ovens. Over the past decades, researchers have developed a wide variety of detection methods ranging from traditional signal-based techniques to advanced data-driven models.

In order to comprehensively understand the research in this field, this chapter introduces the relevant work from multiple aspects. Section 2.1 discusses the mathematical-physical arc model that utilizes mathematical representations of arc behavior to identify arc faults. These models aim to describe the time-varying relationships among voltage, current, and energy in order to guide and assist the arc fault detection. Section 2.2 focuses on detection algorithms based on physical signal characteristics, such as voltage, acoustic, and electromagnetic emissions. These methods require prior knowledge of the arc fault location to effectively perform detection. Section 2.3 reviews the mainstream arc fault detection algorithms based on the current signal data. These approaches detect arc faults by analyzing current waveforms and extracting representative features that capture the characteristics of arc fault signal. In Section 2.4, the requirements of several representative standards are introduced in arc fault detection. Section 2.5 provides a conclusion of research in the field of electric arc faults.

2.1 The Mechanism and Mathematical Models of Arcs

A comprehensive understanding of arc mechanisms is a prerequisite for proposing effective methods to detect arc-fault events. Analyzing arc-related characteristics in conjunction with the behavior of the surrounding circuit enables more efficient arc fault detection.

There are two main ways to simulate an arc fault in the circuit. The microscopic approach describes plasma phenomena with detailed equations, but it quickly becomes mathematically heavy. The macroscopic approach treats the arc as a variable resistor governed by nonlinear differential equations, with resistance set by the balance between input and dissipated energy.

The two classic arc models are Cassie and Mayr, introduced in 1939 and 1943. Cassie assumes a constant arc temperature, with power loss proportional to changes in the arc-column cross-section [23]. Before zero-crossing current, the breakdown keeps the arc resistance low, so Cassie generally matches measurements well.

The expression of the Cassie model is as follows:

$$\frac{1}{g}\frac{dg}{dt}=\frac{1}{\tau}\left(1-\left(\frac{u}{U_c}\right)^2\right) \tag{2-1}$$

In (2-1), g is the admittance of the arc, u is the arc voltage, U_c is the static voltage of the arc, and τ is the arc time constant.

Mayr assumes a fixed arc-column diameter and constant power loss, while the arc temperature varies over time and with radial position [24]. After the zero-crossing point, Mayr is suitable for modeling with experiments due to the highly resistive arc.

The Mayr model is typically expressed as:

$$\frac{1}{g}\frac{dg}{dt}=\frac{1}{\tau}\left(\frac{ui}{P_0}-1\right) \tag{2-2}$$

In (2-2), g is the admittance of the arc, u is the arc voltage, i is the arc current, P_0 is the steady-state power loss of the arc, and τ is the arc time constant.

Scholars have recently undertaken studies on the classical models and proposed a range of model combinations and refinements. In 2000, an improved Mayr-type arc model, known as the Schavemaker model, was introduced with a constant time parameter and a cooling power that depends on the electrical power input [25]. Reference [26] proposed an improved arc model based on the combined Mayr and Cassie arc models. In Reference [27], the authors proposed an improved electrical arc model based on the arc diameter variation to predict the average arc voltage and dynamic behavior closer to the measured ones compared to the conventional arc models. In Reference [28], the authors propose a parameter estimation approach for the Mayr arc model, addressing both linear and nonlinear descriptions. They use heuristic optimization methods to assess the algorithms and to estimate the arc-model parameters. An AC arc model based on the simplified Schavemaker model was investigated using a neural-network-based computational method [29]. In Reference [30], the authors proposed an improved arc model, which can continuously imitate the randomness and intermittence during the “unstable arcing period” of arc faults. As the current model fails to capture the high-frequency and randomness of arc currents, a time-domain simulation model for arc fault currents was developed by enhancing the time constant of the Cassie arc model, while the high-frequency features of arc currents were simulated using a segmented noise model [31].

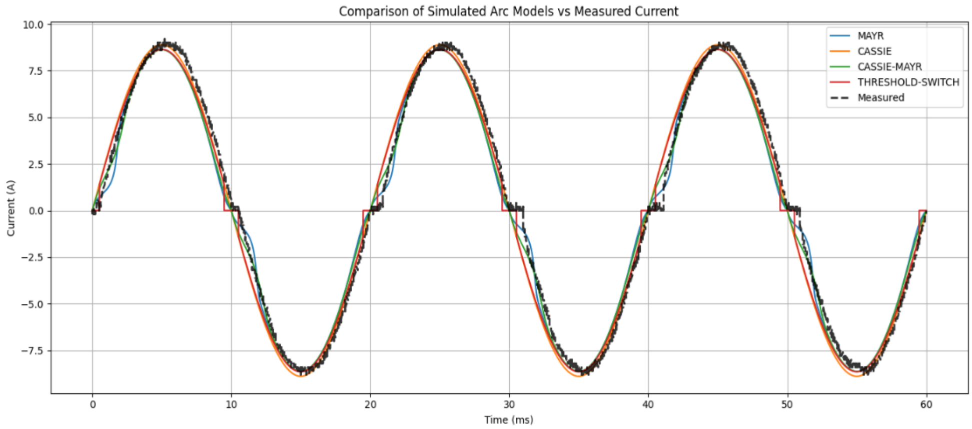

Figure 2.1 Simulated arc models and measured current of resistive loads.

Figure 2.1 compares measured arc-fault current waveforms with several simulated arc models for resistive loads. The results show that these arc models are capable of accurately simulating arc-fault current of resistive loads, including peak current reduction and the stagnation when crossing zero.

Although arc-fault simulated models under resistive loads have achieved a high level of similarity with measured signals, a major challenge remains in simulating the internal components of other practical loads. Many electrical loads contain complex internal components and may involve chemical phenomena, which are challenging to model explicitly using conventional simulation approaches.

For motor-type loads, the presence of inductance, mechanical inertia, and dynamic states leads to complex current behavior, making it difficult for conventional arc models to accurately reproduce high-frequency arc characteristics, as illustrated in Figure 2.2.

For switch mode power supply (SMPS) loads, highly nonlinear characteristics, and diverse internal topologies distort current waveforms, while detailed internal parameters are often unavailable, limiting the effectiveness of physics-based simulations. As a result, existing simulation approaches struggle to capture the complexity of arc behavior under these types of loads. Simulation efforts focus on normal current waveforms, which are used as the training dataset to prevent unwanted trippings in Figure 2.3.

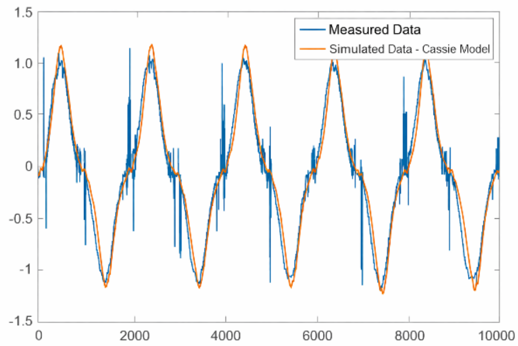

Figure 2.2 Simulated and measured arc data of motor loads.

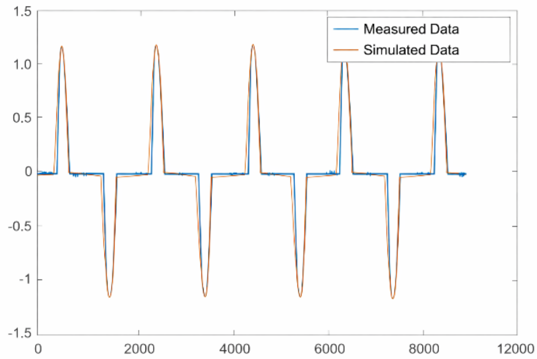

Figure 2.3 Simulated and measured normal data of SMPS loads.

Various Arc models have been developed to study the characteristics of the current or voltage during arc faults, thus detecting the arc fault in the residential circuit. However, the load condition in reality is complex. The temperature, humidity, and the condition of the electrodes can affect the generation of an arc fault [32]. Also, the arc exhibits nonlinear characteristics and randomness in the circuit. It is hard to develop an accurate model to include these factors. The proposed arc models are all based on approximations and assumptions for some particular conditions. Thus, arc models are not suitable for arc diagnosis in the residential circuit.

2.2 Arc Fault Detection Methods based on Physical Phenomena

During an arc fault, energy will be released to the surrounding area due to the discharge in the circuit. The electromagnetic radiation, acoustic emission, luminous phenomenon, and the rise of temperature change can be used as indicators for arc fault detection.

For the light phenomenon, Reference [33] proposed a simultaneous detection of light and overcurrent for air-insulated switchgear. In Reference [34], the study clarified the mechanism of undesired electromagnetic noise from contact-breaking arcs by quantifying the relationship between short-arc sustainable voltage and duration. The authors measured the effect of the external DC magnetic field on the breaking arc of Ag [35]. In Reference [36], the authors utilized radiated electromagnetic energy from a spark/arc source as a means of detecting arcing faults by using two types of simple antennas, stick and loop. Reference [37] proposed a fault detection algorithm based on the randomness of differential voltage at double-ended monitoring points to effectively identify the line voltage drop and fault arc voltage and exclude the impact of load fluctuations.

However, these physical factors are susceptible to the environment and arc location, which results in low feasibility in practical applications. Besides, in the residential building, electrical wires are installed inside the wall, where it's hard to detect these physical factors. Thus, arc fault detection based on physical phenomena is usually used in some particular occasions, such as switch cabinets, switchgears, aircraft, etc.

2.3 Data Processing and Data-Driven Detection Methods

Since the location of the arc fault is unpredictable, the most common method is to detect the arc fault by measuring the bus current. At present, most arc fault detection methods are mainly realized by detecting the difference between the normal current signal and the fault arc current signal.

The AC fault arc detection technology is mainly divided into the following categories. (1) From the perspective of the time domain, these methods analyze the current signal in the time domain and identify the time domain characteristics by extracting the current intensity, the current jump value and peak value, the flat shoulder feature of the current waveform, and the current rate of change. (2) From the perspective of the frequency domain, the Fourier methods transform the current signal and identify the arc based on the characteristic component of the arc fault. (3) Combining artificial intelligence algorithms, other methods to perform statistical analysis on many arc-fault current signals to find out their main characteristics and obtain the identification basis for arc-fault events.

2.3.1 Feature Extraction for Arc Fault Detection

Feature extraction aims to identify characteristic attributes from raw data, enabling algorithms to focus on the most informative features for arc-fault classification. Because the arc-fault waveform is a nonlinear time series, developing an effective identification algorithm requires the extraction of key features. In this field of arc fault detection, commonly used signal processing and feature extraction techniques can be categorized into time-domain, frequency-domain, and hybrid methods. These algorithms require manual threshold setting. When the characteristic value of the current exceeds the threshold, it is confirmed as an arc fault.

Time-domain characteristics are primarily determined by analyzing the differences between arc currents and normal currents in the time domain. In the time domain, phenomena such as stagnation duration, waveform distortion, amplitude decrease, current mean value, mean square deviation (MSD), mean energy deviation (MED) [38], randomness, and transient saltation can be observed in the current waveform [39, 40]. According to Mayr's model [41], some simple but trustworthy features can be recognized as members of the feature pool, such as signal mean, variance, and range, even though they may be affected by load types. Moreover, some complex statistical features are used as descriptors of time-domain signals, such as kurtosis [42], skewness, entropy, norm [43], zero current period, and maximum slip difference [38]. Figure 2.4 shows the current waveform of a 9 A resistive load. After the occurrence of the arc fault, indicated by the red dashed line, the current waveform exhibits some different features, including a reduction in current amplitude and the zero current period.

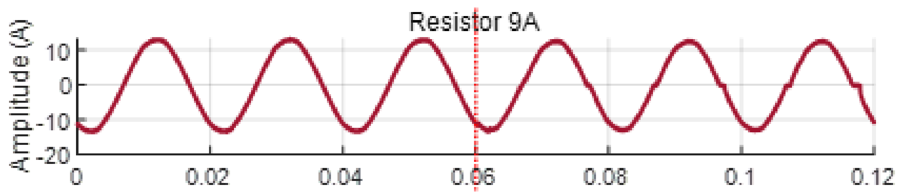

Figure 2.4 9A resistive load current waveform.

When it comes to the frequency domain, the magnitudes of components are normally used as key features to detect arc-fault events. The frequency-domain feature extraction methods transform the time-domain current signals into the spectral domain and determine decomposition coefficients, power spectral density, and other indicators for classification, including the Fast Fourier transform (FFT)

[44, 45], discrete wavelet transform (DWT)[46-48], and chirp-z transform (CZT) [49].

Reference [50] utilizes FFT to select the odd frequencies as threshold indicators for arc fault detection. Qu et al. [51] divide the frequency range (0-2000Hz) into ten intervals. Wang et al. [39] extract frequency domain features such as the fundamental frequency component, the third harmonic component, and the fifth harmonic component, combined with time domain features based on different load types. Kurtosis and skewness of the fifth and sixth principal components were used as a feature vector for identifying arcs [52]. DWT is employed to effectively address the limitation of frequency domain techniques in accurately localizing temporal frequency components. Some methods set the threshold to obtain arc-fault features based on different mother wavelets and the scale parameter defining the observed frequency range of the signal, like 6-layer db1 with a range of 1.9kHz-7.8kHz [53], reconstructed detail coefficients cd2 of db4 [54], and cd1 of 1-layer db2 [55]. The power of the d5 detail signal (623-1250 Hz) is selected through the mother wavelet Db10 with 5 detail levels [56]. Artale *et al.* [49] detect arc faults through a high-resolution low-frequency harmonic analysis of the current signal, based on the CZT and a proper set of indicators.

In current algorithms, time-domain features and frequency-domain features are often put together as an important basis for testing arc faults. Reference [57] proposed a series arc fault identification method based on wavelet transform and singular value decomposition. The method selected the mean, root mean square, and standard deviation of the singular value vector as the arc fault indicators. In the time-frequency domain, Reference [57] extracted the standard deviation of the root mean square of the current, the standard deviation of the DC component, and the sum of odd harmonics as the features of identifying arc-fault events. Reference [51] extracted four time-domain features, namely, current average, current range, difference current average, and current variance, and used the FFT to extract ten frequency domain features. The algorithm [40] adopts a random forest to select the top ten features with a high correlation to the current signals from the aspects of time-domain, frequency domain, and wavelet packet energy analysis. Random Forest (RF) is used to select the combination of linear load and nonlinear load characteristics in the line and then input into the neural network for training. Reference [39] proposed a series arc fault identification method based on time-frequency hybrid analysis.

Overall, feature extraction for arc-fault detection has evolved from simple time-domain indicators to more sophisticated frequency-domain and time–frequency hybrid features. While these approaches effectively capture feature differences between normal and arc-fault currents, most methods rely on manually designed features and fixed threshold settings, making them sensitive to load types, operating conditions, and noise levels. The dependence on manually extracted features and empirical parameters limits their robustness and flexibility in real-world residential environments, thereby motivating the exploration of more adaptive, data-driven detection methods.

2.3.2 Arc Fault Detection Methods based on Artificial Intelligence Techniques

In recent years, more intelligent algorithms have been employed to identify arc faults, primarily using support vector machines (SVMs) [38], artificial neural networks (ANNs) [39, 58, 59], and deep learning methods [60]. In general, AI-based arc-fault detection follows a two-step procedure in Figure 2.5. Unlike low-cost solutions that typically rely on simple algebraic calculations to extract indicators, AI-based approaches usually apply signal transformation methods, such as the FFT, DWT, Empirical Mode Decomposition (EMD), and CZT, to extract informative features. Second, classifiers are used to perform arc fault diagnosis.

Figure 2.5 Flowchart of arc fault algorithms.

SVM-based algorithms can obtain global optimums and have good generalization ability, especially when addressing high dimensions or small samples. In Reference [61], high-frequency energy and current variations are extracted as an input eigenvector for the SVM. To reduce miss or misjudge detection, the multi-characteristic signals, including high-frequency radiation characteristics, current waveform slope, and periodic integral characteristics, are extracted from the normal condition, arc fault condition, and start-up stage of the circuit. Then, the status of the circuit is identified by the SVM [62]. In Reference [38], SVM and principal component analysis are implemented to detect the arc fault as well as load recognition. Reference [38] proposed a comprehensive method based on principal component analysis and support vector machine (PCA-SVM) combined model for compound load identification and series arc detection. It collected 3-time-domain parameters, maximum slip difference (MSD), zero current period (ZCP), and maximum Euclidean distance (MED), as well as nine frequency-domain harmonic information, mixing time domain, and frequency domain information. Based on SVM, a comprehensive load identification and series arc detection model is realized. Reference [52] proposed a recognition method based on Kernel Principal Component Analysis (KPCA) and Firefly Algorithm Optimization Support Vector Machine (FA-SVM). KPCA was used to separate the harmonics and load noise interferences in the voltage and current signals. Kurtosis and skewness of the fifth and sixth principal components were used as a feature vector for identifying arcs.

As an advanced AI technique, ANNs [63] are also employed to detect arc faults, due to threshold methods cannot handle complex situations. Reference [58] proposed a method that uses sparse coding to capture specific signal features by NNs for intelligent feature learning and classification. The preprocessed input samples are converted into a series of sparse coefficients and then input into the neural network for recognition. Reference [39] proposed a fully connected neural network to divide the samples into resistive type, capacitive-inductive type, and switching type according to the fundamental frequency component of the series current. An independent fully connected neural network is used in each category, with custom time and frequency indicators as input, for category recognition and state recognition.

In another aspect, to avoid the complex feature extraction process for arc fault diagnosis, end-to-end classifications are also widely used, for example, deep learning methods [39, 64]. The raw or pre-processed electrical signals are directly leveraged as the input of deep neural networks, using the powerful feature extraction ability of networks to adaptively extract useful features. Some interesting networks are utilized in recent research, such as the AutoEncoder (AE) [65], series arc fault neural network [66], ArcNet [60], and a temporal convolution network (ArcNN) [67]. Reference [60] proposed an arc detection model based on a Convolutional Neural Network (CNN). The research database collects data of 8 different types of loads according to the IEC62606 standard. ArcNet only receives the original sampling data in the form of time series, without any software preprocessing, and directly performs a large number of analysis experiments to verify the effectiveness of the proposed ArcNet. The high detection and classification accuracy implies that these models can discover hidden arc faults through automatically extracted features, including using different sample times. This result-oriented thinking runs through the entire deep learning process, including the construction of additional features, the construction of the model structure, and the selection of hyperparameters.

Many algorithms are performed under a single working condition, so it is challenging to meet the requirements of the diversity and complexity of household loads. Reference [40] used a combination of the feature selection method based on Random Forest (RF) and the Deep Neural Network (DNN) to detect and locate the topological series arc fault of multi-load circuits. Moreover, RF-DNN increased the accuracy of ANN and DNN. Reference [68] proposed a singular value decomposition (WASVD) algorithm based on wavelet analysis. The proposed WASVD-CAN method has a detection accuracy of only 92% in the parallel experiment of electronic dimming lamps, halogen lamps, and fluorescent lamps, and the other experiments have a detection accuracy of 100%.

2.3.3 Arc Fault Detection Applications

Among all the approaches for applications, low-cost detection is most prevalent and widely used today. To reduce computational cost caused by the large number of parameters and training samples, the circuit current is first divided into subsets based on common features. Then, within these refined subsets, lightweight classifiers are employed to perform targeted feature learning and identification [39]. In Reference [69], an easy implementation method based on calculating the algebraic derivative of the current is used for arc fault detection. Short integration times (50 us) are sufficient for arc detection in the AC circuit. However, this method is not suitable for installations with a switching load. In Reference [45], the 5th harmonic of the current in the circuit is used for arc fault detection. By comparing the 5th harmonic of the current in the circuit with the minimum value of the 5th current harmonic indicates the appearance of the arc fault in the circuit, the arc fault in the circuit can be identified. This method is simple and inexpensive. However, this method is only effective when the loads in the circuit can not produce the 5th current harmonic. Other methods based on the harmonic analysis also perform poorly during switching events [70]. Compared to the arc fault detection based on harmonic analysis, arcing fault methods using the crest factor are more reliable and can withstand the disturbances of arcing faults from many switching events and harmonics [71]. A more sensitive and stable indicator is proposed in [72]. By using the inter-period autocorrelation coefficient, the arc fault can be easily identified.

Many algorithms focus more on the accuracy of arc detection, but they do not realize that in some cases, the misjudgment caused by non-arc signals is also worthy of attention. Reference [73] proposed an arc fault coupling identification method based on Short-Observation-Window SVDR, which solved the misjudgment caused by the similar arc and non-arc signals. The traditional current detection methods based on FFT, wavelet transform, and CZT, even with high FR, cannot extract small fault features from the main current. Compared with the methods mentioned above, the coupling method proposed in this article can effectively solve the small-amplitude fault characteristics of the main current. In the coupled signal, the second-order cumulant algorithm is used to distinguish the arc. To guarantee the accuracy and reduce the nuisance tripping of AFDDs in a complex load environment. The Kalman filter, which has the ability to deal with linear systems containing white noise and other inaccuracies in data measurement and processing, is adopted in arc fault detection [74, 75]. In [75] the Kalman filter and a fuzzy logic processor are used to develop a reliable arc fault detection method for a complex load environment, and when masking load exists. In this work, various loads, masking loads, and disturbances of the appliances are considered.

2.4 Testing Requirements in Arc Fault Detection Standards

Due to the appearance of load resistance, the arc current during a series arc fault does not change significantly compared to the normal operating current. Thus, it can not be prevented by the traditional overcurrent protection devices. To reduce fire accidents caused by arc faults, some countries have published standards to require the test configurations for arc fault detection products in Figure 2.6. These include UL-1699 issued by the United States, IEC62606:2013 issued by the International Electrotechnical Commission (IEC), and GB/T31143 and GB14287.4 issued by China.

In the US, the Arc fault circuit interrupter (AFCI) was invented in 1993, and the standard for AFCI has been released and revised by the Underwriters Laboratories since 1999 [20]. Since then, the potential of reducing electrical fires by using AFCI has been recognized. Subsequently, the International Electrotechnical Commission (IEC) and the National Electrical Code (NEC) also released the requirement for the AFCI [21]. In the 2002 version of the NEC code, the AFCIs are required to be installed in all circuits in dwelling unit bedrooms. At the initial stage, the AFCIs can be used only for branch or feeder circuits. Later, the combination-type AFCIs, which can be used for both the outlet circuit and the branch circuit, were invented and are defined by the NEC and the UL1699 in 2005 and 2006, respectively. Since then, the use of AFCIs has expanded from bedrooms to living rooms, libraries, recreation rooms, or similar rooms or areas [76].

The IEC promulgated an international standard for arc fault protection equipment in 2013, namely (IEC62606-2013) [21]. In 2014, based on the international standard IEC62606-2013, China made some modifications according to China's power supply voltage and frequency and formulated the GB/T 31143-2014 standard to regulate arc fault protection equipment [22]. Currently, in China, AFDDs have not been required to be installed compulsorily. Both the AFCI and AFDD standards serve to detect arcs and interrupt the circuit to prevent fires. In 2014, China proposed GB 14287.4 as a standard for arcing fault detectors (AFDs) applicable to industrial and residential buildings with power ratings up to 10kW, which function as alarms [77]. Until 2014, South Korea still did not publish its industrial standards or electrical installation technical standards of the electricity enterprises act on AFDD [78].

Figure 2.6 Standards for arc fault detection products.

In terms of voltage levels, UL-1699 is an American standard primarily targeting applications with AC 60Hz and a rated voltage of 120V. GB/T31143 and GB14287.4 target domestic voltage levels in China, namely AC 50Hz with a rated voltage of 220V. The IEC62606 standard covers most countries and regions worldwide, including both voltage levels used in different situations.

For current levels, UL-1699 specifies that the maximum current for normal operation of arc fault protection products should not exceed 30A, while GB/T31143-2014 sets a maximum current limit of 63A. According to GB14287.4-2014, which defines a power rating of 10kW, the current level will also not exceed 100A. In standard GB/T 31143, the minimum test current is 3A, slightly higher than 2.5A in the standard IEC62606. Therefore, these standards mainly apply to low-current and low-power domestic scenarios.

To assess AFDD/AFCI performance, the evaluation should cover not only the detection of series and parallel faults but also immunity to nuisance tripping under disturbing loads. Accordingly, the standards define test configuration and evaluation criteria for both sensitivity and immunity. Verification of the operating characteristics requires the tests, including series arc fault tests, parallel arc fault tests, masking tests, and unwanted tripping tests.

However, unwanted tripping and missing trips of AFDDs often happen. According to an investigation [79], the accuracy of arc fault detection devices is only 50%. This is mainly due to the following two reasons: the first is that the fault arc current is small. The normal current easily submerges the characteristic signal, especially when the arc fault happens in the subcircuit. Secondly, due to the complex loads used in the residential building, high-frequency signals and the 'flat shoulders' phenomenon can appear in the circuit without an arc fault. This will lead to the unwanted tripping of the AFDDs.

2.5 Conclusions

This chapter reviewed the main research in AC arc-fault detection from four perspectives: arc modeling, physics-based arc fault detection, data processing and data-driven detection, and relevant standards. Traditional mathematical and physical arc models, such as the Cassie and Mayr models, provide theoretical foundations for understanding arc behavior but are limited by environmental uncertainties, nonlinearity, and the randomness of real-world arc phenomena. physics-based detection methods rely on optical, acoustic, or electromagnetic emissions, which are easily affected by environmental factors and installation conditions, restricting their use to specific industrial applications.

Data-driven detection methods, particularly those based on current-signal analysis, have shown great potential. Time-domain, frequency-domain, and hybrid feature extraction techniques form the basis of most algorithms. Artificial intelligence (AI)-based methods such as SVM, ANN, and deep learning models have significantly improved recognition accuracy and automation. Nevertheless, these models often rely on limited datasets and specific load types. When faced with untrained or new load conditions, their performance tends to degrade, leading to false detections or missed faults. Moreover, the complex loads and strong masking effects in household environments remain a major challenge.

Existing standards, including UL-1699, IEC62606, GB/T31143, and GB14287.4, provide the foundation for testing and evaluating arc fault detection products, but unwanted tripping and missed detections continue to occur due to the small amplitude of fault currents and the overlap between arc and non-arc characteristics.

In summary, although significant progress has been made in both model-based and data-driven detection techniques, challenges remain in ensuring robustness, adaptability, and real-time performance under diverse load conditions.

3 Assessment of Arc Fault Detection Devices

Arc-fault circuit-interrupters (AFCIs) and arc fault detection devices (AFDDs) have been developed to reduce electrical fire risks by interrupting arc faults in low-voltage residential circuits. As discussed in Section 2.4, several standards specify test requirements for assessing the operating characteristics of arc fault detection products.

However, the standardized tests are limited in both complexity and scope, addressing only a narrow range of load conditions and circuit configurations. As a result, despite widespread claims of meeting standard requirements, the real-world effectiveness of arc fault detection products under diverse residential scenarios remains insufficiently validated. A systematic evaluation of arc fault detection products is therefore needed to assess practical performance and to identify weaknesses in existing test methodologies.

This chapter provides a comprehensive assessment of commercial AFDDs and the weaknesses of the existing tests, and provides recommendations for strengthening standardized tests. Section 3.1 describes the development of the arc fault detection platform used for testing. Section 3.2 summarizes the tests of GB/T 31143 and presents results for AFDDs. Section 3.3 and Section 3.4 examine additional masking tests and additional unwanted tripping tests. Section 3.5 proposes improvements to the operating-characteristic tests in current standards. Section 3.6 concludes with key findings and recommendations.

3.1 Development of the Arc Fault Platform

To conduct comprehensive arc fault detection product testing and systematically collect experimental datasets, an experimental platform was constructed in a real building, as shown in Figure 3.1. The test configuration is shown in Figure 3.2. The platform comprises three units: an Arc Fault Unit (AFU), a Data Acquisition Unit (DAU), and an Appliance Load Unit (ALU). This platform is powered by a 220 V AC, 50 Hz source.

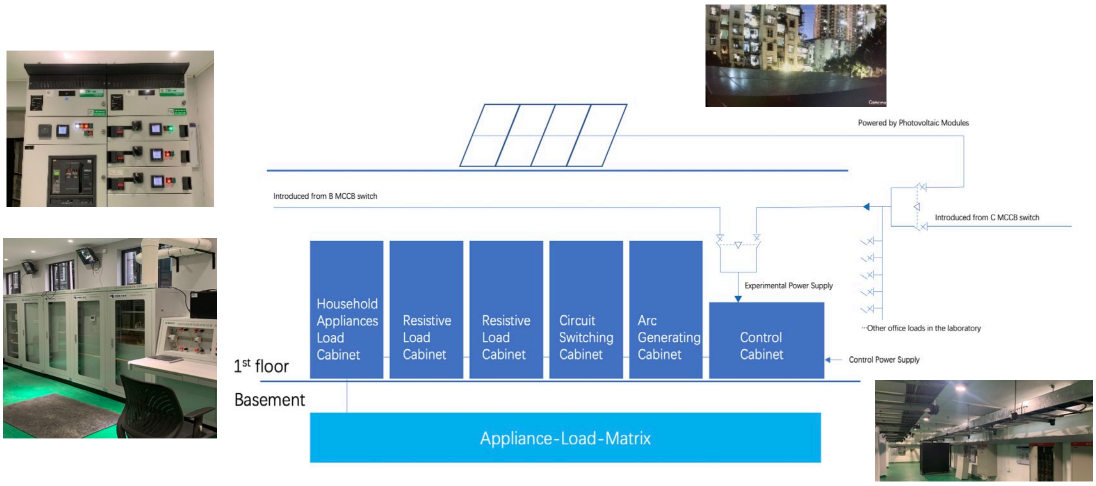

Figure 3.1 Layout of the experimental platform.

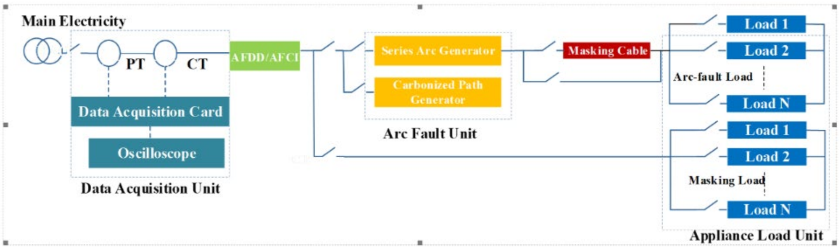

Figure 3.2 Configuration of the arc testing platform.

3.1.1 Arc Fault Unit

Series arcs are generally generated in two different ways. Figure 3.3 shows the point contact arc fault generator to produce arcs caused by the interruption of the line connection. This device consists of a stationary electrode and a moving electrode based on GB/T 31143. The stationary electrode is a 6mm diameter graphite carbon rod, and the moving electrode is a copper rod.

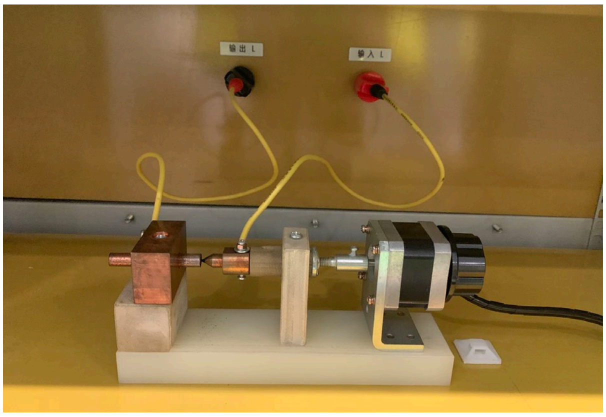

Figure 3.3 Point contact arc fault generator.

Figure 3.4 shows the carbonized path generator designed to generate arcs caused by damage to the insulation layer. The transformer in this generator is used to provide a current source for creating a carbonized conductive path across the insulation of the cable specimens.

Figure 3.4 Carbonized path generator.

3.1.2 Data Acquisition Unit

The current and voltage are respectively measured by a current probe (CP8050A with the bandwidth of DC-50MHz) and a voltage probe with a bandwidth of 250MHz. The signals are recorded by an oscilloscope (Rigol Oscilloscope MSO5000 with 250 MS/s) as shown in Figure 3.5.

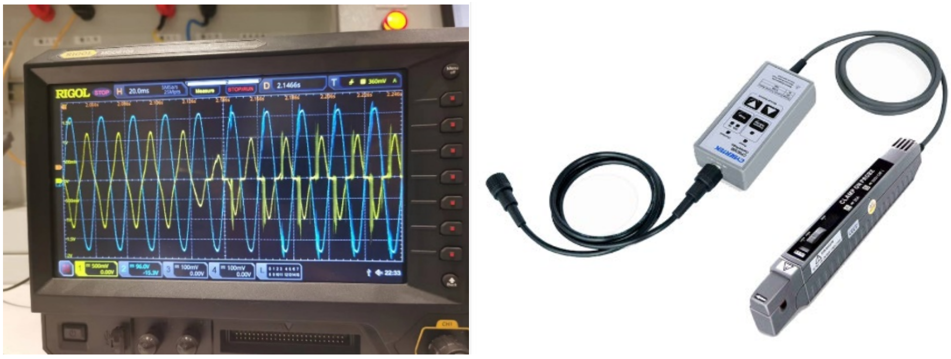

(a) (b)

Figure 3.5 Data acquisition device (a) Oscilloscope (b) Current probe

3.1.3 Appliance Load Unit

Loads and circuit configurations in the standard are relatively simple and narrow in scope. The ALU extends some typical household appliances in Figure 3.6, incorporating devices such as air conditioners, electric kettles, hair dryers, and various lighting systems. The platform recreates comprehensive household scenarios in which arc faults may occur on the main feeder, on individual branches, or across multiple branches.

Figure 3.6 Household appliances.

3.1.4 Selection of AFDDs

Arc fault detection devices are designed to detect hazardous arc faults in electrical circuits and thereby reduce fire risk. Thirteen AFDD/AFCI products available in the Chinese market were collected for testing, as shown in Figure 3.7. An anonymized list is provided in Table 3.1. The products employ diverse feature-extraction and detection techniques. Most devices on domestic and commercial applications have a rated current up to 40 A, which are typically used to detect series arc faults in the circuits.

Figure 3.7 Selected AFDDs.

Table 3.1 The parameters of selected products

Product	Feature Extraction	Detection Algorithm	Rated Current(A)
A	None	Artificial intelligence	32
B	Typical time-domain features and FFT	Trip thresholds	40
C	A low-frequency and high-frequency signal	Trip thresholds	20
D	FFT, spectrum analysis	Trip thresholds	32
E	RSSI in the frequency domain	Trip thresholds	25
F	Typical time-domain features and FFT	Trip thresholds	32
G	None	None	25

3.2 Standard Tests

This section presents the standard tests performed on AFDDs to evaluate their performance, reliability, and safety. Section 3.2.1 outlines the general requirements and test procedures of standard tests. Section 3.2.2 summarizes the test results and analysis of AFDDs.

3.2.1 The Requirements of Standard Tests

All AFDD/AFCI products entering the Chinese market must undergo a sequence of tests defined in GB31143 [22] to verify the ability to capture the arc-fault event and ensure a basic level of unwanted tripping. In this section, standard tests are presented, which were performed on the selected AFDDs to reveal their detection performance against arc faults.

The verification of the operation characteristics is mainly made by conducting three types of tests, namely

- series arc fault tests,
- masking tests, and
- unwanted tripping tests.

3.2.1.1 Series Are Fault Tests

In the series arc fault tests, a representative product shall clear the arcing fault in case of sudden appearance of a series arc in the circuit, by inserting a load with a series arc fault, and closing on series arc fault. The test circuit is shown in Figure 3.8. According to the switch position of S1, S2, S3, and S4, the test arc current is adjusted to the rated current through the resistive load, and the breaking time is measured three times.

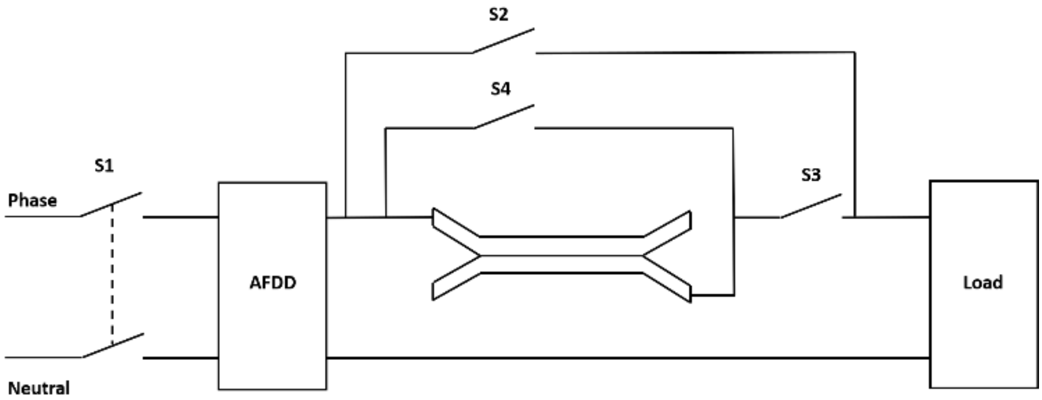

Figure 3.8 Circuit diagram of the series arc fault experiment.

3.2.1.2 Masking Tests

In the masking tests, the correct operation of AFDDs shall be checked in different inhibition configurations: inhibition loads, an electromagnetic interference (EMI) filter, and a line impedance.

The masking test with inhibition loads is divided into two groups. In the first group, the resistive load is adjusted so that the current flowing through the AFDD is 2.5A. The circuit diagram is shown in Figure 3.9. The second group of tests is applied with inhibition loads, using the same resistive load in different configurations. The circuit diagram is shown in Figure 3.10. The current and power of the masking load in the experiment are shown in Table 3.2.

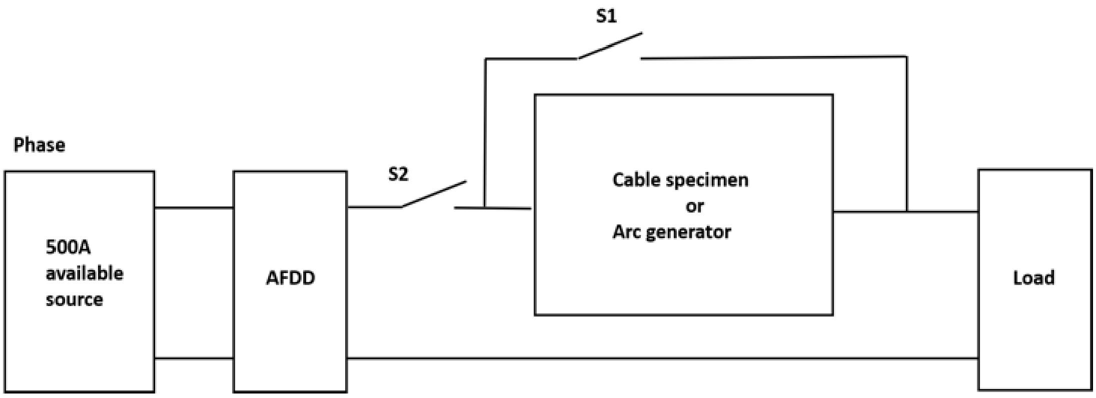

Figure 3.9 Test circuit for masking tests.

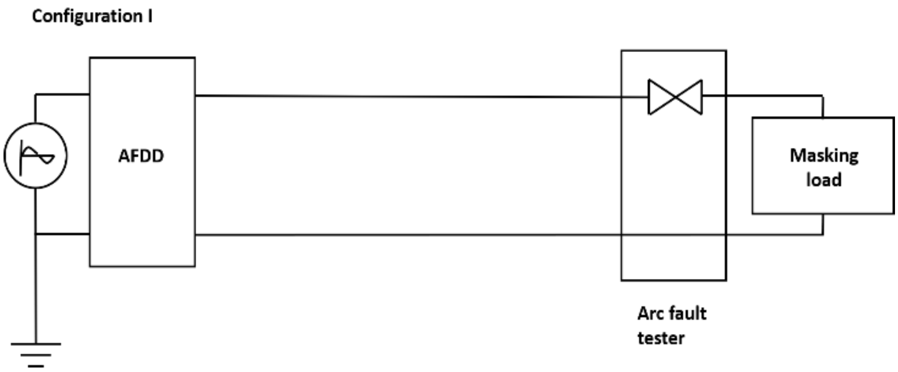

（a）

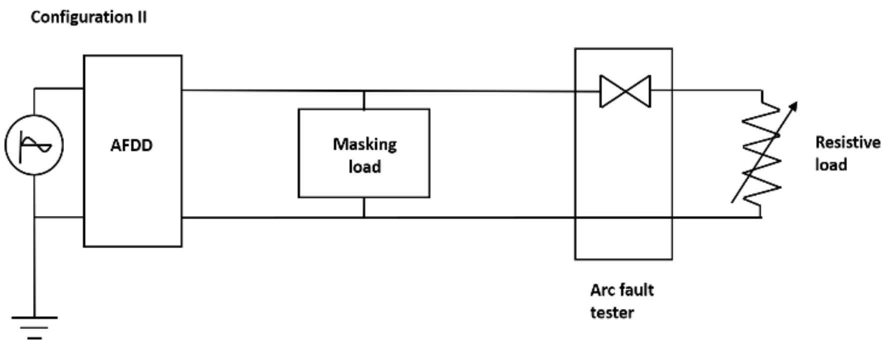

（b）

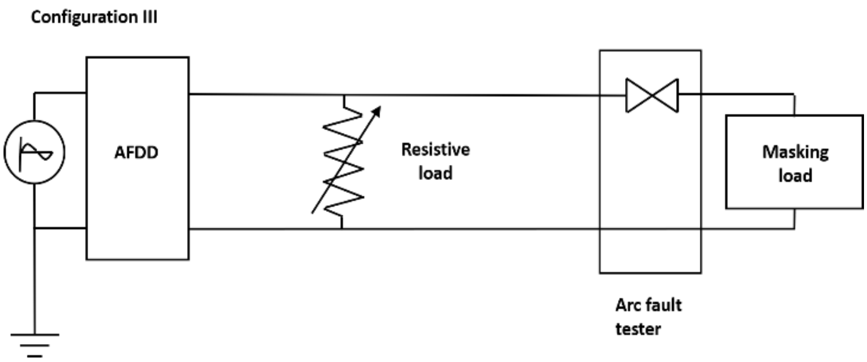

(c)

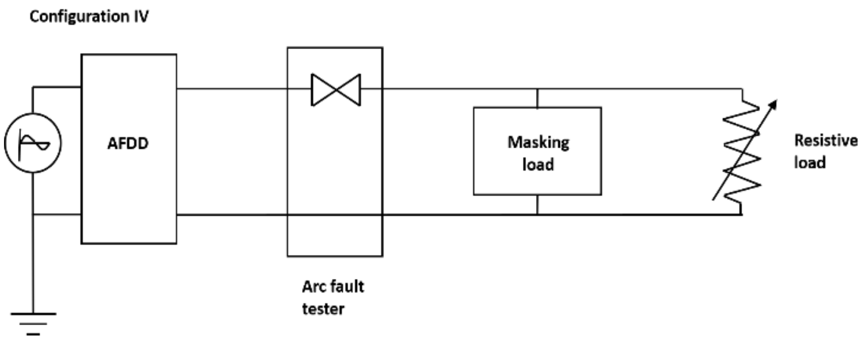

(d)

Figure 3.10 Test configurations for masking tests (a) configuration I (b) configuration II (c) configuration III (d) configuration IV.

Table 3.2 Load parameters

No.	Load type	GB31143	Lab
a	A vacuum cleaner	5A-7A	6.8A
b	Electronic switching mode power supplies	At least 3A	3.95A
c	A capacitor start motor	P=2.2kW	P=2.2kW
d	An electronic lamp dimmer controlling a tungsten load	P=600W	P=600W
e	Two fluorescent lamps plus a resistive load 5A	P=80W	P=80W
f	12 V halogen lamps powered with electronic transformer plus a resistive load 5A	P=300W	P=300W
g	Drill	P=600W	P=600W

The EMI filter masking tests include two types, one using two capacitors and the other using an EMI filter at the end of the cord.

The line impedance consists of an armored cable with a length of 30 m and a cross-section of 2.5 mm². The load is a 3 A resistive load. The circuit is shown in Figure 3.11.

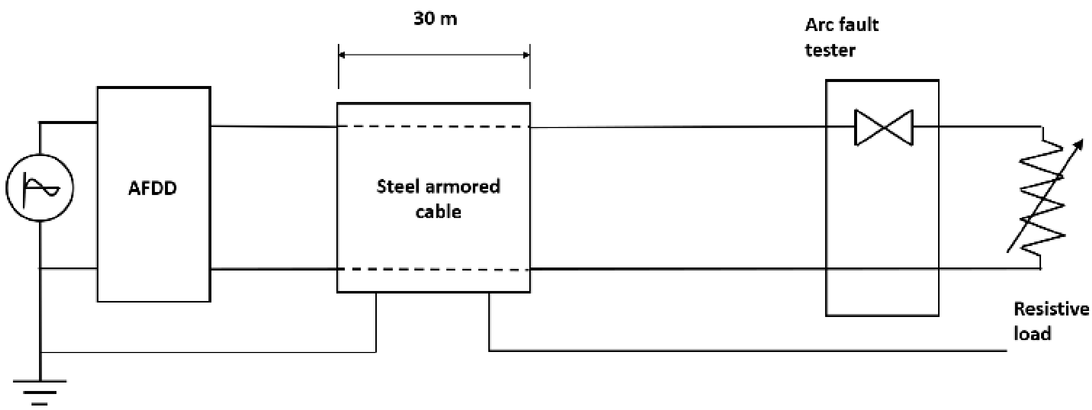

Figure 3.11 Line impedance for masking tests.

3.2.1.3 Unwanted Tripping Tests

Unwanted tripping tests consist of cross talk test and test with various disturbing loads. The cross talk test mainly tests whether an AFDD will trip incorrectly in a branch when an arc occurs in another branch without an AFDD. Tests with various disturbing loads are shown in Figure 3.9 without an arc generator or cable specimen (S1 being closed). The parameters of loads are presented in Table 3.2.

3.2.1.4 Testing Procedure

In the series arc fault tests and masking tests, the breaking time is measured three times. No measurement shall exceed the limiting value in Table 3.3 when using the carbonized path generator. When using the arc generator, the AFDD/AFCIs shall clear the arcing fault in less than 2,5 times the break time in Table 3.3. In the unwanted tripping tests, the loads are energized for a period of at least 5 s. Five Start/Stop operations shall be performed and the products shall not trip.

Table 3.3 Limit values of break time

Test arc current (r.m.s. values)	3A	6A	13A	20A	40A	63A
Maximum time	1	0.5	0.25	0.15	0.12	0.12

3.2.2 Results and Analysis of AFDD Standard Tests

Seven AFDDs are installed at the side of the power supply to detect arc faults, as listed in Table 3.1. In the masking tests and unwanted tripping tests, seven loads are selected, as shown in Table 3.2.

3.2.2.1 Results of the Standard Tests

Since the rated currents of the AFDDs are different, the series fault arc test is mainly based on the rated current to determine the test items, so the number of arc test items between AFDDs with different rated currents is not the same. Table 3.4 shows the results of the series fault arc tests on seven different brands. Among the seven AFDDs, two AFDDs ultimately passed the series arc fault tests in GB31143, and five AFDDs did not.

In the three fail-to-pass experiments of AFDD Sample C, the tripping time under the current of 20A is 0.2s, which is greater than 0.15s required by the standard. In the fail-to-pass experiment of AFDD Sample E, the AFDD tripped at 0.6 s under the 20A current, which exceeded the max. limit of 0.15s. The situation shows that the algorithms in the two AFDDs are too complicated to protect the circuit in time. Furthermore, the performance of circuit breakers is different in the three experiments of the same item.

Table 3.4 Results of the series fault arc tests

AFDD	Rated Current	Overall Items	Failed items	Remark
A	32A	4*3=12	0	
B	40A	5*3=15	0	
C	20A	4*3=12	3	Time out
D	32A	4*3=12	11	
E	25A	4*3=12	5	Time out
F	32A	4*3=12	12	
G	25A	4*3=12	12	

The results of masking tests for AFDDs were presented in Table 3.5. It can be seen that seven AFDDs, four AFDDs passed the test, and the remaining three circuit breakers failed in the test. From the number of failed projects, these three AFDDs can hardly identify arcs in the masking tests.

Table 3.5 Results of the masking tests

Brand	3A	a	b	c	d	e	f	g	EMI	Line	Fail
A	√	√	√	√	√	√	√	√	√	√	0
B	√	√	√	√	√	√	√	√	√	√	0
C	√	√	√	√	√	√	√	√	√	√	0
D	√	√	√	√	√	√	√	√	√	√	0
E	×	×	×	×	×	×	√	×	×	×	22
F	×	×	×	×	×	×	×	×	×	×	20
G	×	×	×	×	×	×	×	×	×	×	28

The tests with various disturbing loads are aimed at the current waveforms of some loads having flat shoulders and other arc current features to prevent AFDDs from unwanted tripping under normal operation. In Table 3.6, AFDDs performed very well in the unwanted tripping test. Among the seven AFDDs, only one AFDD failed in the test.

Table 3.6 Results of the unwanted tripping tests

Brand	Cross	a	b	c	d	e	f	g	Fail
A	√	√	√	√	√	√	√	√	0
B	√	√	√	√	√	√	√	√	0
C	√	√	√	√	√	√	√	√	0
D	√	√	√	√	√	√	√	√	0
E	√	√	√	√	√	√	√	√	0
F	√	√	√	√	√	√	√	√	0
G	√	×	×	√	√	×	√	√	3

In Table 3.7, among the seven brands of AFDDs, two circuit breakers have passed ultimately, and the rest of the AFDDs are not satisfactory. This result evaluated the operating characteristics of seven AFDDs in the Chinese market and found that not all circuit breakers can detect the arc fault within the specified time. The main problem is the arc fault identification under the masking experiment. When there is a masking load in the circuit, the current feature of the arc-fault signal is easily masked. In the series arc fault experiment, the challenge of the circuit breaker is that AFDDs cannot recognize the fault arcs and trip in a standard fixed time under high currents. In the unwanted tripping experiment, the overall performance of AFDDs is outstanding.

Table 3.7 Results of the AFDD standard tests

Brand	Series arc fault tests		Masking test		Unwanted tripping test		Total tests	
Test	Total	Fail	Total	Fail	Total	Fail	Total	Fail
A	12	0	28	0	8	0	48	0
B	15	0	28	0	8	0	51	0
C	12	3	28	0	8	0	48	3
D	12	11	28	0	8	0	48	11
E	12	5	28	22	8	0	48	27
F	12	12	28	20	8	0	48	32
G	12	12	28	28	8	3	48	40

3.2.2.2 Waveform Analysis

Figure 3.12 presents the normal current and arc current of a 3A resistive load in the series arc fault tests. It is observed that the normal current is a sinusoidal alternating current. When an arc appears in the circuit, the current waveform is distorted with an amplitude increase and a flat shoulder.

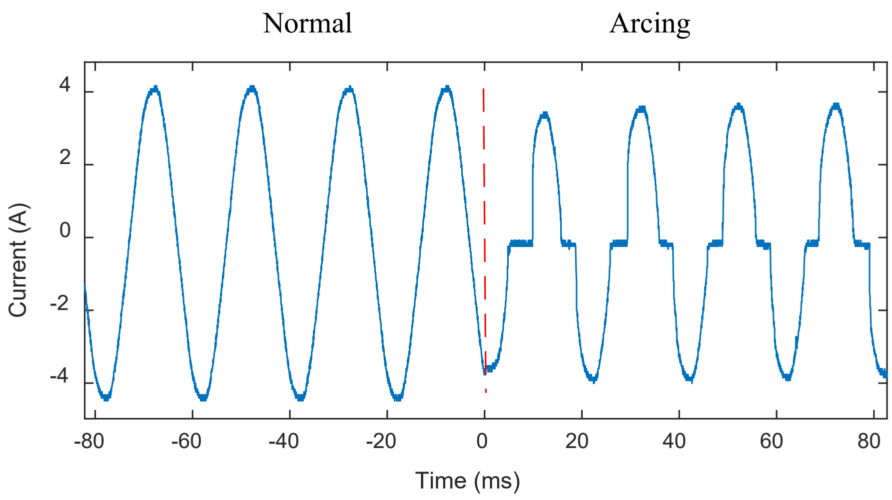

Figure 3.12 3A resistive load current waveform.

In the masking tests, the arc-fault current of the vacuum cleaner has high-frequency components at the zero-crossing point. The arc-fault current waveform of the electric drill shows a flat shoulder and high-frequency characteristics. However, when there is a masking resistance in the circuit with the arc on the resistance branch, the feature of the fault arc current is easily masked. In Figure 3.13, when a switching power supply or an electric drill is used as a masking resistor in the circuit, arc-fault current waveforms exhibit less pronounced features than typical resistive arc-fault current waveforms in Figure 3.12. The masking of this parallel load has caused difficulties for the AFDDs to judge the arc current.

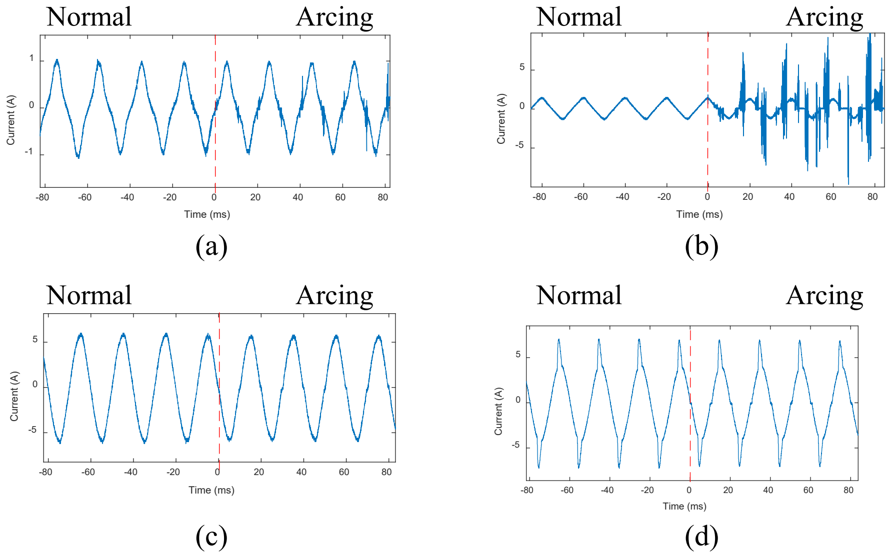

Figure 3.13 Normal and arc waveforms of different types of appliances. (a)Vacuum cleaner (b) Drill (c) Drill and 3A resistive load-arc fault in the resistive load branch (d) Power supplies and 3A resistive load-arc fault in the resistive load branch

3.3 Additional Masking Tests

Based on the results in Table 3.7, several AFDDs achieve a good operating performance in the standard tests. However, in complex and dynamic scenarios at home, whether these AFDDs can still identify fault arcs and protect circuits correctly is not clear.

The additional masking tests are designed to evaluate the performance of these AFDDs under real-world conditions. The test circuit follows configuration I, as illustrated in Figure 3.10. The detailed power ratings of the selected appliances are listed in Table 3.8. In total, thirty-three load types are included, covering many common household loads and operating modes.

Table 3.8 Power rating of the home appliances available for tests

ID	Load type	Power	ID	Load type	Power
1	Tungsten bulb	200	18	Fluorescent lamp	20
2	Kettle	1800	19	Computer	300
3	Handheld garment steamer	1200	20	Electronic switching mode power supplies	460
4	Electric baking pan	1200	21	LED bulb	16
5	Vacuum cleaner	1600	22	LED tube	14
6	Hair dryer-Heating	1000	23	Electronic lamp dimmer	600
7	Hair dryer-Cold	500	24	Air purifier	38
8	Sliding resistor	660-8800	25	Fluorescent lights with magnetic ballast	30
9	Drill	600	26	Induction cooker	2100
10	Capacitor start (air compressor type) motor	1600	27	Microwave Oven-Micro	1300
11	Industrial electric fan	550	28	Microwave Oven-Light	850
12	Washing machine	400	29	Fixed-frequency air conditioner	3500
13	Dishwasher	1200	30	Changeable frequency air conditioner Cold	1390
14	Disinfection cabinet	800	31	Changeable frequency air conditioner Heating	1780
15	Fluorescent lights with electronic ballast	36	32	Halogen lamps powered with electronic transformer	50
16	Refrigerator	130	33	Dehumidifier	178
17	Electric bike charger	180			

3.3.1 Additional masking tests with inhibition loads

AFDDs A, B, C, D, and E are collected for the additional masking tripping tests due to the performance in Table 3.7. In the additional masking tests, the test configurations for the loads are classified into three groups: 1) the arc fault current below the minimum current defined by the GB/T 31143, 2) the variation of the masking load current, and 3) the variation of masking loads other than those listed in the standard.

Table 3.9 reveals the results of the masking tests with Group 1 loads. As shown in the table, Product D cannot detect the arc fault current of the fan or drill with the masking loads. Product B fails to capture the signal of arc-fault events with the tungsten bulbs as the arc-fault load and the motor or switching-mode power supply as the masking load. Product B functions incorrectly with the arc fault load of the fan and the masking load of the switching-mode power supply. It is apparent that these common home appliances have significant masking effects on the identification of arcing in a circuit with loads of the current rating less than 3A.

Table 3.9 Results of the masking load tests(Group 1)

Arc-fault Loads / Masking loads	Fan		Drill		Tungsten bulbs	
AFDD/AFCI products	D	B1	D	B1	D	B1
3A resistive load	×	√	×	√	√	√
6A resistive load	×	√	×	√	√	√
10A resistive load	×	√	×	√	√	√
16A resistive load	×	√	×	√	√	√
Drill + 3A resistive load	×	√	×	√	√	×
Drill + 6A resistive load	×	√	×	√	√	×
Drill + 10A resistive load	×	√	×	√	√	×
Vacuum cleaner + 3A resistive load	×	√	×	√	√	×
Vacuum cleaner + 6A resistive load	×	√	×	√	√	×
Vacuum cleaner + 10A resistive load	×	√	×	√	√	×
Vacuum cleaner + 16A resistive load	×	√	×	√	√	×
Switching power supplies + 3A resistive load	×	×	×	√	√	×
Switching power supplies + 6A resistive load	×	×	×	√	√	×
Switching power supplies + 10A resistive load	×	×	×	√	√	×

'×' failure in the test, '√' pass in the test.

In the second group of tests, a sliding rheostat is inserted in the branch for the masking load to provide an adjustable current of up to 25A. Figure 3.14 shows the testing results of Products A, E, and D with various arc fault loads. In the figure, the symbol of '○' depicts a pass in the test under a combination of an arc-fault load and the masking load current, and '×' depicts a failure in the test. It is found that Product E could fail in the test with the masking load current of 25A, and Product A could fail in the test with the masking load current of 16A or above. This means a large masking current could cause the detection failure of the products.

(a)

(b)

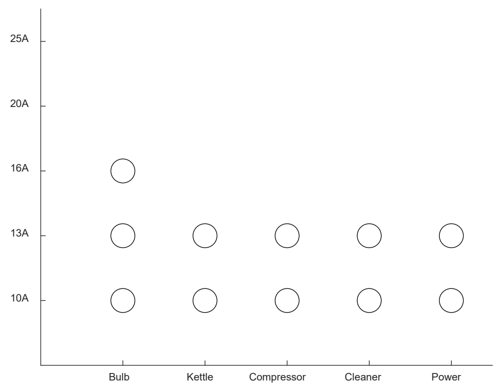

(c)

Figure 3.14 Results of the masking load tests (Group 2). (a) Product E (b) Product A (c) Product D

In the third group of tests, different combinations of appliances in the list are made for the masking load to mimic realistic working conditions. The available loads include the 3A/25A resistive load, kettle, induction cooker, tungsten bulbs, disinfection cabinet, vacuum cleaner, air compressor, switching-mode power supply, and fluorescent light with magnetic ballast. Table 3.10 shows the testing results of Products A, C, and E. It is found that Products A and C fail to detect the arc fault current in the resistive loads, and Product E fails to detect the arc fault current in other loads. Note that these products pass the standard masking tests. Figure 3.15 shows the arc-fault currents in the resistive load and disinfection cabinet, respectively. It is seen that the arc-fault signals of the resistive load and disinfection cabinet are masked by the masking loads, which leads to detection trouble to the algorithms in these products.

Table 3.10 Results of the masking load tests (Group 3)

Arc-fault Load	Masking loads	A	C	E
A 3A resistive load	Fluorescent lamps Kettle Switching power supplies Vacuum cleaner	√	×	√
Kettle	A 25A resistive load Tungsten bulbs	√	×	√
A 3A resistive load	Tungsten bulbs Kettle Induction Cooker	√	×	√
A 3A resistive load	Tungsten bulbs Kettle	×	√	√
A 3A resistive load	Tungsten bulbs Kettle Switching power supplies	×	√	√
Disinfection cabinet	Vacuum cleaner Switching power supplies Fluorescent lights with magnetic ballast Kettle	√	√	×
Kettle	Disinfection cabinet Vacuum cleaner Switching power supplies Fluorescent lights with magnetic ballast	√	√	×
Vacuum cleaner	Disinfection cabinet Switching power supplies Fluorescent lights with magnetic ballast Kettle	√	√	×
Disinfection cabinet	Vacuum cleaner Switching power supplies Fluorescent lights with magnetic ballast Kettle Tungsten bulbs Air compressor	√	√	×

'×' failure in the test, '√' pass in the test.

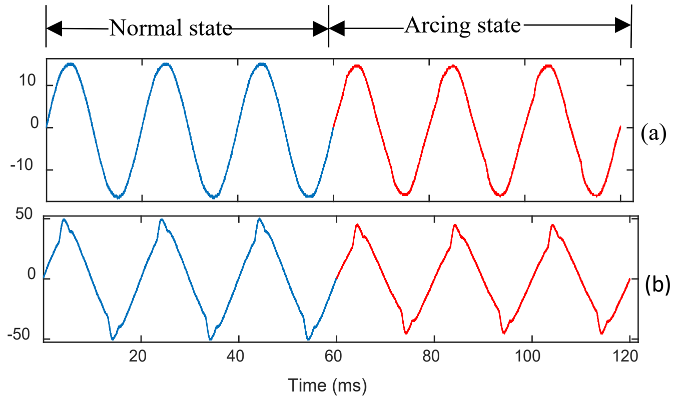

Figure 3.15 Arc-fault current waveforms in masking experiments. (a) 3A resistive (arc-fault load), tungsten bulbs, kettle (b) Disinfection cabinet (arc-fault load), vacuum cleaner, switching-mode power supply, fluorescent lights with magnetic ballast, kettle, tungsten light, air compressor

The products passing the standard tests could fail in the masking tests with the arc-fault loads of a current of less than 3A, with a large masking current, or with a marking circuit consisting of a group of home appliances. It seems that resistive loads in an arc fault circuit could cause some difficulty in the identification of arc faults in these cases.

3.3.2 Masking Tests with Line Impedance

The experimental platform is constructed to investigate the impact of cable length on arc fault detection in Figure 3.2. The circuit configuration is shown in Figure 3.11. Experiments are conducted on combinations of load and various lines. The line impedance between the load and the current sensor can be adjusted from 0 to 100 m with a cross-sectional area of 1 mm². For experimental validation, seven common appliances are chosen, and the rated power or current is shown in Table 3.11.

Table 3.11 Power rating of the home appliances available for tests

ID	Load type	Category	Power/Current
1	2.5A resistive load	Resistive	2.5A
2	9A resistive load	Resistive	9A
3	Kettle	Resistive	1800W
4	Tungsten bulbs	Resistive	800W
5	Vacuum cleaner	Inductive	1600W
6	Capacitor start motor	Inductive	2200W
7	Electronic switching mode power supplies (ESMPS)	Switched-mode power supply	3.95A

The results are summarized in Tables 3.12 to 3.14, where numerical values represent the percentages of successful tests. An "X" denotes an invalid or inapplicable test group. These results show that the accuracy of AFDDs decreases to varying extents as the cable length increases.

Table 3.12 shows that as the cable length increases, AFDD2, AFDD3, and AFDD4 experience a significant decline in their ability to detect tungsten lamp arc signals, eventually failing when the masking effect exceeds a certain threshold. In the electric kettle tests, AFDD2 and AFDD3 become vulnerable to interference beyond 60 meters of cable length, while AFDD4 exhibits notable instability after only 20 meters. With a 2.5A resistive load, AFDD1, AFDD2, and AFDD3 demonstrate progressively diminished accuracy beyond 20 meters, whereas AFDD4 ceases to operate effectively beyond 60 meters. However, under a 9A resistive load, AFDD1 remains unaffected by variations in cable length, while AFDD3 and AFDD4 begin to generate erroneous results beyond 40 meters.

Table 3.12 Results of resistive loads

Tungsten bulb	0m	20m	40m	60m	80m	100m
AFDD1	100%	80%	80%	60%	100%	100%
AFDD2	100%	100%	100%	100%	0	0
AFDD3	100%	100%	0	0	0	0
AFDD4	100%	100%	0	0	0	0
Kettle	0m	20m	40m	60m	80m	100m
AFDD1	100%	100%	100%	80%	100%	60%
AFDD2	100%	100%	×	40%	40%	40%
AFDD3	100%	100%	100%	80%	40%	60%
AFDD4	100%	20%	40%	0	20%	0
2.5A resistive load	0m	20m	40m	60m	80m	100m
AFDD1	100%	80%	80%	60%	20%	60%
AFDD2	100%	80%	×	×	×	40%
AFDD3	100%	60%	0	0	0	0
AFDD4	100%	100%	100%	0	20%	0
9A resistive load	0m	20m	40m	60m	80m	100m
AFDD1	100%	100%	100%	100%	100%	100%
AFDD2	100%	×	0	0	0	0
AFDD3	100%	100%	80%	80%	80%	20%
AFDD4	100%	100%	20%	40%	0	0

Table 3.13 presents the experimental results for inductive loads. Increasing cable length has minimal impact on AFDDs for vacuum cleaners. For the signals of a capacitor start motor, cable lengths up to 100 meters do not interfere with AFDD2's detection capability. However, AFDD1 and AFDD4 fail to detect arc signals when cable lengths exceed 20 meters and 40 meters, respectively. AFDD3's efficiency decreases gradually beyond 60 meters.

Table 3.13 Results of inductive loads

Vacuum Cleaner	0m	20m	40m	60m	80m	100m
AFDD1	100%	100%	100%	100%	100%	100%
AFDD2	100%	100%	100%	100%	100%	100%
AFDD3	100%	100%	100%	100%	100%	100%
AFDD4	100%	100%	100%	100%	100%	100%
Capacitor start motor	0m	20m	40m	60m	80m	100m
AFDD1	100%	20%	0	0	0	0
AFDD2	100%	100%	100%	100%	100%	100%
AFDD3	100%	100%	100%	60%	20%	40%
AFDD4	100%	100%	0	0	0	0

Table 3.14 presents the test results of ESMPs. The performance of AFDD1 remains unaffected by cable lengths within 100 meters. The accuracy of AFDD2 gradually decreases beyond 80 meters. AFDD3 exhibits low identification efficiency when the cable length exceeds 40 meters. AFDD4 begins to show performance degradation at 20 meters and completely fails beyond 80 meters.

In general, the accuracy and stability of AFDDs decline as cable length increases. And, the attenuation characteristics vary across different load types, leading to distinct impacts on detection performance.

Table 3.14 Results of switched-mode power supply loads

ESMPs	0m	20m	40m	60m	80m	100m
AFDD1	100%	100%	100%	100%	100%	100%
AFDD2	100%	100%	100%	100%	80%	40%
AFDD3	100%	100%	20%	0	20%	20%
AFDD4	100%	60%	60%	60%	0	0

3.4 Additional Unwanted Tripping Tests

The five products in Section 3.3.1 are selected for the additional unwanted tripping tests. The test procedures are described in Section 3.2.1. Table 3.15 shows the pass/failure results obtained from the tests. It is found that many failures are associated with the loads, such as hairdryers, compact fluorescent lamps, and fluorescent lights with magnetic ballast.

There are three different groups of tests. Table 3.15 shows the test results when the fluorescent light with a magnetic or electronic ballast is switched on or off. It is observed that three of five products (B, C, and E) fail the test. Figure 3.16 (a) shows the current waveform when fluorescent lights with a magnetic ballast alone are turned on. Figure 3.16 (b) shows the current waveform of multiple loads connected in series. It is clearly seen that these currents contain high-frequency components, which may lead to the misjudgment of these products. Figure 3.16 (c) presents the normal current of the fluorescent light with an electronic ballast, which is similar to the arc current waveform with flat shoulders.

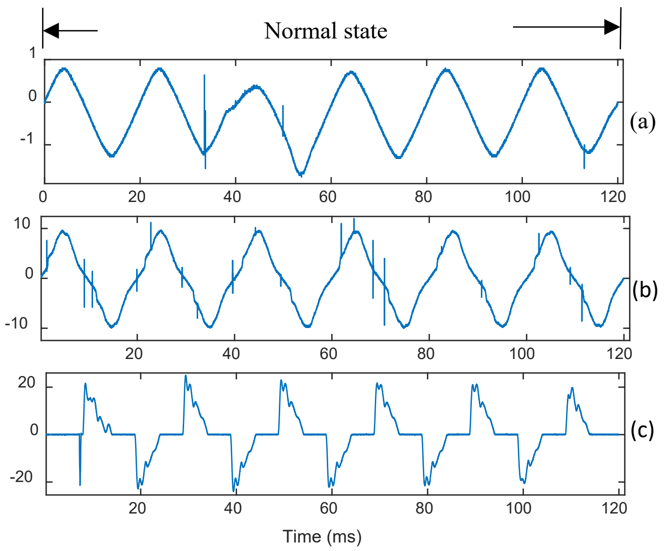

Figure 3.16 Normal current waveforms. (a) Fluorescent lights with magnetic ballast (b) Fluorescent lights with magnetic ballast, vacuum cleaner, drill, compact fluorescent lamps (c) Fluorescent lights with electronic ballast

Table 3.15 Pass/Failure results of the unwanted tripping tests

The loads on/off	Load in other branches	A	B	C	D	E
1. first case-starting process						
Fluorescent lights with magnetic ballast	3A Resistive	√	×	√	√	×
	Refrigerator Switching power supplies Fixed-frequency air conditioner	√	√	√	√	×
	3A Resistive Vacuum cleaner	√	√	√	×	×
	Vacuum cleaner Drill Fluorescent lamps	√	√	√	×	√
	Vacuum cleaner	√	√	√	×	√
	Vacuum cleaner Hairdryer LED bulbs	√	√	√	×	√
	3A Resistive Fluorescent lamps	√	√	√	×	√
	Vacuum cleaner Drill LED bulbs	√	√	√	×	√
	3A Resistive Hairdryer	√	√	√	×	√
	3A Resistive Hairdryer Fluorescent lights with electronic ballast	√	√	√	×	√
Fluorescent lights with electronic ballast	None	√	√	√	√	×
	3A Resistive	√	×	√	√	√
2. Second Case- mode change						
Hair dryer	None	×	×	×	×	×
	3A Resistive	×	√	√	√	√
	3A Resistive Fluorescent lights with electronic ballast Fluorescent lights with magnetic ballast	×	√	√	√	√
	3A Resistive Fluorescent lights with magnetic ballast	×	√	√	√	√
	3A Resistive Electronic lamp dimmer	√	√	×	√	√
3. Third Case- change states among different cases						
Vacuum cleaner	Disinfection cabinet upper floor 3A Resistive	√	√	√	√	×
6A Resistive	Fluorescent lights with electronic ballast	√	√	√	√	×
3A Resistive	Fluorescent lights with magnetic ballast	√	√	√	√	×
	Fluorescent lamps	×	√	×	√	√

Electronic lamp dimmer	3A Resistive					
	Fluorescent lamps 3A Resistive Switching power supplies	×	√	√	√	√
	3A Resistive Halogen lamps with electronic transformer	×	√	√	√	√
	3A Resistive	√	×	√	√	√
Halogen lamps with electronic transformer	3A Resistive Switching power supplies Electronic lamp dimmer	√	√	×	√	√
Industrial electric fan	None	√	√	√	√	×
Changeable frequency air conditioner	6A Resistive	√	√	√	√	×
Fluorescent lamps	3A Resistive Kettle	√	√	√	√	×
	6A Resistive	√	√	√	√	×
	3A Resistive Electronic lamp dimmer	×	√	×	√	√
	3A Resistive Halogen lamps with electronic transformer	×	√	√	√	√
	3A Resistive Halogen lamps with electronic transformer Fluorescent lights with magnetic ballast	×	√	√	×	√
	3A Resistive Halogen lamps with electronic transformer Fluorescent lights with magnetic ballast Fluorescent lights with electronic ballast	×	√	√	×	√
Switching power supplies	3A Resistive Electronic lamp dimmer	×	√	√	√	√
	3A Resistive Electronic lamp dimmer Fluorescent lamps	×	√	×	√	√
3A Resistive Fluorescent lights with electronic ballast	None	√	√	√	√	×

'×' failure in the test, '√' pass in the test.

The second group of tests is performed to check the performance of these products when switching the operation mode of a hairdryer. It is found in Table 3.15-2 that all five products could fail the tests. Figure 3.17 shows the current of the hairdryer when the hairdryer is switched from cold mode to hot mode. It is found that the current waveform changes from the half-wave and full-wave, which is similar to the arc current of resistive loads. When the hairdryer is operated with other loads connected in parallel, a sudden change in the current waveform is observed. This could lead to misjudgment as well.

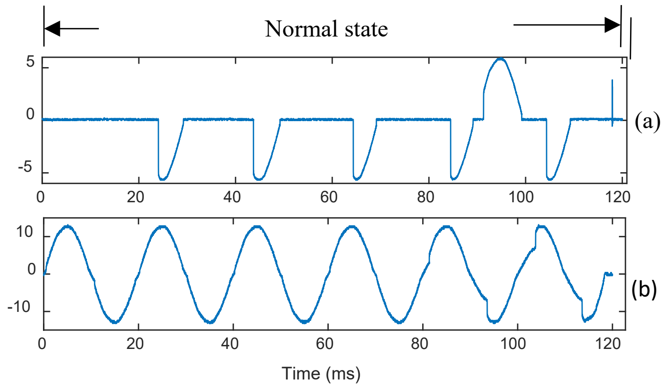

Figure 3.17 Normal current waveforms. (a) Hairdryer (b) 3A resistive load, hair dryer, fluorescent lights with magnetic ballast

The third group of tests is performed by switching a load other than fluorescent lamps and a hairdryer on or off. As shown in Table 3.15-3, the switching of tungsten lamps with an electronic dimmer and fluorescent lamps in the presence of other loads could cause misjudgment of three products. The startup and shutdown of some small current loads could cause misjudgment of the tested products as well, e.g., an electronic lamp dimmer, compact fluorescent lamps, and fluorescent lights with electronic ballast. There is a phenomenon of zero-crossing, accompanied by high-frequency components in the normal state of an electronic lamp dimmer in Figure 3.18. (a).

In the test with the tungsten bulbs with an electronic dimmer connected in parallel with a 3A resistive load, the turn-off current waveform has several cycles with zero-crossing, followed by an irregular current waveform. The zero-cross waveform is also observed when the compact fluorescent lamps are switched off (Figure 3.18(b)) or a switching power supply is switched on (Figure 3.18(c)). This could lead to misjudgment. When the upper room of a disinfection cabinet is working, the closing of a vacuum cleaner results in a current distortion, accompanied by high-frequency components, and leads to misjudgment, as shown in Figure 3.18 (d). Figure 3.18(e) shows the current waveform in the case that two loads are turned on simultaneously. The distorted current waveform causes the malfunctions of Product E.

For the first case-starting process, a reasonable dataset, including fluorescent lights with magnetic ballast and fluorescent lamps with electronic ballast, for training can be very helpful in reducing the false positive rate of the products. It is known from the tests that unwanted tripping of products could be caused by the transient load current during the switching of loads. Such a transient current may contain high-frequency components or zero-cross current, which are similar to those observed in the arc-fault current. It is also noted that the transient current lasts for just a few cycles. Therefore, it is possible to avoid unwanted tripping by ignoring arc-like signals that appear just in a few cycles. If the arc-like signals continue for a long time, tripping of the product shall be made in the circuit.

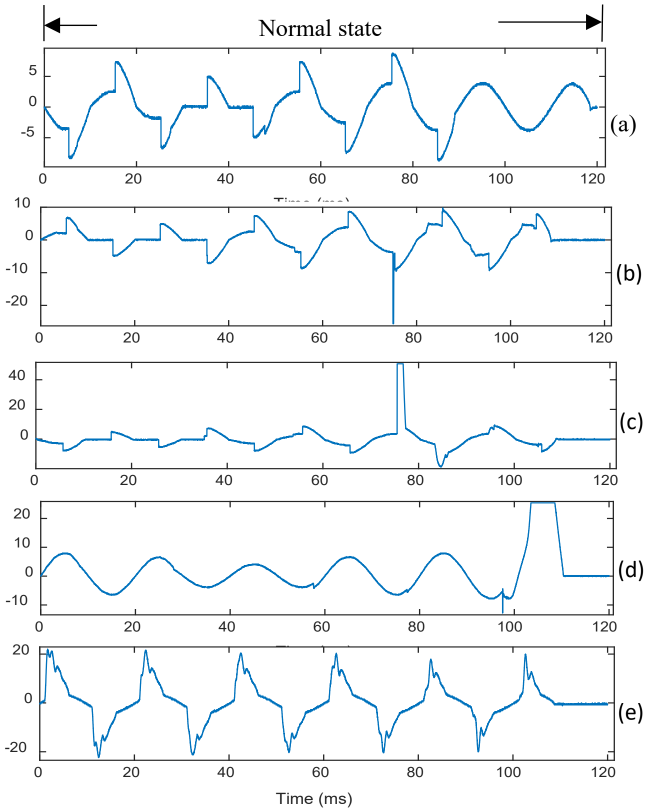

Figure 3.18 Normal-state current waveforms. (a) 3A resistive, electronic lamp dimmer (b) 3A resistive, fluorescent lamps, electronic lamp dimmer (c) 3A resistive, switching power supplies, Electronic lamp dimmer (d) Disinfection cabinet upper floor, vacuum cleaner, 3A Resistive (e) Fluorescent lights with electronic ballast, 3A resistive (together)

3.5 Suggestion on the Operating Characteristic Tests of the Standard

This assessment uncovers the performance of AFDD/AFCI products available in the Chinese market. Unfortunately, less than half of the collected products passed the standard tests. All these products failed in the additional tests in which more diverse appliances and more complicated configurations were considered. A revision should be proposed to retain the core framework of standard tests while adding broader test scenarios and stricter anti-interference requirements in order to align AFDD performance with real-world needs and enhance safety.

The investigation results in Section 3.3.1 reveal a demand for more comprehensive and diverse additional tests as part of the certification process. To address the limitation of test load types in the current standard, it is recommended to expand the scope from the original 7 types of standard loads to 33 types in Table 3.8. With this expansion, the coverage of test loads will extend beyond traditional single scenarios to more diverse and realistic operating conditions. This adjustment allows AFDD testing to better capture the typical characteristics of modern residential electricity usage, thereby enhancing the representativeness and applicability of the standard.

The unwanted tripping tests aim to evaluate whether AFDDs can maintain stable and reliable arc fault detection under multi-level operating conditions. The selected load should have at least three operating levels, such as: induction cooker (low, medium, and high power levels), electric fan (low, medium, and high speed levels), electric drill (stepped or continuous speed control), and LED lighting with multi-level brightness or dimming modes. A reasonable dataset, including fluorescent lights with magnetic ballast and fluorescent lamps with electronic ballast, for training can be very helpful in reducing the false positive rate of the products.

3.6 Conclusions

Standards have been implemented for a decade, initially meeting the typical arc fault detection needs of residential power environments. However, against the background of technological advancement and increased electrification, the proliferation of household appliances, diversification of types, and complexity of user scenarios have exposed significant limitations in the standard's operating characteristic tests. These limitations include narrow coverage of masking test loads, inadequate consideration of unwanted tipping loads, and overly simplistic masking configurations.

To address these gaps, this chapter presents a comprehensive investigation into the AFDDs on the ability to clear the arcing fault under series arc faults and avoid unwanted trips in the standard and additional tests. The products passing the standard test failed in additional tests with more diverse appliances or more complicated circuit configurations. Through analyzing the current waveforms collected in failure cases, realistic tests with diverse appliances and complex load configurations were provided for inclusion in the dataset creation for detection algorithm development and in the standard for certification.

These improved test methods comprehensively address the shortcomings of the current standard, enabling more accurate, comprehensive, and realistic evaluation of AFDD performance. By better aligning with modern residential electrical environments, the methods enhance the relevance and guidance of IEC62606 or GB/T 31143, providing stronger technical support for ensuring the safe and reliable operation of AFDDs in real-world applications and promoting the healthy development of the arc fault detection industry.

4 Lightweight AC Arc Fault Detection Method By Integration of Event-Based Load Classification

4.1 Introduction

Arcing creates excessive heat [80] that can easily ignite surrounding materials, such as wood framing or insulation, resulting in a potentially hazardous fire. Various methods based on different features and detection algorithms have been developed in Chapter 2. Features based on the spectral domain (transformations) and time domain (statistical descriptors) have been adopted [42, 81, 82]. Transformation is one of the commonly used feature extraction techniques for arc fault detection. These methods transform the time-domain arc signals into the spectral domain and determine decomposition coefficients, power spectral density, and other indicators for event classification. Transformations require manually configuring the algorithm. The choice of base functions, level of decomposition, and sampling frequency greatly influences the detection performance [47], thus should be carefully selected for fault detection [19, 38, 39, 82]. Descriptors developed for mechanical systems [38] are also employed to analyze arc signals such as MSD, MED, etc. All these features are manually selected by researchers based on their own experiences. There still lacks a general specification to determine which feature is more reasonable for AC arc fault detection.

After features are extracted, detection algorithms are adopted to diagnose the arc fault. Initially, constant thresholds or algebraic expressions are employed as the detection criteria due to their simplicity. Detection according to constant thresholds cannot handle complex situations. Recently, artificial intelligence (AI) techniques have begun to be used in arc fault detection [44, 52, 75, 82]. The performance of Artificial Neural Network (ANN) is determined by its structure, which requires manual design. Due to the limitation of computation capacity, the calculation of deep learning is too complicated to perform in an industrial chip of AFCIs. Thus, a suitable detection algorithm should be selected from the viewpoint of both configuration convenience and computation complexity.

Another key issue for arc fault detection is the selection of data characteristics, including sampling rate and sampling period, which is seldom studied in previous studies. Theoretically high sampling rate and a long sampling period will bring high detection accuracy. However, it will certainly lead to a high computational burden. Therefore, it is necessary to consider both accuracy and efficiency when selecting the reference sampling rate and period.

Despite detection methods, the complex waveforms of arc fault currents induced by different loads are also a significant challenge for arc detection. The additional tests in Chapter 3 reveal that the complex waveforms of arc fault currents generated by different loads present a significant challenge for arc fault detection. The waveforms of arc fault currents are various, especially in the presence of nonlinear or switching loads [52, 72, 83] What is more, multiple loads operate simultaneously in practical conditions, making arc fault detection more difficult. The widely adopted AC arc detection methods are constructed using a given and fixed basis. However, it may limit their ability to adapt to various load conditions. Experimental results show that their performances are not always satisfactory, and they have a high possibility of nuisance tripping or miss tripping when the load condition is complex [83].

To address the mentioned issues, this chapter proposes a high-performance AC arc fault detection method that is implemented by integrating load identification with fault detection. With the assistance of load identification, different discriminative features and rules are extracted for arc detection of different categories of loads, which can greatly improve the generality and accuracy of arc detection under complex operating load conditions.

In Section 4.2, three load categories are specifically defined for arc fault detection. An event-based load classification method is implemented, which works in real-time and can perfectly integrate with arc fault detection. Section 4.3 proposes a lightweight arc fault detection method, which integrates event-based load identification with arc fault detection. The experiment validation in Section 4.4 proves that the proposed method achieves high detection accuracy with low computational cost. The proposed method works well with complex load conditions, including multiple operating loads. In Section 4.5, the sensitivity analysis of classifiers, deep learning algorithms, sampling rates, and sampling periods for arc fault detection is carried out. It provides a reference for developing arc fault detection devices.

4.2 Arc Characteristics Analysis with Different Loads

According to the designed function and operation principle, common electric appliances can be roughly categorized as [84]: resistive, inductive, capacitive, power electronic, and composite loads. Figure 4.1 shows the typical waveforms of different types of appliances and corresponding arc fault waveforms. Their corresponding waveforms under arcing conditions also vary.

Most of the resistive loads are related to heating, such as heating kettles, incandescent lighting, etc. They have almost no harmonic content with synchronized current and voltage, as shown in Figure 4.1(a). The arcing current for resistive loads has a 'flat shoulder' of current across the zero-crossing region without showing significant spikes.

Inductive loads are mainly appliances equipped with transformers and motors, such as vacuum cleaners, drills, etc. As shown in Figure 4.1(b), in motor-based inductive loads, a large inrush current occurs at the turn-on moment of operation when the motor is switched from the standstill into movement. When an arc occurs, transient spikes are also observed for inductive loads.

Capacitive loads are barely found in residential usage. Although many loads have capacitive elements (e.g., an air compressor with a starting capacitor as shown in Figure 4.1(c)), their overall behavior is dominated by inductive and resistive characteristics [85]. Thus, loads with capacitive elements are not considered as a load category for arc fault detection.

Power electronic loads with switch-mode power supply can produce a large number of harmonic contents, such as a dimmer displayed in Figure 4.1(d). A short but very high-amplitude transient can be observed at its turn-on moment. Meanwhile, this category of load draws current in a non-sinusoidal form with a period of zero current, making it difficult to discriminate from arc faults. It can also be observed that the short-duration transient also appears for arcing.

The others are the combination of different loads, which are called composite loads. For example, a dehumidifier consists of a motor and a heating element that has a complicated current waveform, as shown in Figure 4.1(e). The currents of this category of load show a composite effect rather than a pure resistive, inductive, or switchable current. In this situation, loads are classified by their turn-on characteristics. For example, the switchable load's turn-on spike is commonly larger than the inductive spike, making it the dominant component. Thus, a composite load is classified as a switchable load if it contains a switchable component. Similarly, if a composite load consists of inductive and resistive components, it is classified as an inductive load. Therefore, based on the characteristics of the transient spike and load category, we separate the loads into three categories: resistive, inductive, and switchable (power electronic) loads.

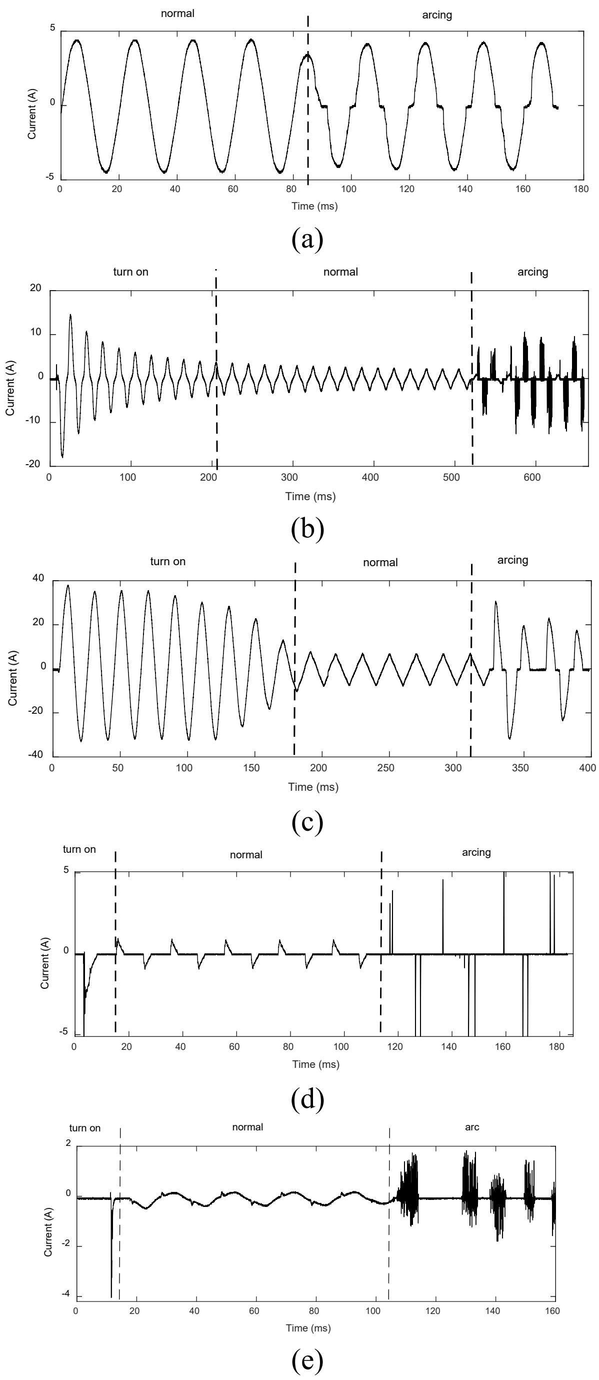

Figure 4.1 Typical waveforms of different types of appliances and corresponding arc fault waveforms. (a) Heating kettle – resistive, (b) Drill – inductive, (c) Air compressor – inductive with capacitance, (d) Dimmer – switch, (e) Dehumidifier – composite.

4.3 The Proposed AC Arc Detection Method

Figure 4.2 shows the comparison of the traditional arc fault detection method and our proposed method. Traditional methods commonly detect arc faults directly based on current waveforms, as shown in Figure 4.2 (a). But the waveforms of arc faults vary according to load categories. To take advantage of this, an arc fault detection method is proposed by integrating load identification as described in Figure 4.2 (b). The proposed arc fault detection method has two major parts: load classification and arc fault detection. Different feature sets are extracted based on the load category. This section presents the details of the proposed method.

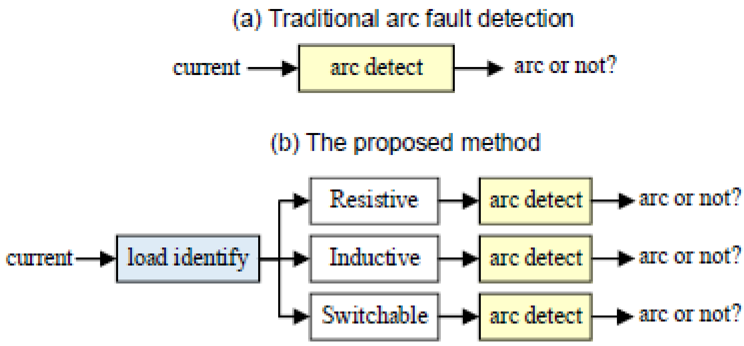

Figure 4.2 The comparison of (a) the traditional arc fault detection method, and (b) the proposed method.

4.3.1 Load Classification Based on Transient Events

The waveform of an arcing current is mainly determined by the category of load. As indicated in [39], to detect series arc faults successfully, the detection system should first identify the category of the load, allowing it to extract corresponding features for that category of load.

As analyzed in Chapter 4.2, the loads are divided into three categories, namely, resistive, inductive, and switchable loads. A rule-based event detector [86] using the change of mean concept [87] is developed by avoiding the use of any kind of complex mathematical technique that may cause a high computational cost.

The event detector calculates the log-likelihood ratio of the change-of-mean in each sliding window to detect transient events [87]. For a sliding window with the length of $2n$ samples, the signal is divided into pre- and post- parts, and the following relation is obtained,

$$D_k = \begin{cases} \dfrac{\mu_{post} - \mu_{pre}}{\sigma^2} \cdot \left| p_k - \dfrac{\mu_{post} + \mu_{pre}}{2} \right| & \left| \mu_{post} - \mu_{pre} \right| > P_{thr} \\ 0 & \left| \mu_{post} - \mu_{pre} \right| \le P_{thr} \end{cases} \tag{4-1}$$

$$\text{where} \quad p_k = v_k i_k \quad \mu_{post} = \frac{1}{n} \sum_{k=n+1}^{2n} p_k \quad \mu_{pre} = \frac{1}{n} \sum_{k=1}^{n} p_k$$

in which μ_{pre} and μ_{post} are the mean of the pre- and post- parts respectively, σ^2 is the variance of the transient power in the sliding window. Parameters p_k, v_k and i_k are the transient power, voltage and current for sample k. P_{thr} is the threshold to screen the influence of the noise.

The likelihood of the signal for a sliding window is then obtained by its maximum as

$$D = \max\left(\left| D_k \right| \right) \quad k = 1, \ldots 2n \tag{4-2}$$

An event can be detected when the amplitude of D exceeds a threshold D_{thr}. It is noted that we use a constant threshold for the detection which has a possibility of reporting wrong (false) events. False events (e.g. noise or power fluctuations) should be eliminated from the detected events. Power changes and time limits are set to remove false detections [88].

- A minimum power change is set to eliminate the influence of noise or power fluctuations. Based on the typical rating power of major household appliances, we only consider the power events with a minimum absolute power change of 20 Watts.
- In order to remove false events, the minimum time interval between two continuous events is set. Considering the turn-on transient periods of major household appliances, the time limit is set to 0.1s, which means multiple events within 0.1s are treated as one event.

Besides removing false events, the time interval between events is also an indicator to separate different categories of loads. Figure 4.3 shows the current, transient power, and likelihood of turn-on events of loads. A resistive load has the shortest turn-on duration. As multiple spikes occur, an inductive load has a turn-on duration of more than 0.4 s. While, this value becomes less than 0.15 s for a switchable load because just one spike occurs for this load category. Arcing is mistaken as a continuous event because it reacts as a switch, repeating opening and closing operations. Thus, this type of false event can be removed by using the duration time.

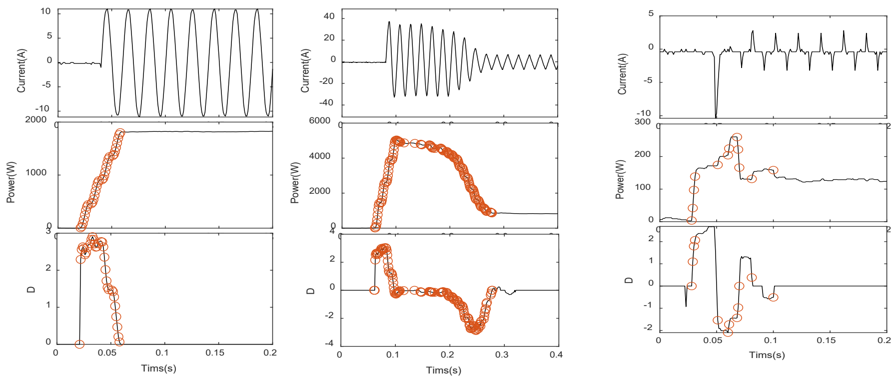

(a) (b) (c)

Figure 4.3 The current, transient power and likelihood of turn-on events, (a) Heating kettle - resistive, (b) Air compressor – inductive, (c) Switch power+resistance – switch. (○ indicates the detected event.)

Assuming Δt is the duration of an event, the category of load C can be obtained as

$$C = \begin{cases} resistive & \tau_0 \le \Delta t < \tau_1 \\ switch & \tau_1 \le \Delta t \le \tau_2 \\ inductive & \Delta t < \tau_3 \\ false & others \end{cases} \tag{4-3}$$

According to the previous analysis, we set the time thresholds as $\tau_0 = 0.02$ s, $\tau_1 = 0.08$ s, $\tau_2 = 0.15$ s and $\tau_3 = 0.4$ s.

4.3.2 Feature Selection Based on the SFFS Method

After load classification, arc fault feature extraction is carried out for each category of load. The selection of features [43] is key to the success of arc fault detection. In this algorithm, both transformation and statistical descriptors are adopted to construct a feature pool. In terms of efficiency, FFT and statistical descriptors are used, listed in Table 4.1, resulting in a total of 25 features. However, not all these features can discriminate well the differences between normal and arc states. Feature selection is evaluated to remove irrelevant features. Obtained features can provide a better learning performance and lower computational cost.

Table 4.1 List of features for arc fault detection

Descriptor	Expression
Range	$\max(x)-\min(x)$
Mean	$\frac{1}{N}\sum_{i=1}^{N}x_i$
Integral	$\frac{1}{N}\sum_{i=1}^{N}\lvert x_i\rvert$
Root Mean Square (RMS)	$\sqrt{\frac{\sum_{i=1}^{N}x_i^2}{N}}$
Variance	$\frac{1}{N\text{-}1}\sum_{i=1}^{N}(x_i-\overline{x})^2$
Skewness	$\frac{\frac{1}{N}\sum_{i=1}^{N}(x_i-\overline{x})^3}{\left(\sqrt{\frac{1}{N}\sum_{i=1}^{N}(x_i-\overline{x})^2}\right)^2}$
Kurtosis	$\frac{\frac{1}{N}\sum_{i=1}^{N}(x_i-\overline{x})^4}{\left(\frac{1}{N}\sum_{i=1}^{N}(x_i-\overline{x})^2\right)^2}$
MSD	$\max\left[\left(\sum_{i=1}^{i+m-1}x_i-\sum_{i+m}^{i+2m-1}x_i\right)\Big/2m\right]$
ZCP	$n_{x_i<\theta}\,/\,N$
Entropy	$-\sum_{i=1}^{N}x_i^2\cdot\log\left(x_i^2\right)$
FFT	15 harmonics

The maximum value is used between precision and recall of a predetermined classifier as the criterion to determine the quality of selected features. K-Nearest Neighbor (KNN) is employed as the classifier for arc fault detection. A sequential floating forward selection (SFFS) [89] is used to deal with feature selection. SFFS consists of two different steps, a forward step and a conditional backward step that partially avoids the local optima.

- The first step is sequential forward search (SFS), which adds one feature from a candidate subset at a time while evaluating the criterion. The feature subset with the highest classification accuracy becomes the initial feature set for the next round of feature selection.
- The second step consists of performing a sequential backward search (SBS), which excludes one feature at a time from the subset obtained in the first step and evaluates the new subset. If excluding a feature increases the value of the objective criterion, then that feature is removed and goes back to the first step with the new reduced subset.

- This process is repeated between SFS and SBS until the required number of features is added or the required performance is reached.

Assuming m is the size of the current feature, M is the required dimension, the scheme of SFFS can be visualized as in Figure 4.4. Based on the category of the load, SFFS is evaluated for three categories of loads using corresponding data. Three groups of decisive features are obtained. They are fed to KNN classifiers to implement the arc fault detector.

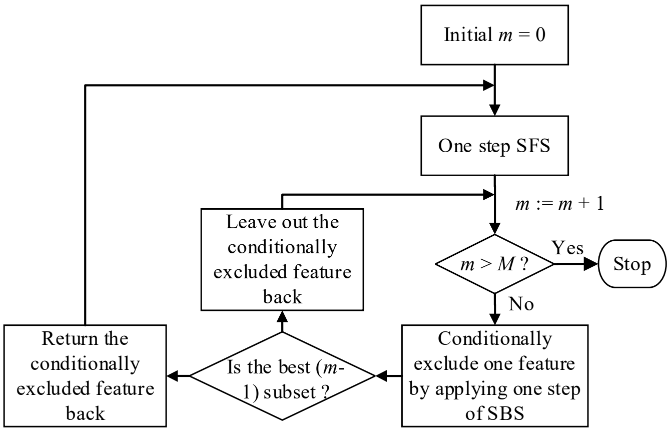

Figure 4.4 The flowchart of sequential floating forward selection

4.3.3 Strategy of the Method

The whole framework of the proposed method is displayed in Figure 4.5. The voltage and current are captured in the acquisition window timely. Event detection is evaluated based on the likelihood of transient power. If an event is detected, false event removal is followed according to the duration of the event. Once the event is confirmed, the load category is recognized from its duration, and the load index is updated. Load classification is only triggered when an event is detected. Otherwise, load classification is paused, and arc fault detection continues with the last classified load. While, if an event is not detected, the acquired current is processed to determine whether the arc occurs or not. The load index indicates which of the three categories of arc detectors to activate. Integrating load classification into arc fault detection makes the proposed method more accurate. As no complex computation is involved, the proposed method is efficient.

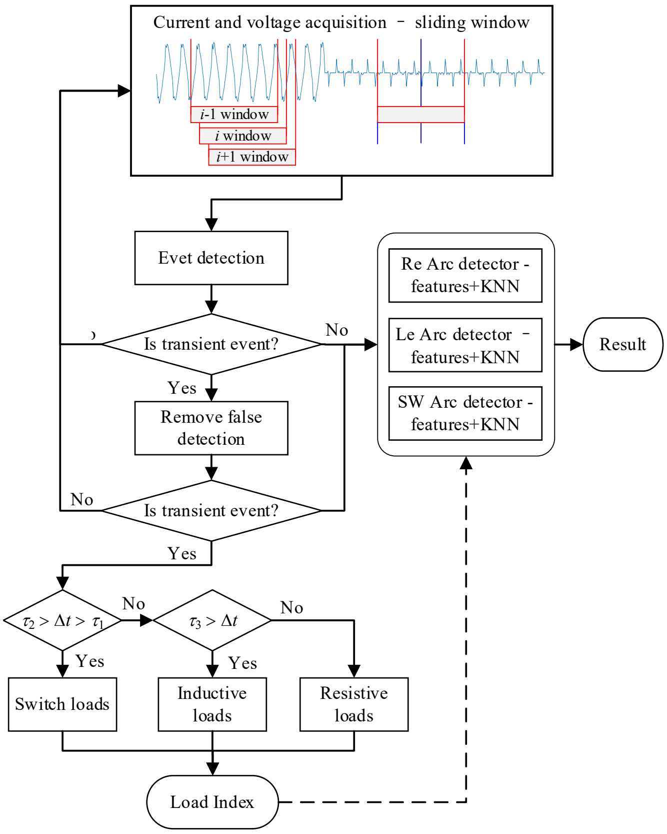

Figure 4.5 The flowchart of the proposed hybrid arc detection method.

4.4 Validation of the Proposed Method

This section presents the arc detection performance of the proposed method. The arc fault detection method constructed using Floating Forward Feature Selection is first validated using the experimental data. Then, the proposed hybrid arc fault detection method with load classification is validated using 15 sequences of data.

Precision and Recall are chosen to be the evaluation metrics. Assuming the minority class to be positive class (P) and the majority class to be negative class (N), classified samples can be separated into four groups as denoted in the confusion matrix. A confusion matrix consists of information about actual and predicted classifications returned by a classifier. Precision is defined as the proportion of the number of correctly predicted samples in the total number of the positive class as Eq. (4-4). Recall is defined as the classification accuracy of correctly identifying a positive class, and it is expressed by Eq. (4-5).

$$\text{Precison} = \frac{TP}{TP + FP} \tag{4-4}$$

$$\text{Recall} = \frac{TP}{TP + FN} \tag{4-5}$$

4.4.1 Experimental Configuration and Dataset

To verify the efficiency of the proposed method, common electric appliances with/without arcing are tested. As the experiment configuration in Figure 4.6, the arc generator and current probe are presented in Section 3.1.

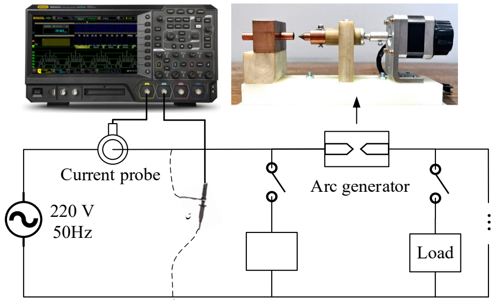

Figure 4.6 Experimental platform

As listed in Table 4.2, 14 common electric appliances are tested. The dataset is obtained for a single load or combined loads. Firstly, series arc fault current signals for each load are generated for measurement. As fault detection is more difficult to achieve with combined loads, series arc fault signals for multiple loads are arranged for measurement. More complicated configurations with 1 or 2 masking loads are also evaluated. A total of 165 sequences of data with 10-second long are recorded, each of which has a 6s normal operation and 4s arcing operation. The dataset is constructed by using 150 sequences. Each sequence of data is randomly split in order to have 70% data for training, and 30% data for validation. Additionally, the other 15 sequences of data are used for verifying the proposed method in time series, which are not included in the training.

Table 4.2 Categories of common electric appliances

Load Category	**Appliance**	**Power (W)**
Resistive	Resistance (105 Ω, 52 Ω and 32 Ω)	/
	Heating kettles	1200
	Incandescent lighting	4×200
Inductive	Vacuum cleaner	1600
	Drill	600
	Fan	550
	Air compressor	1600
Capacitive	/	
Switchable	Switch mode power + resistance	120
	Computer	400
	Dimming lamp	800
	LED lamp	4×22
	Microwave oven	1300
	Air conditioner	1360
	Dehumidifier	400

4.4.2 Validation on Arc Fault Data

Firstly, the detection method is verified by classifying normal and arcing data. The recorded data are downsampled to 10 kHz and divided using a sliding window of 3-cycle length. In the proposed method, load classification and arc fault detection need to be constructed based on the dataset. The proposed method is tested on 150 sequences of data, and all of them succeed.

The arc fault detection is implemented by feature extraction through SFFS. The dataset is divided into three groups according to the load categories, and feature extraction is carried out separately for them. For each group, 70% of the data is used as the training set and the remaining 30% is used as the testing set. 5-fold cross-validation is employed. The arc fault detection results of the Re, Le, SW categories are shown in Figure 4.7 with a confusion matrix, and the extracted features are shown in Figure 4.8.

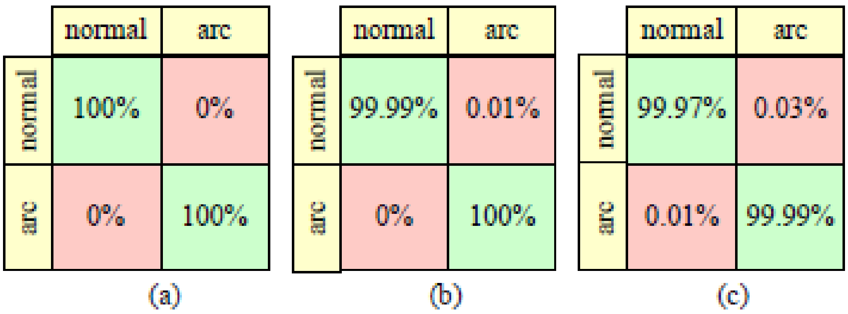

Figure 4.7 The confusion matrix for detection performances of three load categories. (a) Resistive load, (b) Inductive load, (c) Switchable load.

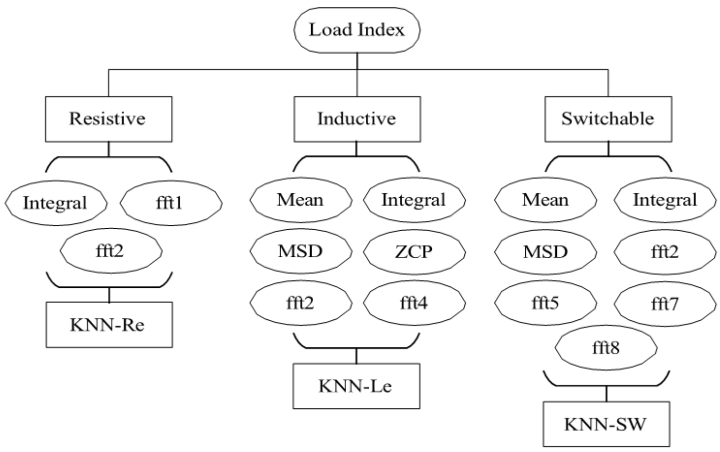

Figure 4.8 Extracted features and classifier for arc fault detection of three load categories.

The average detection precision of normal and arcing states for Re category, Le category, and SW category are 100%, 99.99%, and 99.98%, respectively. The result validates that the proposed method is effective and reliable in complex load conditions with various categories. Different sets of features are extracted for three load categories. As Figure 4.9 shows, extracted features have significant changes when the arc occurs for different load categories. A resistive load has the least features and the highest detection accuracy, which is the most easily handle. Arc detection for Le load is more complicated and requires 6 features to guarantee a high detection accuracy. Arc detection for SW loads is the most difficult with 7 features extracted. These features contain many FFT information indicating SW loads generate many harmonics.

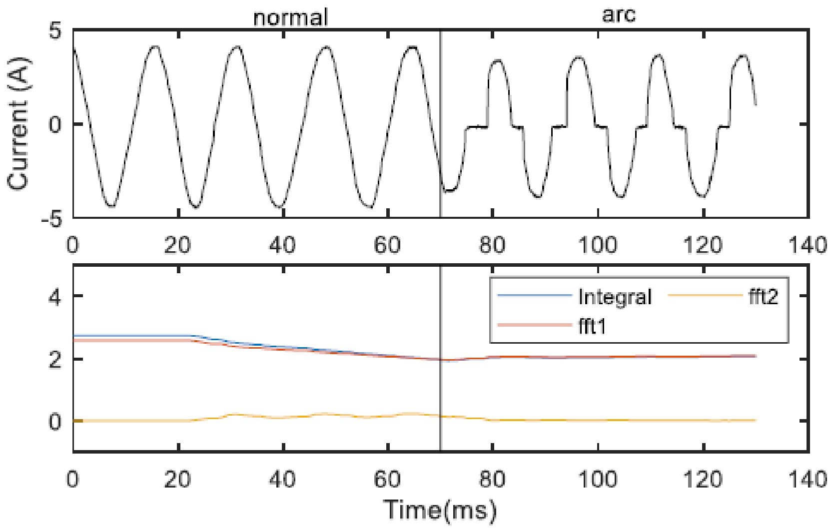

(a)

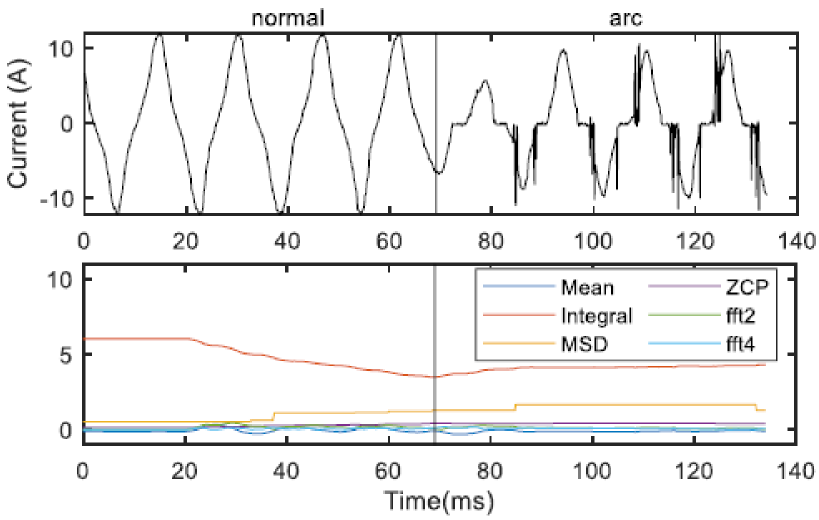

(b)

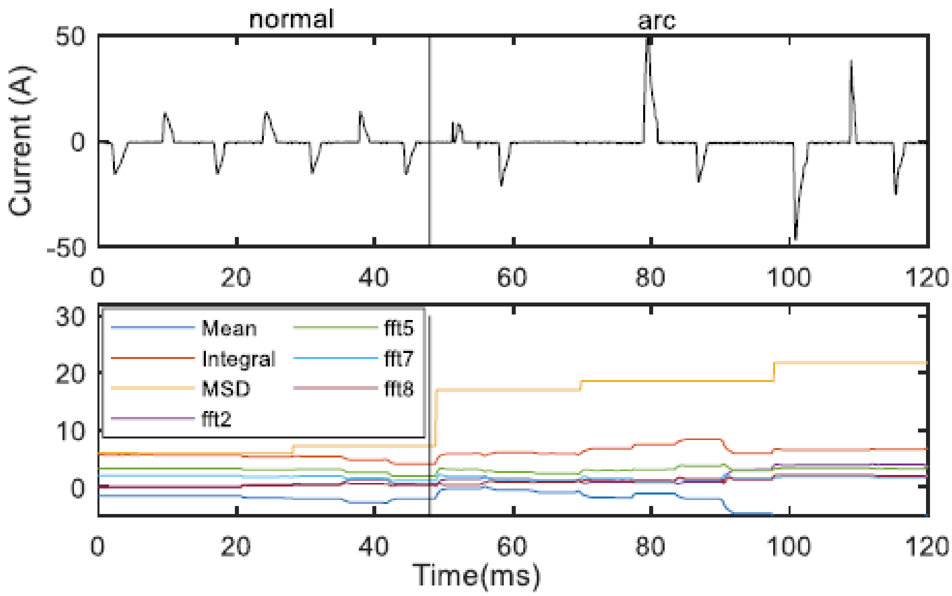

(c)

Figure 4.9 Extracted features for three load categories with/without arcing.(a) Resistive load (b) Inductive load (c) Switchable load.

4.4.3 Validation on Practical Data Sequence

Secondly, the effectiveness of the proposed hybrid method is presented, where both load classification and arc fault detection are implemented. The method is tested using 15 sequences of data in a time series. Load classification is implemented using the method, which are determined according to the turn-on characteristics of loads. The proposed method succeeds in all 15 sequences. Three sequences of data are presented in Figure 4.10 to show their efficiency and mechanism.

Figure 4.10 (a) shows a sequence of data with two resistive loads opened at different time instances. Resistive load 1 is opened at 0.58s, and resistive load 2 is opened at 2.59s. The arc occurred at 4.24s. The proposed method classifies the load as resistive and detects an arc fault in time.

Figure 4.10 (b) shows a sequence of data with a resistive load and an inductive load opened at different time instances. The resistive load is opened at 0.53 s and the inductive load is opened at 0.92s. The proposed method initially classifies the load as resistive. Then, it turns into an inductive category at 1.24s. To avoid the false event, we set a time threshold of τ_3 = 0.4s corresponding to the period from the start of the inductive load (at 0.84s) to determining the load category (at 1.24s). The arc detection method for the inductive load is activated at 1.24 s. Finally, the arc occurs at 2.64 s and is correctly detected.

Figure 4.10 (c) shows a sequence of data with a resistive load, an inductive load, and a switchable load opened at different time instances. The resistive load is opened at 0.53 s. Then, the inductive load is opened at 1.41 s, and the load category turns to be inductive at 1.75 s ($<\tau_3$). The switchable load is opened at 2.87 s, and the load category turns switchable at 2.97 s ($<\tau_2$). The arcing is detected at 5.48 s.

The proposed method successfully classifies the load category and detects arc faults in time sequences. The result proves its efficiency.

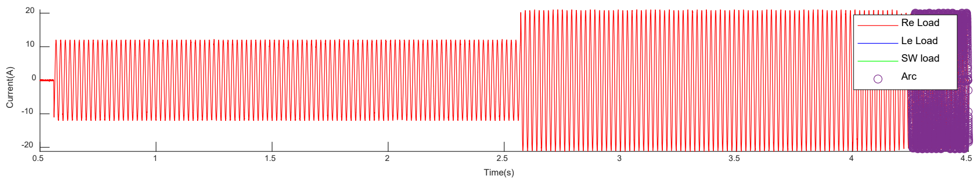

(a)

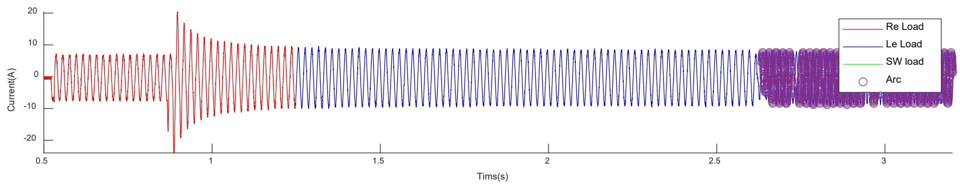

(b)

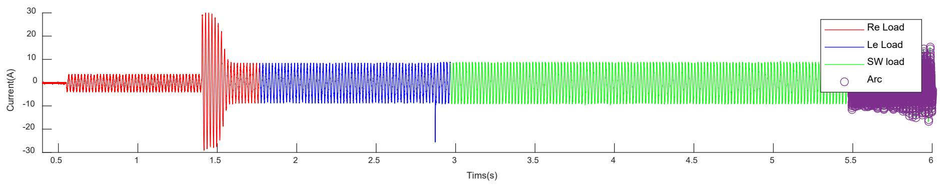

(c)

Figure 4.10 Three sequences of data for validation of the proposed hybrid method. (a) With two resistive loads. (b) With a resistive load and an inductive load. (c) With a resistive load, an inductive load, and a switchable load.

4.5 Sensitivity Analysis and Discussion

The selection of AI algorithms and sampling parameters is important for developing fault detection methods. This section presents the sensitivity analysis of AI algorithms and sampling parameters. Meanwhile, to validate the superiority of the proposed method, a comparison with other reported arc fault detection methods is presented.

4.5.1 Discussion on AI algorithms for AC Arc Detection

As summarized in Table 4.3, various AI algorithms have been employed for arc fault detection. Thus, the performances of six popular AI algorithms are evaluated, including SVM, KNN, DT, and three sigmoid-activated ANNs. Considering the variant structures of ANN, three configurations are evaluated, namely

SVM: with radial basis function (RBF) kernel and optimizes parameters using iterative single data algorithm;

KNN: with Euclidean distance metric, the number of nearest neighbors is 5, and uses a kd-tree to find nearest neighbors;

DT: a standard CART tree is adopted;

ANN1: 1-layer ANN with 10 neurons, the activation function is sigmoid;

ANN2: 2-layer ANN where the first hidden layer is composed of 20 neurons and the second one of 8 neurons, the activation function is sigmoid [82];

ANN3: 3-layer ANN that the first and second hidden layer is composed of 12 neurons and the third one of 4 neurons, the activation function is sigmoid [39].

Extracted features (as in Figure 4.8) are used as the input to six AI algorithms and their detection results are listed in Table 4.3. The comparison of three ANNs reveals that the performance of an ANN is heavily affected by its structure. More hidden layers and neurons can improve the detection performance but bring a high computational burden. Despite SVM and DT being more complex classifiers, KNN performs best among the six AI algorithms with the highest precision and recall for all three load categories. The superior performance of KNN is due to the following reasons. KNN computes the distance among all features. It is not suitable for high-dimensional problems but can provide accurate results for low-dimensional problems. For each category of load, a few features are extracted in our method. KNN performs great on arc fault detection problems of such a low dimension.

Table 4.3 The performance comparison of different classifiers

	Re		**Le**		**SW**	
	Precision	***Recall***	***Precision***	***Recall***	***Precision***	***Recall***
SVM	99.91	99.98	98.44	98.46	96.42	96.42
KNN	**100**	**100**	**99.99**	**99.99**	**99.98**	**99.98**
DT	99.98	99.98	99.93	99.93	99.67	99.67
ANN1	99.7	99.52	92.23	92.26	91.0	91.1
ANN2	100	100	98.74	98.75	98.15	98.16
ANN3	100	100	99.34	99.35	98.29	98.32

4.5.2 Discussion on Sampling Frequency and Period

Both the sampling frequency and sampling period are decisive factors influencing the computation cost and reaction time. The influence of these two factors on arc fault detection performances is evaluated. The sampling frequency from 1 kHz to 20 kHz and the sampling period from 1 circle to 3 circles are evaluated. The arc fault detection method is used for all cases.

The average precision and recall are listed in Table 4.4. It can be seen that the arc fault detection performance improves with the increase of sampling frequency and sampling period. The sampling frequency is more important than the sampling period. In other words, a high sampling frequency can significantly improve detection performance. While, the sampling period can only contribute a little improvement. By comparing all combinations of these two factors, the sampling frequency of 10 kHz with a 3-cycle sampling period is the best.

Table 4.4 The performance comparison under different sampling frequencies and sampling periods

	T=1		**T=2**		**T=3**	
	Precision	***Recall***	***Precision***	***Recall***	***Precision***	***Recall***
1 kHz	78.1	78.87	83.11	83.39	87.92	88.07
2 kHz	85.52	85.58	94.37	94.36	96.72	96.72
5 kHz	97.62	97.62	98.89	98.88	99.48	99.48
10 kHz	99.89	99.88	99.97	99.96	**99.99**	**99.99**
20 kHz	99.95	99.96	99.98	99.97	**99.99**	**99.99**

4.5.3 Discussion on Integration of Load Classification

To show the effect of load classification, the AI algorithms tested are evaluated for arc detection without load classification, where all data from the three categories are mixed up. A total of 11 features are adopted for arc detection, which are selected by combining features for three load categories in Figure 4.8. The data is also sampled at 10 kHz and 3-cycle long. The average precision and recall are obtained as listed in Table 4.5. The results show that arc detection performance is greatly improved when load classification is integrated. It proves the advantage of the proposed method.

Table 4.5 The performance comparison of different classifiers with/without load classification

		Precision	*Recall*
Without Load Classification	**SVM**	95.27	95.27
	KNN	96.93	96.93
	DT	96.62	96.62
	ANN1	83.31	83.31
	ANN2	93.59	93.63
With Load Classification	**ANN3**	95.39	95.43

4.5.4 Comparison with Adopted Features in Other Methods

To test the advantage of the proposed method, six reported methods are compared. Fault features are selected according to the compared methods as listed in Table 4.6, respectively, and the KNN is used to identify an arc fault.

Table 4.6 Adopted features of the compared methods

	Ref.	Feature
①	[38]	MSD, ZCP, MED, FFT
②	[39]	FFT, Integral, variance, skewness, kurtosis, Shannon entropy
③	[19]	mean, median, variance, RMS, range
④	[83]	FFT using 1-15 harmonics
⑤	[46]	DWT with mother wavelet of Daubechies 10 level 5 under descriptor signal energy
⑥	[82]	DWT with mother wavelet of Daubechies 4 level 5 and CZT 10-20 kHz under descriptors mean, variance, skewness, kurtosis, max value, etc.

The same dataset is used in the evaluation with the 10 kHz sampling rate and 3-cycle sampling period. The average precision and recall are obtained as listed in Table 4.7. From the results, we can find:

1) Series arc faults that occur on resistive loads are easily detected. All methods have a high performance. Series arc faults on inductive and switchable loads show more difficulty for detection.

2) The comparison of results ② and ③ , ④ reveals that more features do not provide a better detection accuracy. The results of ③ and ④ show both statistical descriptors and harmonics can be great candidate features for arc fault detection.

3) Wavelet related techniques show worse performance than others. A wavelet technique requires a long sampling period. A 3-cycle sampling period is not long enough to take advantage of wavelet decomposition. Meanwhile, as the wavelet technique has massive variables and combinations [82], it should be carefully designed for identification.

4) The proposed method shows superior performance for all types of loads, which verifies its advantage.

Table 4.7 The comparison of arc fault detection performance

Method	Re		Le		SW	
	Precision	***Recall***	***Precision***	***Recall***	***Precision***	***Recall***
①	99.99	99.99	99.97	99.95	97.98	97.98
②	98.38	98.37	95.71	95.71	95.15	95.16
③	100	100	99.27	99.28	98.69	98.69
④	100	100	99.99	99.99	99.87	99.87
⑤	96.97	96.7	90.8	90.8	90.66	90.67
⑥	97.01	96.58	82.66	82.66	78.43	78.43
Proposed	**100**	**100**	**99.99**	**99.99**	**99.98**	**99.98**

4.5.5 Comparison with Deep Learning Methods

Recently, deep learning models have also been adopted for arc fault detection. For comparison, four deep learning methods are evaluated with the detailed network structures as follows:

LSTM: the model includes two layers of Long Short-Term Memory Networks (LSTMs) and a fully connected (FC) layer. The first LSTM layer has 20 hidden units, and the second one contains 10. Each LSTM layer is followed by a dropout layer with a probability of 0.2. The FC is the output layer followed by the softmax layer for classification.

AE [65]: AutoEncoder (AE) is composed of an encoder and a decoder. The encoder consists of a convolution (CNN) layer (filter size = 4, stride = 1, number of filters = 8, and activation function is leaky ReLU), and an FC layer (number of hidden units = (sequence length − 3)×8 and activation function is ReLU). Then the FC layer with 128 hidden units and the activation function of ReLU is followed for the latent representation. The decoder is then connected with the inverse structure of the encoder (an FC layer followed by a CNN layer). Finally, the output is implemented by an FC layer with softmax activation.

CNN [65]: this is a basic CNN network with 5 CNN layers followed by 2 fully connected layers. All CNN layers are set with a stride of 1 and activated by ReLU. The sizes of these layers vary as (1st: filter size = 10, stride = 1, number of filters = 30; 2nd: filter size = 8, stride = 1, number of filters = 30; 3rd: filter size = 6, stride = 1, number of filters = 40; 4th: filter size = 5, stride = 1, number of filters = 50; 5th: filter size = 5, stride = 1, number of filters = 50)

ArcNet [60]: the model has 4 CNN layers and is followed by 2 FC layers. The 1st and the 3rd CNN layers have 96 filters each. The 2nd CNN layer has 128 filters each. The 4th CNN layer has 64 filters. Each CNN layer has the same kernel size of 5 × 1 and is followed by a ReLU and a MaxPooling layer of pooling size 2 × 1 with stride 1. At the end of the last MaxPooling layer, 2 FC layers having 64, and 32 neurons are appended.

All these models are trained using the Adam optimizer with a minibatch of 150 for 30 epochs. The learning rate is initial to be 0.001. The diagnosis results of these models are listed in Table 4.8. The results show that all these models can achieve high diagnostic accuracy of more than 99% for three categories of loads. While, the proposed method is better than theirs. Deep learning models have many parameters and require careful tuned for better performance. Meanwhile, as summarized in [65], the memory cost and computation complexity of deep learning models are much larger than shallow AI methods. For series arc fault detection, the dominant features are limited. Shallow AI algorithms are recommended for arc fault detection.

Table 4.8 The performance comparison with deep learning models

	Re		**Le**		**SW**	
	Precision	***Recall***	***Precision***	***Recall***	***Precision***	***Recall***
LSTM	99.86	99.81	99.42	99.41	99.04	99.03
AE	99.85	99.86	99.93	99.93	99.64	99.63
CNN	100	100	99.99	99.99	99.78	99.78
ArcNet	99.89	99.92	99.84	99.84	99.38	99.38
Ours	**100**	**100**	**99.99**	**99.99**	**99.98**	**99.98**

4.6 Conclusion

In this Chapter, an efficient AC arc fault detection method is proposed where an event-based load classification method is integrated. In the proposed method, loads are divided into resistive, inductive, and switchable categories based on their turn-on patterns. Three groups of features are extracted using Sequential Floating Forward Feature Selection for three load categories separately. In the practical detection process, load classification is first evaluated to decide the load category. Then, a specific arc fault detection is activated according to the load category. The proposed method improves the arc detection performance with complex load conditions, including multiple operating loads. Meanwhile, it is fast and easy to implement and requires no complex mathematical calculation. It achieves a high diagnosis accuracy under a relatively low sampling frequency with low computational complexity features.

The experimental results show that the proposed method works well for practical arc fault detection with multiple loads. The proposed method has strong applicability in arc fault detection and better performance than other reported methods, even for deep learning models. The sensitivity analysis shows that both statistical descriptors and harmonics can provide great arc fault detection. It is also noted that more features do not mean better detection.

5 Series AC Arc Fault Detection with Line Impedance Based on Multi-band Feature Fusion and Catboost

5.1 Introduction

In response to the concern regarding fire incidents caused by arc faults, standards have established masking tests with line impedance as shown in Section 2.4. American standard UL-1699 specifies a line impedance test for arc-fault circuit interrupters (AFCIs) involving a parallel arc with a current of 500A [20]. Other standards mandate series arc fault tests. The requirements of the international standard IEC 62606 [21] and the Chinese standard GB/T 31143 [22] for arc fault detection devices (AFDDs), include a branch circuit comprising 30 meters of 2.5 mm^2 armored cable with two conductors and steel armor in the masking test with line impedance. In real residential homes where cable lengths can reach 100 meters or more, it remains unclear whether the tests specified in these standards are sufficient for detecting arc faults under such practical conditions.

Masking tests with various line lengths are designed to evaluate the performance of AFDDs under seven loads in Section 3.3.2. Our findings indicate that an increase in line length negatively affects the accuracy and stability of AFDDs.

In recent years, many algorithms have been studied for arc-fault detection, as outlined in Chapter 2 [60, 65-67]. However, these algorithms lack datasets with line impedance and typically restrict circuit lengths to 10 meters or less, and the impact of line length has not been sufficiently considered in the design and training process of the algorithm. Such limitations reduce their applicability to real-world residential scenarios.

Some researchers have investigated arc fault location techniques under varying line lengths in household AC power systems. A low-voltage AC series arc fault location method based on an RBF neural network has been introduced, with a maximum applicable line length of 200m [90]. The algorithm [91] utilizes line impedance parameters in conjunction with a neural network to estimate the distance of a series arc fault in short AC low-voltage indoor power lines. However, these approaches have certain limitations: all of them require multiple sensors to measure both current and voltage at both ends of the arc faults [90-92], which restricts their direct applicability to practical products.

Although many methods have reported accuracies above 95% in controlled experiments [93-96], the practical performance of commercial products remains considerably lower [97]. A key reason is the inconsistent emphasis on frequency bands of the features between algorithmic designs and product implementations. AFDDs commonly employ high-pass filters to capture high-frequency features and reduce misjudgment. In real-life scenarios, lines can extend up to 30-100 meters or even longer. The filtering effect of lines amplifies interference and enhances the high-frequency masking phenomenon, posing a significant challenge. Moreover, the deployment of algorithms at the edge imposes specific requirements on both the data sampling rate and the model complexity. Although certain large-scale deep neural networks exhibit strong performance in classification tasks, their deployment on resource-constrained edge devices presents considerable challenges, as they require extensive pre-extraction of basic features [98].

To address the problem, this chapter analyzes the influence of cable masking on high-frequency characteristics within the 100 kHz range and proposes a Multi-band Feature Fusion and Catboost (MFFC) model, incorporating a transient-event load classification and recursive feature elimination (RFE) feature selection, to detect arcing events within 100-meter cables.

Section 5.2 presents the masking effect analysis with line impedance. In Section 5.3, the proposed MFFC is introduced to extract relevant features and identify arc faults. In Section 5.4, the performance of the proposed method is evaluated on the test set of various line lengths. Section 5.5 provides a conclusion.

5.2 Masking Effect Analysis with Line Impedance

Due to the presence of capacitance and inductance in a long line, the line exhibits low-pass filtering characteristics. As a result, the current signal undergoes considerable attenuation in the high-frequency range, while low-frequency components are transmitted with minimal loss. To investigate the variations of different frequency bands of the current signal as the line length changes, we apply the Short-Time Fourier Transform (STFT) to perform a series of time-frequency analysis to capture the dynamic evolution of the frequency of the current signal over time.

Figures 5.1 to 5.3 present the signal spectrum distributions of three representative load categories (a 2.5A resistive load, a vacuum cleaner, and ESMPs). Each graph consists of three distinct segments: load start-up, normal current, and arc-fault current. The upper portion of the graph displays the time-domain waveform of the current, while the lower section presents the time-frequency distribution derived from STFT, with each pixel indicating the energy magnitude at the corresponding frequency and time.

When an arc fault occurs, the high-frequency components of the current signal exhibit a significant increase compared with the normal state. Generally, as the line length increases, the attenuation of the high-frequency components becomes apparent. As the line length of a 2.5A resistive load rises to 100 meters, the high-frequency components decrease from approximately 80 kHz to 30 kHz in Figure 5.1.

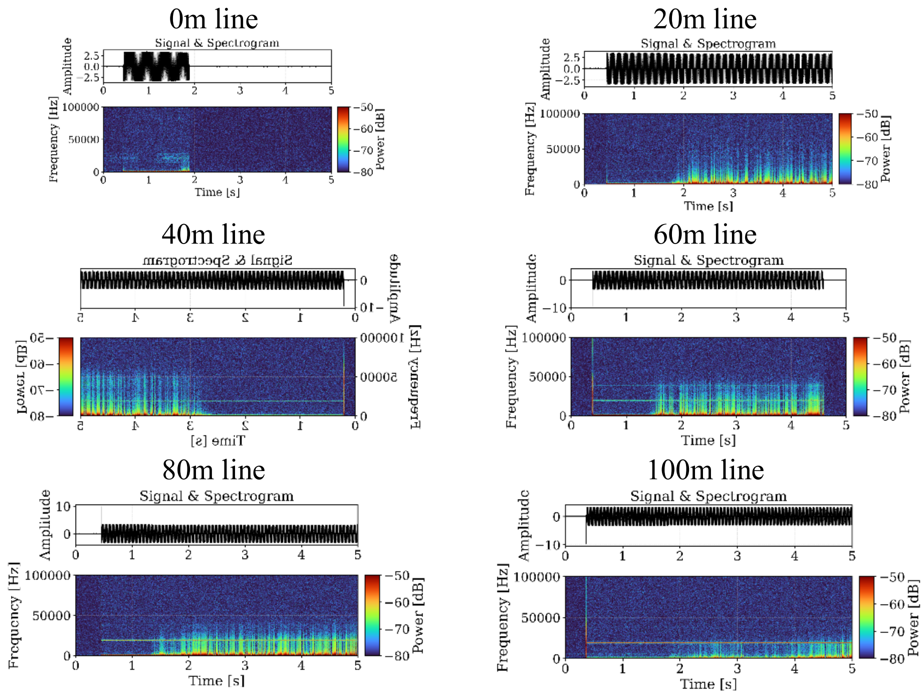

Figure 5.1 The signal spectrum distribution of a 2.5A resistive load at different line lengths

In Figure 5.2, the high-frequency components of the vacuum cleaner remain unaffected by line lengths to 100 meters, which aligns with the results presented in Table III, where these products can still identify arc fault signals. In Figure 5.3, the high-frequency components of the ESMPs decrease from 100 kHz to approximately 50 kHz with increasing line length. By analyzing the attenuation characteristics of high-frequency components across different load types concerning line length, corresponding characteristic intervals can be determined, thereby enabling the efficient identification of arc-fault events.

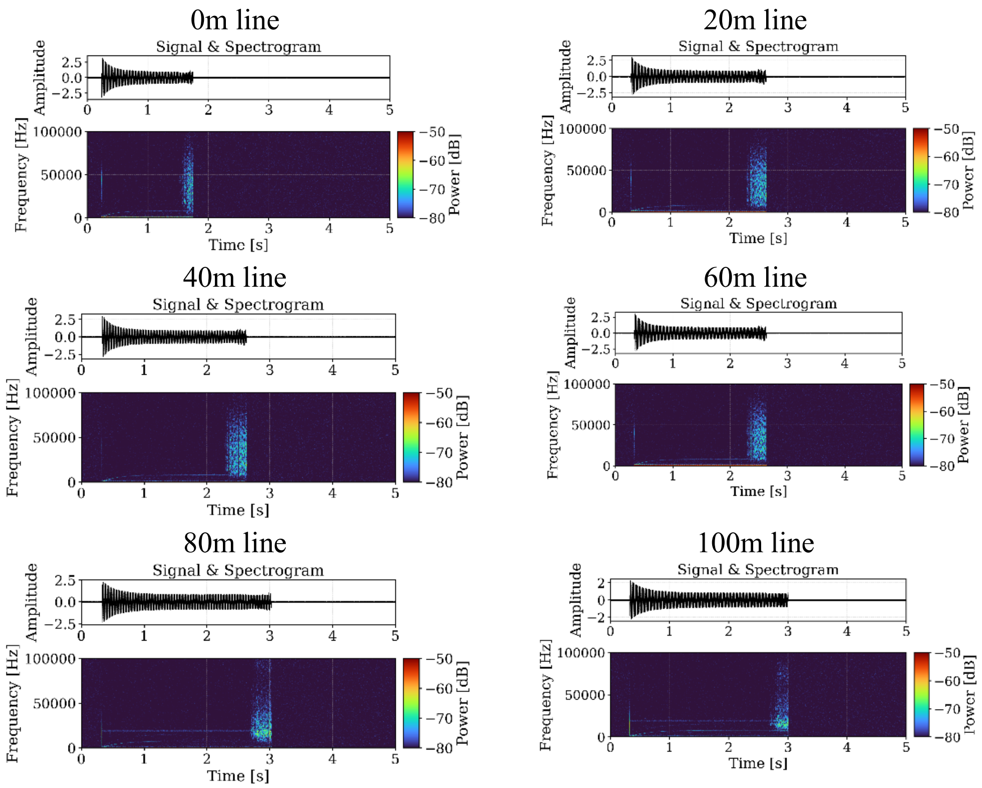

Figure 5.2 The signal spectrum distribution of the vacuum cleaner at different line lengths

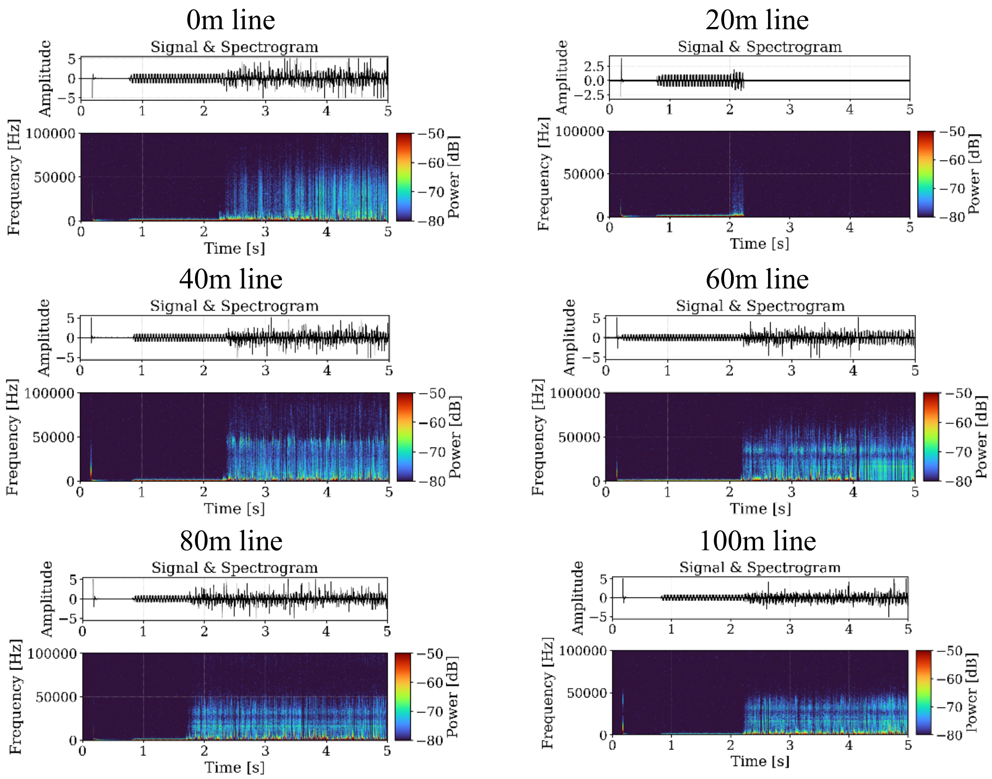

Figure 5.3 The signal spectrum distribution of ESMPs at different line lengths

Overall, the test results reveal that a longer line length leads to a higher probability of missing detections by AFDDs. Through signal analysis using STFT, the energy of high-frequency components diminishes progressively as the line length increases. Moreover, when arc faults occur under different load types, the high-frequency components of the current exhibit different distributions. These frequency components serve as key characteristic indicators for arc fault detection.

5.3 The Proposed Multi-band Feature Fusion Catboost

Based on the comprehensive analysis presented in Section 5.2, we propose a robust detection framework that systematically integrates load classification, feature extraction and selection, and a classification model to achieve accurate arc fault detection across varying operational conditions and line lengths.

5.3.1 Load Classification based on Transient Behavior

As analyzed in Section 5.2, the impact of line length on current signal distortion varies with the load category. Therefore, incorporating load identification into the detection framework enables more adaptive feature analysis, thereby enhancing robustness under a variety of line conditions. After analyzing the current waveform characteristics during the start-up transient phase, two metrics, initiation peak and initiation time, are defined to describe the initiation behavior of the current signal and are used to identify electrical load categories in the load classification module.

According to the classification method [39, 60, 99], the loads can be classified into three representative categories. Figure 5.4 (a) shows the original current among the three electrical load categories:

a. Resistive loads (Re): typical linear elements such as electric kettles, tungsten lamps, and resistive loads, which exhibit a smooth and stable current (and power) rise with no overshoot or high-frequency content.
b. Inductive loads (In): loads such as motors and transformers. The vacuum cleaner and air compressor fall into this category. They typically display a prominent inrush current with a large peak followed by a slow decay due to magnetic field build-up and saturation effects.

c. Switched-mode power supply loads (Sw): nonlinear loads, such as switching power supplies. The type of loads often presents high-frequency noise, sharp current spikes, and significant non-stationary components at start-up.

After defining the categories and their features, we use a start-up detection algorithm based on moving average difference, which enables precise identification of the actual load energization moment. The idea of moving average difference is as follows.

At each time index t, two adjacent sliding windows are defined: preceding window$W_{pre} = [t - w_1 : t]$ and posterior window $W_{post} = [t : t + w_2]$. Given the current value at time i is $I[i]$, the instantaneous power can be calculated as $P[i] = I[i]^2$, and the average power of both windows is given by:

$$\mu_{pre} = avg\left(P[W_{pre}]\right) = \frac{1}{w_1} \sum_{i=t-w_1}^{t} I[i]^2 \tag{5-1}$$

$$\mu_{post} = avg\left(P\left[W_{post}\right]\right) = \frac{1}{w_2} \sum_{i=t}^{t+w_2} I[i]^2 \tag{5-2}$$

$$\delta_{tran} = |\, \mu_{post} - \mu_{pre} | \tag{5-3}$$

A transient event is detected if the transient difference δ_{tran} exceeds a predefined threshold. Once the start-up point is identified, the first-order derivative of the current is calculated to characterize the rate of change:

$$\frac{dI[n]}{dt} \approx (I[n+1] - I[n]) \cdot f_s \tag{5-4}$$

where f_s is the sampling rate of the current.

As illustrated in Figure 5.4 (b) and Figure 5.4 (c) , different types of loads exhibit distinct initiation characteristics. Resistive loads tend to have relatively low peaks in the first-order derivative of current, while inductive and switched-mode power supply loads show significantly higher values. To further distinguish between the two types, the duration for which $dI[n]/dt$ remains above a threshold can be used, as inductive loads tend to have a long duration, while switched-mode power supply loads have a short spike. Then two metrics are defined to describe the initiation behavior of the current signal.

a. Initiation peak: maximum value of $dI[n]/dt$ in 0.5 second after the start-up point.
b. Initiation time: range of $dI[n]/dt$ greater than threshold in 0.5 second after the start-up point.

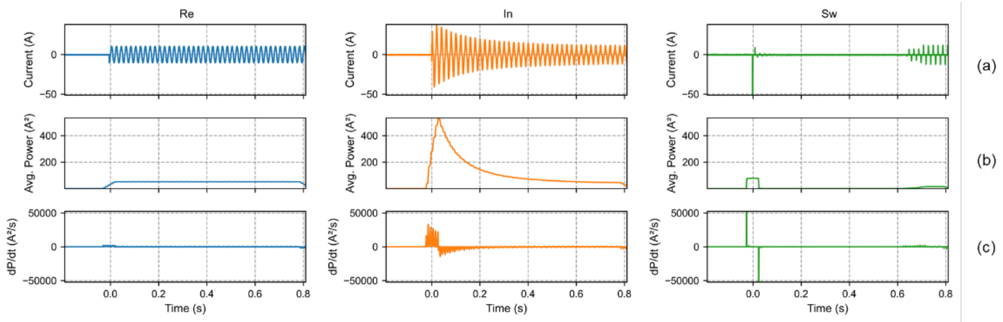

Figure 5.4 Comparison of (a) original current (b) average power of current (c) first-order derivative of average power among three electrical load categories: resistive loads (Re), switched-mode power supply loads (Sw), and inductive loads (In).

Based on these metrics, a three-class classification strategy is proposed. First, the peak derivative is used to separate resistive loads. Then, the initiation time is used to distinguish between inductive and switched-mode loads. The classification thresholds are summarized in Table 5.1.

Table 5.1 Load classification thresholds

Category	Initiation peak (A^2/s)	Initiation time (s)
Resistive loads	0~5000	-
Switched-mode power supply loads	>5000	0~0.15
Inductive loads	>5000	> 0.15

5.3.2 Multi-band Feature Extraction

To accurately capture arc fault signatures under various lines and load categories, a multi-band feature extraction strategy is designed, incorporating both specific features for each load category and global signal features. A total of 19 representative features are extracted from each current signal segment, as summarized in Table 5.2 and Table 5.3. To account for the high-frequency attenuation and interference caused by long lines, the raw current signal is decomposed into three frequency bands: 0–20 kHz, 20–40 kHz, and 40–80 kHz. Although the main frequency components of the current signal are concentrated around 30 kHz, 50 kHz, and 80 kHz, as shown in Section 5.2, the signals are divided into broader bands (0–20 kHz, 20–40 kHz, 40–80 kHz) to balance resolution and generalization. This approach captures energy variations near key frequencies while mitigating the effects of load differences and noise, ensuring robustness for subsequent feature extraction and classification.

0–20 kHz: This band is minimally affected by line attenuation and primarily contains load harmonics and steady-state current behavior. However, variations caused by normal load operation may introduce significant interference.

20–40 kHz: This band captures the initial emergence of arc-related spectral energy and exhibits moderate sensitivity to line length. It provides a balance between arc-fault signal content and transmission robustness.

40–80 kHz: This high-frequency band typically contains strong arc fault signatures, but is significantly attenuated by line masking and transmission effects, especially at long lengths.

Each band is isolated using either a Butterworth low-pass or band-pass filter. The filtered signals are subsequently mean-centered to remove DC bias, ensuring stability and comparability in feature extraction.

For each frequency band, the following five features are extracted to describe signal amplitude, impulsiveness, spectral distribution, and structural characteristics in Table 5.2. These band-level features in 3 bands generate 15 features in total and enhance robustness to line distortion.

In the following tables and analyses, x denotes the time-domain signal, X denotes its corresponding frequency-domain representation and p denotes power spectrum density. The symbol μ is the sample mean, and σ is the sample standard deviation.

Table 5.2 Band signal feature indicators

Indicator	Expression
Energy ratio	$ER = band\_energy/total\_energy$
RMS	$RMS = \sqrt{\frac{1}{n}\sum_{i=1}^{n} x_i^2}$
Zero crossing rate	$ZCR = \frac{1}{n-1}\sum_{i=1}^{n-1} 1(x_i \cdot x_{i+1} < 0)$
Entropy	$Entropy = -\sum_{i=1}^{n} p(i) \cdot log(p(i))$
Kurtosis	$Kurtosis = \frac{\frac{1}{n}\sum_{i=1}^{n}(x_i-\mu)^4}{\sigma^4}$

To capture the overall signal morphology regardless of frequency decomposition, four global features are directly calculated from the full-band current signal in Table 5.3. These four global features complement the band-signal set with 15 features, resulting in a comprehensive 19-dimensional feature vector that balances frequency resolution and generalizability.

Table 5.3 Global feature indicators

Indicator	Expression
Crest factor	$CF = \frac{max(x)}{\sqrt{\frac{1}{n}\sum_{i=1}^{n} x_i^2}}$
Spectrum Centroid	$Centroid = \frac{\sum_{i=1}^{n} f_i * \lvert X(i)\rvert}{\sum_{i=1}^{n}\lvert X(i)\rvert}$
Spectrum Bandwidth	$BW = \sqrt{\frac{\sum_{i=1}^{n}\lvert X(i)\rvert * (X(i) - Centroid)^2}{\sum_{i=1}^{n}\lvert X(i)\rvert}}$
Flatness	$Flatness = \frac{(\prod_{i=1}^{n}\lvert X(i)\rvert)^{\frac{1}{n}}}{\frac{1}{n}\sum_{i=1}^{n}\lvert X(i)\rvert}$

5.3.3 Feature Selection based on Recursive Feature Elimination (RFE)

To reduce feature redundancy and enhance the model's generalization capability, RFE is employed for the feature selection of arc fault signals. This approach systematically reduces computational complexity and accelerates training by iteratively removing less relevant features. RFE refines the feature set by evaluating feature importance, thereby enhancing model generalizability and mitigating overfitting.

To reduce feature redundancy and enhance the model's generalization capability, RFE [100] is employed for the feature selection of arc fault signals. This approach systematically reduces computational complexity and accelerates training by iteratively removing less relevant features. RFE refines the feature set by evaluating feature importance, thereby enhancing model generalizability and mitigating overfitting.

Initially, a base model is trained to assess the importance of all features. The least important feature is then eliminated, and the model is retrained on the remaining features. This iterative process continues until only the K's most critical features are retained. As Table 5.4 shows:

Table 5.4 Pseudocode for RFE algorithm

Algorithm: Recursive Feature Elimination (RFE)
Input: dataset D = [(x_1, y_1), ..., (x_n, y_n)], model M, feature set F = [$f_1, f_2, \ldots, f_d$], desired number of features k.
Output: Selected feature subset $F_{current}$
Initialize $F_{current} \leftarrow F$
While $\lvert F_{current} \rvert > k$ **do**:
Train model M on D using features in $F_{current}$
Evaluate feature importance scores
Identify f_{min} with the least importance
Remove f_{min} from $F_{current}$
Return $F_k \leftarrow F_{current}$

5.3.4 Model Construction based on Catboost

To achieve accurate arc fault detection in the masking tests with line impedance, the Catboost [101] is employed as the core classifier, which is a gradient boosting decision tree (GBDT) model that provides excellent performance with tabular data, strong handling of categorical variables, and robustness against overfitting. However, traditional GBDT models are prone to prediction shift, a bias that can adversely affect the convergence rate and generalization performance of the model [101]. To address these limitations, CatBoost introduces two key innovations: Ordered Boosting and Ordered Target Encoding.

Ordered Boosting first generates one or more random permutations σ of the training indices. In iteration m, for the i-th sample in the permutation σ, CatBoost calculates the gradient using a partial model that is only trained on the first i-1 samples in that permutation. The gradient for sample σ(i) can be written as:

$$g_{\sigma(i),m} = -\frac{\partial L\left(y_{\sigma(i)}, F(x_{\sigma(i)})\right)}{\partial F(x_{\sigma(i)})}\Bigg|_{F=F_{m-1}^{(\sigma,i-1)}} \tag{5-5}$$

where $y_{\sigma(i)}$ is the label of the σ (i)-th sample, $L(\cdot)$ represents the loss function and $F_{m-1}^{(\sigma,i-1)}$ donates the model obtained after the previous iteration (m−1) and after processing the first i−1 samples in permutation σ. These sequentially calculated gradients (one per sample, respecting ordering) are used to fit the weak learner. Then the model is updated:

$$F_m^{(\sigma)}(x) = F^{(\sigma)}{}_{m-1}(x) + \nu \cdot h^{(\sigma)}{}_m(x) \tag{5-6}$$

Although internally, CatBoost maintains partial updates as it progresses through the permutation.

Ordered Target Encoding uses only the portion of data preceding the current sample to compute means or other statistics. Specifically, σ represents random permutations of the sample indices. The target encoding is calculated as:

$$\hat{\mu}_{\sigma(i)} = \frac{\sum_{j=1}^{i-1} \mathbf{1}[x_{\sigma(j)}=x_{\sigma(i)}] \cdot y_{\sigma(j)}}{\sum_{j=1}^{i-1} \mathbf{1}[x_{\sigma(j)}=x_{\sigma(i)}]+\alpha} \tag{5-7}$$

where $x_{\sigma(j)}$ is the categorical feature value of the sample at position j in the permutation σ, $y_{\sigma(j)}$ is the target value of the preceding samples in the permutation and α is a smoothing parameter. This dramatically reduces the likelihood of data leakage. Although the application may primarily involve numerical features, this mechanism remains advantageous for any discrete or inherently categorical features.

5.4 Verification of the Proposed Method

5.4.1 Framework of MFFC

A structured processing framework is proposed, as illustrated in Figure 5.5. The entire pipeline encompasses three principal stages, namely data acquisition, load classification and feature extraction, and arc fault detection.

In the first stage, raw current signals are acquired from the experimental platform. To ensure temporal resolution and local analysis, the current waveform is segmented using a sliding window method. Each window, covering five complete cycles of the 50Hz signal, serves as the basic analysis unit for downstream processing. The second stage focuses on load classification and feature extraction. The first-order derivative of the signal is calculated to identify potential transient points. If a transient is detected, its peak magnitude and initiation timing are compared against predefined thresholds to distinguish among three typical load categories in Table 5.1. The current signals are further processed using frequency-domain decomposition and normalization. In the final stage, the extracted features, combined with the inferred load type, are fed into a pre-trained CatBoost classification model to perform arc fault detection and output the classification result.

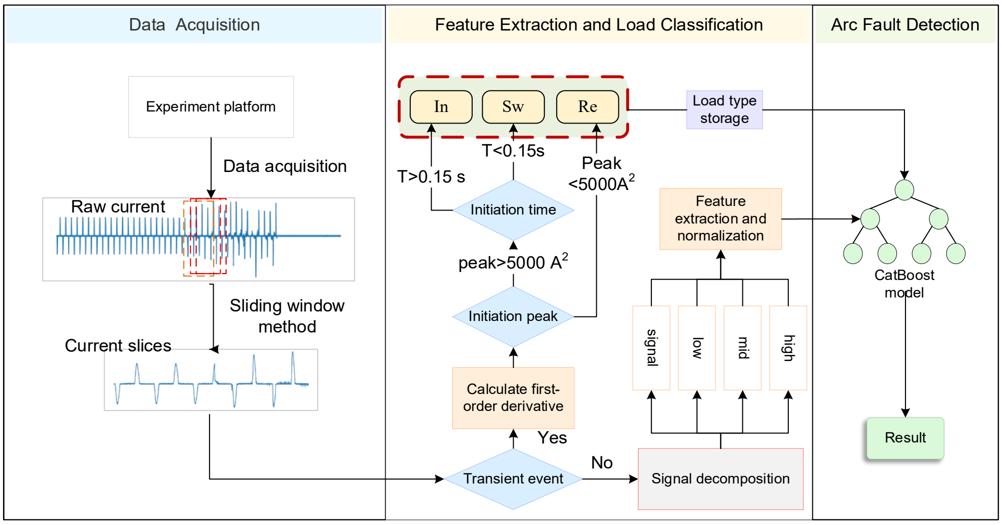

Figure 5.5 Process of MFFC.

5.4.2 Dataset Establishment

Data are collected on the experimental platform mentioned in Section 3.21, followed by preliminary screening and processing to construct a dataset for subsequent processing. The dataset encompasses a variety of loads, including 2.5A and 9A resistive loads, a kettle, tungsten bulbs, a vacuum cleaner, a capacitor-start motor, and switch power supplies. The sampling rate of the current signal is 200 kHz. Then, a sliding window method is applied to segment the data. Each window contains 5 cycles of 50Hz current signals. Detailed data for each load is provided in Table 5.5.

Table 5.5 Samples for loads

Samples	0m	20m	40m	60m	80m	100m
Kettle	2769	907	379	591	718	746
Vacuum Cleaner	2346	487	453	483	361	417
Switch power supply	2473	605	353	476	717	766
Air compressor	2525	1342	634	818	902	803
Incandescent lamp	2496	971	708	815	676	598
2.5A Resistor	1883	1156	1151	1232	1180	1129
9A Resistor	3251	1356	671	1235	1445	814
Total	17743	6824	4349	5650	5999	5273

5.4.3 Multi-band Feature Fusion

Feature engineering mainly consists of feature extraction, normalization, and selection. 19 features (mentioned in Section 5.3.2) and the load category are extracted from each current segment. Subsequently, Z-score standardization is applied to eliminate unit discrepancies and improve model stability. After that, RFE is conducted based on a simple Decision Tree model to select features from the 20 features. An optimal feature subset containing 10 features is selected for model training in Table 5.6. Specifically, these features include 4 low-frequency (below 20 kHz) features, 2 middle-frequency (20~40 kHz) features, 1 high-frequency (40~80 kHz) feature, and 3 global features.

In the low-frequency band, features primarily characterize waveform impulsiveness, zero-crossing behavior, and energy distribution. In contrast, features in the middle-frequency and high-frequency bands capture subtle variations in transient energy.

Table 5.6 Selected multi-band features

Type	Features
Low frequency （0~20 kHz）	Kurtosis, ZCR, Spectral Entropy, Energy Ratio
Middle frequency （20~40 kHz）	RMS, Kurtosis
High frequency （40~80 kHz）	RMS
Global	Spectral Bandwidth, Crest Factor, Load Category

5.4.4 Classification Model Performance

For model training, we split the 0m dataset into 80% for training and 20% for testing, using other datasets as additional test sets to demonstrate the generality of the algorithm. For the CatBoost model, the hyperparameters are constrained: iterations = 200, learning rate = 0.1, and depth = 8.

To evaluate the effectiveness of the proposed method in detecting arc faults under varying line lengths, a CatBoost classifier [101] is trained using only the dataset corresponding to the 0 m line. Subsequently, the model is tested on datasets associated with six distinct line lengths, namely 0 m, 20 m, 40 m, 60 m, 80 m, and

100 m. The generalization capability of this model can be evaluated across different lengths of lines.

Four evaluation metrics are employed to comprehensively assess model performance, including Accuracy, Precision, Recall, and F1 Score in Table 5.7. The model achieves an accuracy of 99.73% on the seen data (0 m line), indicating near-perfect classification performance on seen samples. When tested on unseen line lengths, the model still maintains high Accuracy (>95%) and F1 score (> 94%) across all cases, demonstrating strong generalization ability. Notably, while precision remains consistently high across different line lengths, recall shows a gradual decline as line length increases, which indicates that some arc faults are missed at longer lengths. This might be due to the attenuation of high-frequency components and weakened signal features after long-distance propagation.

Overall, the model exhibits robust performance in detecting arc faults even when trained on a single-length dataset. The results confirm the discriminative power of the selected multi-band features and the capacity of the model to capture load-dependent transient characteristics under varying lengths of lines.

Table 5.7 Metrics comparision for each length data

Length (m)	Accuracy	Precision	Recall	F1 Score
0	99.73%	99.36%	99.45%	99.41%
20	98.09%	97.90%	93.67%	95.74%
40	97.27%	99.26%	93.06%	96.06%
60	95.87%	99.62%	90.81%	95.01%
80	95.51%	97.67%	90.77%	94.10%
100	95.76%	99.45%	91.38%	95.25%
Average	97.04%	98.88%	93.19%	95.93%

5.4.5 Ablation Study and Model Comparison

To further investigate the contribution of the load classification module and the impact of different classifiers on the proposed framework, we conduct ablation studies and model comparison.

Two configurations are compared: one with the load classification module integrated into the framework and another with the module removed. In Figure 5.6, the results present the arc fault detection accuracy across various line lengths for both the original method and the ablation variants. The incorporation of load classification consistently enhances detection performance for long line lengths (e.g., 80m and 100m), with an accuracy improvement of up to 2%. This result confirms that the inclusion of the load classification module provides prior knowledge to the model, enabling it to adaptively distinguish load-specific signal patterns from arc faults, especially when the signal is degraded due to line attenuation.

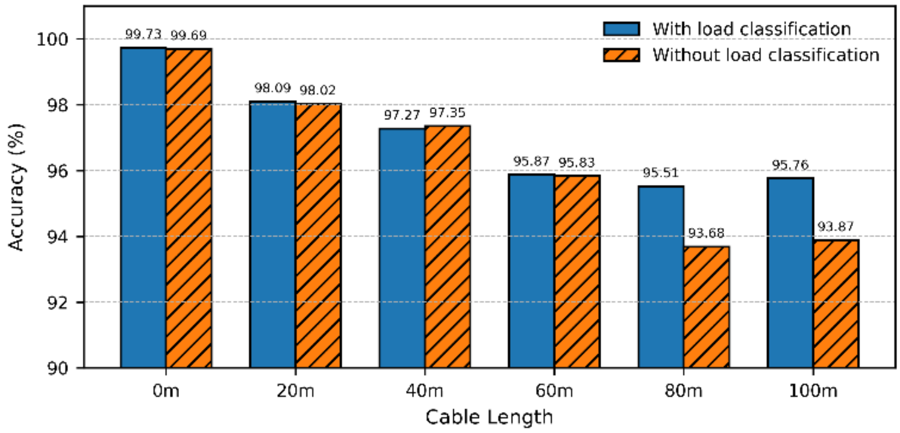

Figure 5.6 Accuracy comparison with and without the load classification module across different cable lengths.

The choice of the best classifiers is evaluated in the proposed task. By average results across all datasets, CatBoost is compared with Multi-Layer Perceptron (MLP), Decision Tree (DT), Random Forest (RF), and two other popular boosting models, XGBoost and LightGBM. The evaluation results are summarized in Table 5.8. CatBoost achieves the best performance across three out of four average metrics, including accuracy (97.04%), precision (98.88%), and F1-score (95.93%). In contrast, MLP performs relatively poorly due to its sensitivity to hyperparameter tuning and data scale. Meantime, tree-based ensemble methods—particularly XGBoost and LightGBM—also demonstrate strong overall performance, with F1-scores exceeding 95%. These results confirm the effectiveness of gradient boosting models in arc fault detection and highlight that CatBoost is the most robust classifier under the current feature set and data configuration.

Table 5.8 Average metrics comparison

Model	Accuracy	Precision	Recall	F1 Score
CatBoost	**97.04%**	**98.88%**	93.19%	**95.93%**
MLP	88.57%	91.78%	73.35%	81.47%
DT	93.06%	91.99%	88.51%	90.11%
RF	96.22%	98.71%	91.00%	94.67%
XGBoost	96.81%	98.00%	93.45%	95.65%
LightGBM	96.71%	96.94%	**94.34%**	95.61%

5.5 Conclusion

Arc-fault signal characteristics in low-voltage residential environments are often masked by long-distance lines. Although many algorithms achieve high accuracy, commercial products still have difficulty preventing fires caused by arc faults. Although IEC62606 mandates regulations for a 2.5A resistive load with 30-meter lines, the behavioral pattern of arc signals under longer lines and more complex load configurations has not been adequately addressed by existing algorithms and arc fault detection products.

Our work assesses the performance of AFDDs under diverse loads and line lengths. The attenuation characteristics of lines are analyzed to investigate the impact on the arc-fault signal. Then, during model training, filtering techniques are applied to enhance robustness. The RFE is utilized to select the top 10 most significant features from 20 multi-band features as inputs for the learner. Finally, CatBoost can accurately identify arc-fault events for seven loads within the 0-100 meter line length range, with an accuracy rate consistently exceeding 97%.

6 An Explainable Assessment Scheme for Arc Fault Diagnosis

6.1 Introduction

As reviewed in Chapter 2, arc fault detection methods have been extensively developed to provide early warning and prevent fires in recent years. Except for the physical-signal approaches in Section 2.2, most techniques fall into two categories: (i) time- and frequency-domain analysis techniques and (ii) deep-learning techniques (Section 2.3).

Traditional ML classifiers [19] analyze electrical signals in time and frequency domains using the Fourier transform [102] or wavelet transforms [48, 103] to manually select features, for arc fault detection [38, 42, 43]. These features, chosen based on researchers' experience without standardized criteria, are fed into ML classifiers [19, 88, 99]. Detection performance depends mainly on the rationality and accuracy of feature selection rather than the ML algorithm [19].

End-to-end approaches [39, 64] bypass complex feature extraction by directly feeding raw or preprocessed electrical signals into deep neural networks, which adaptively extract features. High detection and classification accuracy indicate these models uncover latent arc fault patterns through automatically learned features. This result-driven approach guides the construction of features, design of models, and selection of hyperparameters in deep learning [64].

However, a key challenge is whether these methods locate the real arc fault feature, for example, the 'flat shoulder'. A unified evaluation metric is needed to represent whether the arc fault is correctly located quantitatively. To address this issue, explainable artificial intelligence (XAI) [104, 105] can be used to create a unified assessment framework for AI-based arc fault diagnosis. XAI enhances model interpretability and transparency using game theory, gradient-based methods, or attribution techniques, and is widely applied in fields like building energy management [106], load disaggregation [107], and power quality disturbances classification [108]. Aligning with causal inference and engineering needs, XAI helps experts and researchers understand and assess model operations [104, 105].

In this Chapter, the primary objective is to fully utilize the ability of XAI to establish a posterior assessment scheme for AI-based arc fault diagnosis to improve practitioners' confidence in models. A unified explainable assessment scheme (XAS) is proposed for both artificially defined arc features-based and automatic arc feature extraction-based methods. It defines the correct explanation of arc faults and leverages SHapley Additive exPlanations (SHAP) [109, 110] and occlusion sensitivity [111] to quantitatively explain whether the arc fault is correctly located. By examining the consistency of these explanations under different sampling rates and noise levels, the proposed XAS can be used to evaluate the robustness and reliability of arc fault diagnosis models. By checking whether the models remain consistent under different sample times and noise levels, the proposed XAS can be used to assess the robustness and reliability of arc fault diagnosis models. It helps distinguish models that only perform well on clean, high-quality data from those that remain trustworthy under more realistic conditions.

Section 6.2 proposes a definition for the correct explanation of machine learning-based arc fault diagnosis, building a bridge between physical feature locating and machine learning methods. A novel unified explainable assessment scheme is designed to evaluate the AI-based arc fault diagnosis methods, using XAI techniques (SHAP and occlusion sensitivity). In Section 6.3, an arc fault experiment is conducted by using a standard arc fault test platform to demonstrate the effectiveness of the assessment scheme. The XAS is tested across several traditional machine learning methods and deep learning methods using an arc fault dataset with different sample times and noise levels. Section 6.4 proposes a lightweight balance neural network to guarantee the competitive classification accuracy and feature extraction scores by analyzing arc faults. Section 6.5 concludes with a summary of findings.

6.2 Explainable Assessment Scheme

The key reason machine learning models can identify arc signals is that they capture high-frequency characteristics from the feature pool. Therefore, the ground truth features should be able to directly reflect the changes in arc current at high frequencies, instead of blindly stacking useless features. Therefore, in this section, an explainable assessment scheme (XAS) is introduced for both feature pool-based and deep learning-based methods, including the ground truth features definition, the feature extraction score, and the explainable assessment scheme.

6.2.1 Definition of Ground Truth Features

1) Ground truth features in feature pool: The features currently used can be defined into three categories: original signal variants, primary, and secondary features. Original signal variants are based on signal decomposition, for example FFT, to find out the key sub-signals or corresponding properties. It can be considered as the extension of the original data instead of the statistical description. Therefore, although the data contain the most information, they are not discussed in this paper. The primary features are the fundamental arc fault features, which are generally basic characteristics of the data, such as the mean and variance. Considering that the high-frequency arc occurs under different loads and the current is periodic, the efficient features are normally based on the absolute and square value or the bias of the input signal, such as variance, entropy, range, RMS, and integral [39], [65]. The secondary features are usually the extensions of primary features and are artificially designed, such as Skewness, Kurtosis, L1 normalization, and L2 normalization. However, they lack a general specification. Therefore, for arc fault diagnosis, five basic features (Variance, Entropy, Range, RMS, and Integral) are selected as the ground truth features set S.

2) Ground truth features in deep learning: The ground truth features in deep learning methods are defined as the regions r $= [r_1, r_2, \dots, r_N]$ where the arc fault happens. Assuming that the normal input signal at a certain type of load is x and the corresponding arc fault signal is $\hat{x}$, they can be cut into N independent regions respectively. The ground truth features at the region r_n can be defined as:

$$r_n = \begin{cases} 1 & \text{if } x_n \neq \hat{x}_n \\ 0 & \text{if } x_n = c \end{cases} \tag{6-1}$$

where $n = 1,2,3, \dots, N$. x_n and $\hat{x}_n$ are the n-th independent region being cut in x and $\hat{x}$.

6.2.2 Feature Extraction Score

The principle of explainable machine learning methods applied in this chapter can be summarized as "local feature attribution". In this approach, individual predictions are explained by an attribution vector, $\psi \in \mathbb{R}^d$. Mathematically, for any ML model f, input $x \in \mathbb{R}^d$, and output $y \in \mathbb{R}^c$, there is a map $g \in \mathbb{R}^d$ that describes the input feature importance to target class output y_c.The feature importance $g = G(x, f, y_c)$ is calculated by a coalitional game, or heat-mapping function, based on the model being explained [110]. Two XAI techniques are presented in this section: SHAP and occlusion sensitivity.

6.2.2.1 SHapley Additive ExPlanations

The feature attributions based on SHAP depend on defining a coalitional game, or set function. The core idea of SHAP is assigning credits (contributions) to players (features) in coalition games ($G(x, f, y_c)$) in the form of shapley values based on game theory [110].

For a ML model f and input $x \in \mathbb{R}^d$, supposing that the coalition game G is determined by the sets of features $s \subseteq d$ that are chosen to be applied in the model f. For the i-th feature x_i, shapley values assign credit to the individual x_i by calculating a weighted average of the G increase when x_i is in s versus when x_i does not in s (a quantity known as x_i's 'marginal contribution'). The definition of the x_i's shapley value ϕ_i's is

$$\phi_i(G) = \sum_{s \subseteq d \setminus \{x_i\}} \frac{|s|!(|d|-|s|-1)!}{|d|!} (G(s \cup \{x_i\}) - G(s)) \tag{6-2}$$

It follows that when the features contribute more, they should have higher credit in the game. If the features have the same contribution, they have equal credit, and when the feature has no help, the credit is zero.

There are several ways to remove x_i from $d(s \subseteq d \setminus \{x_i\})$, including baseline sample replacement, randomly sampled replacement, and marginal distribution replacement [112]. The choice of the removal approaches is determined by the complex of problems.

6.2.2.2 Occlusion Sensitivity

As the basic perturbation method, occlusion sensitivity analysis [111] is normally used to generate local post-hoc explanations, specifically in the context of neural networks. By measuring the slight variation of the class score to occlusion in different regions of an input signal using small perturbations of the signal, occlusion sensitivity analysis can summarize a heat-map of the input signal based on the resultant variation of each region.

Assume that there is a mask M replacing signal regions with a given baseline (blur, constant, or noise) and an ML model f outputting a probability score $p \in [0,1]$. The new signal with masks can be described as $x \odot M$, where $\odot$ is the Hadamard product and the input signal x is one-dimensional data. Then, the degree of responsibility of the masked region is [113]

$$Res = 1 - \frac{p(x \odot M)}{p(x)} \tag{6-3}$$

Assume that the masked region is defined as R_{mask}. When all the signal is masked, keeping nothing but R_{mask} and the output prediction score p is unchanged, the masked region can be considered as the core part of the signal, and vice versa. Simply put,

$$\begin{aligned} p(x - R_{mask}) = 0 \Leftrightarrow p(R_{mask}) = p(x) \\ p(x - R'_{mask}) = 0 \Leftrightarrow p(R'_{mask}) = 0 \end{aligned} \tag{6-4}$$

where R'_{mask} is an irrelevant area. Masking it should not affect the output score.

6.2.2.3 Definition of Feature Extraction Score

For feature pool-based methods, considering the efficient features vector v as the ground truth and the feature extraction score of the model f_i can be defined as:

$$g(f_i) = \frac{S \cap S_{SHAP,i}}{S \cup S_{SHAP,i}} \tag{6-5}$$

where $S_{SHAP,i}$ is the SHAP based top-5 features in the model f_i when we use Eq (1). $S \cap S_{SHAP,i}$ is the number of overlap features and $S \cup S_{SHAP,i}$ is the number of union features. For deep learning methods, considering the arc fault ground truth features r in the input signals, and the feature extraction score of the model f_i can be defined as:

$$g(f_i) = \frac{\mathbf{r} \cap \mathbf{r}_{Occlusion,i}}{\mathbf{r} \cup \mathbf{r}_{Occlusion,i}} \tag{6-6}$$

where $\mathbf{r}_{Occlusion,i}$ is the region marked as arc faults in model f_i by occlusion sensitivity experiments. $\mathbf{r} \cap \mathbf{r}_{Occlusion,i}$ is the overlap of the two regions, and $\mathbf{r} \cup \mathbf{r}_{Occlusion,i}$ is the union of the two regions. The above two scores are from $0 \sim 1$ ($g(f_i) \in [0,1]$).

6.2.3 Explainable Assessment Scheme

Based on the definitions of ground truth features and the feature extraction score, an assessment scheme can be used to measure the confidence of multiple AI-based arc fault diagnosis models and serve as the basis for potential ensemble learning models.

The assessment scheme is summarized in Figure 6.1 and described in Algorithm 1. Depending on the model, the raw current signal is used to calculate various features or as a direct input to the model for arc fault diagnosis. The input x, output $\tilde{y}$, and the corresponding model f_i are then used to extract the estimated key features using SHAP or occlusion sensitivity experiments. Compared with ground truth features, the feature extraction score of all models can be calculated for practitioners to determine which models are trustworthy and whether to ensemble the models.

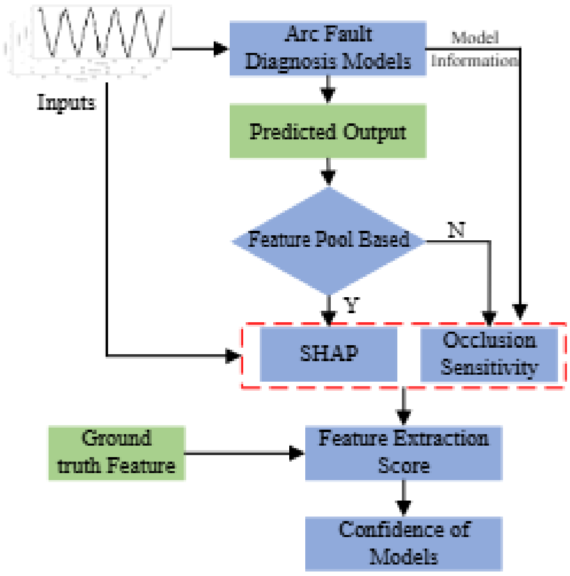

Figure 6.1 The schematic diagram of the assessment scheme.

Algorithm 1: Explainable Assessment Scheme Algorithm

Input:

x: input signal or features in feature pool,
f: AI-based arc fault diagnosis models,
S: Ground truth features in feature pool,
r: Ground truth features input signals,
M: The masks in occlusion sensitivity
L: The number of models

for $i = 1, \ldots, L$ do
  $\tilde{y} \leftarrow f_i(x)$
  if f_i $is\ feature\ pool\ based$ then
    $S_{SHAP,i} = Top_5(SHAP(x, f_i, \tilde{y}))$
    $g(f_i) = \frac{S \cap S_{SHAP,i}}{S \cup S_{SHAP,i}}$
  else
    for $j = 1, \ldots, N$ do
      $r_{Occlusion,i,j} =$
      $OcclusionSensitivity(x \odot M_j, f_i, \tilde{y})$
    end
    $\mathbf{r}_{Occlusion,i} =$
    $[r_{Occlusion,i,1}, r_{Occlusion,i,2}, \cdots, r_{Occlusion,i,N}]$
    $g(f_i) = \frac{\mathbf{r} \cap \mathbf{r}_{Occlusion,i}}{\mathbf{r} \cup \mathbf{r}_{Occlusion,i}}$
  end
end

$$g(f) = [g(f_1), g(f_2), \ldots, g(f_L)]$$

Output: Scores of all models: $g(f)$

6.3 Verification of the Assessment Scheme

6.3.1 Experimental Configuration and Dataset

Before testing the explainable assessment scheme, an arc fault experiment is conducted in the low-voltage electrical safety laboratory for electric appliances with/without arcing and analyzing the corresponding current signals as shown in Section 3.1. To ensure the effectiveness of the proposed scheme, different arc fault currents under various loads are explored, including the heating-kettle, drill, air compressor, dimmer, dehumidifier, and so on. Meanwhile, two datasets is designed to validate the extension of XAS in different arc fault datasets. Dataset 1 is a complex dataset with more arc faults, while dataset 2 is a simple dataset with fewer arc faults.

The experiments are conducted on several types of loads, including resistance, heating kettles, air compressors, vacuum cleaners, switch-mode power, dehumidifiers, microwave ovens, and disinfection cabinets. The arc fault dataset is obtained for a single load or combined loads. In the experiments, each fault has ten experiments, and each experiment contains 1,000,000 samples and two features (current and voltage). The arc fault occurs at a random time to simulate the real situation. The duration of each experiment is five seconds. In dataset pre-processing, the normal and arc fault data are split, cut into several slices with a length of 10,000 (window = 10,000, step = 5,000), and downsample the data. Due to the sampling time of 5 × 10−3ms, which means the high resolution of the data set, low-resolution downsampling on the dataset was performed, such as 1 × 10−2ms, 2.5 × 10−2ms, 5 × 10−2ms, and 1 × 10−1ms for the dataset diversity.

Figure 6.2 takes two examples to show the normal and arc current data (1000 samples) and performs FFT analysis. The figure contains the original signal, the detailed frequency, and the sub-signal at each frequency.

The load of example 1 is a combined load, including the resistance, air compressor, and switch-mode power. For a normal current signal in Figure 6.2a, it has many small but high-frequency fluctuations while maintaining a sinusoidal signal due to the inherent switch-mode power. These fluctuations are hard to observe when an FFT frequency spectrum is performed unless the sub-signal of each frequency is described. For this kind of complex load, the current changes greatly when an arc fault occurs. The current signal has completely changed into a periodic signal of other shapes instead of a sinusoidal signal. There is significant distortion in the peak value of the current, and some other high-frequency signals can be detected in both the frequency spectrum and sub-signals.

The load of example 2 is a combined load as well, including the resistance and the vacuum cleaner. Unlike Example 1, the normal current of Example 2 is more like a smooth sinusoidal signal. There are only some high-frequency noises that can be ignored. The arc fault current approximates a triangle signal with observed transient spikes, which is different from Figure 6.2b.

The two complex current signal examples with combined loads both show differences from arc fault currents with a single load [99]. Whereas the core obstacle in arc fault diagnosis is the same, that is, finding the high-frequency fault signal in the current signal without being affected by noise and sampling rate. In addition, since the laboratory experiments are relatively simple, to simulate more practical and complex engineering problems, additional noise with different levels of signal-to-noise ratio (SNR) is added to the dataset.

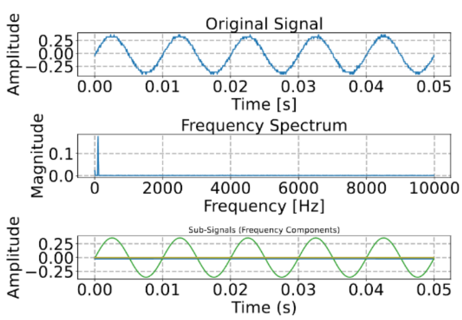

(a) Normal current of example 1

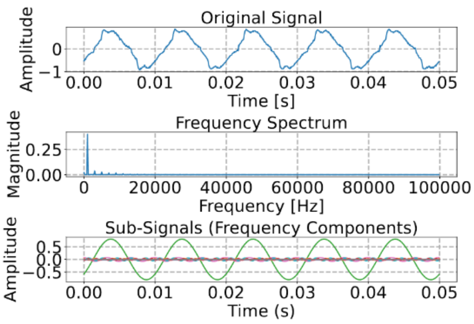

(b) Arc current of example 1

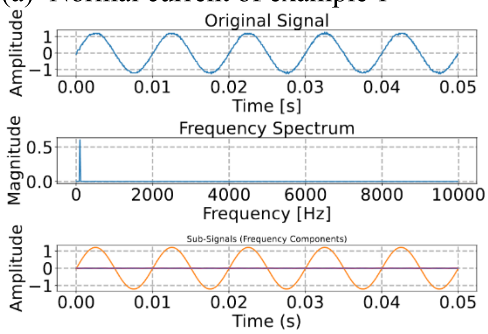

(c) Normal current of example 2

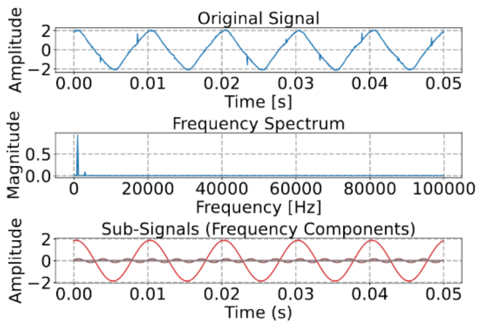

(d) Arc current of example 2

Figure 6.2 Data analysis of experimental dataset.

6.3.2 Model Setup and Accuracy

To further assess the efficacy of the proposed assessment scheme, a wide range of models are evaluated, including several ML models (KNN [99], SVM [88], CART tree [99], L2/L1 norm [114], SEmodel [19], Lightgbm [115], XGBoost [116], NSKSVM [117], TVARF [118]) and several deep learning models (AutoEncoder (AE) [65], lightweight CNN (LCNN) [66], ArcNet [60], and ArcNN [67], IFWA-1DCNN [67]). The ML models contain the most popular clustering, classification, and tree models, as well as ensemble models. The deep learning models are the recently proposed arc fault diagnosis models that have been proven to have good performance. The methods are evaluated on arc-fault datasets with multi-resolution and multi-level noise.

For ML models, the setups of the corresponding research are followed. For deep learning models, training is performed with a batch size of 32 using the Adam optimizer with an initial learning rate of 0.001. The learning rate decays every 30 epochs, and the epoch is set to 100. The dataset is split into training, validation, and test sets with a ratio of 0.8:0.1:0.1. The experiments are implemented in 'Pytorch' using a CPU Intel i7-11800H processor at 2.3Hz and a GPU NVIDIA T600.

Table 6.1 summarizes the test accuracy of arc fault diagnosis when the sample time is 2.5×10^{-2}ms and SNR is 5. It can be seen that all models except SVM have comparative performance. When ML models are applied for fault diagnosis, test accuracy is greatly affected by model selection. The tree models, including L2/L1 norm, LightGBM, XGBoost and TVARF, all have better performance than other ML models. In contrast, all deep learning models have stable performance. The lowest test accuracy is 98.28% (ArcNN), which is higher than the test accuracy of all ML models. However, this result-oriented analysis cannot guarantee that the model is correct and effective. Higher test accuracy cannot guarantee that the models locate the real fault features instead of finding some similar noise.

Table 6.1 The basic test accuracy of arc fault diagnosis using dataset 1

Model	SVM	L2/L1	KNN	SEmodel	CART
Accuracy	43.75%	92.41%	76.11 %	90.17%	90.18%
Model	LightGBM	XGBoost	NSKSVM	TVARF	AE
Accuracy	92.19%	92.19%	83.31%	94.19%	98.65%
Model	LCNN	ArcNet	ArcNN	FWA-1DCNN	-
Accuracy	99.79%	99.47%	98.28%	100.00%	-

6.3.3 Assessment Scheme

The proposed assessment scheme explores the soft feature extraction scores of each model at different data resolutions and noise. By choosing different sample times, the dataset can be downsampled with various resolutions. Meanwhile, noise with different levels of signal-to-noise ratio is added to the dataset for comparison.

1) Results using datasets with multiple sample times: Table 6.2 and Table 6.4 summarize the test accuracy and soft feature extraction scores of each model on different datasets with multiple sample times and SNR=5. For ML model-based arc fault diagnosis, the large sample time limits the precision of soft feature extraction, leading to a decrease in test accuracy of all models. Due to the excellent structure of the tree models, they perform better than other models in test accuracy, especially L2/L1 norm, LightGBM, XGBoost, and TVARF. However, considering the average XAS, the SEmodel performs better than others, instead of models with high accuracy, benefiting from the ensemble mechanism. Meanwhile, although NSKSVM improves the test accuracy of SVM through Newton-optimization, the soft feature extraction score does not improve much, only by 0.09. Generally, high accuracy means high interpretability, for example, the interpretability of XGBoost is always better than KNN. Whereas it is not always correct. When the accuracy is comparable, the soft feature extraction score varies depending on the choice of ML model, for example, when the sample time is 1×10^{-2}, the soft scores of LightGBM and SEmodel are higher than XGBoost, while the test accuracy is lower than it.

Table 6.2 The test accuracy and soft score of arc fault diagnosis using dataset 1 with different sample times

Sample Time	5×10^{-3}ms		1×10^{-2}ms		2.5×10^{-2}ms		5×10^{-2}ms		1×10^{-1}ms		Average	
	Acc	Score	Acc	Score	Acc	Score	Acc	Score	Acc	Score	Acc	Score
SVM	24.44%	0.14	28.89%	0.14	43.75%	0.14	47.75%	0.14	48.32%	0.14	38.36%	0.14
L2/L1 norm	91.12%	0.66	96.01%	1.00	92.42%	1.00	91.89%	0.45	86.67%	0.66	91.62%	0.75
KNN	76.67%	0.14	77.77%	0.33	76.11%	0.40	76.46%	0.17	74.67%	0.14	76.34%	0.24
SEmodel	90.00%	1.00	92.22%	0.80	90.17%	1.00	91.52%	0.67	83.87%	0.67	89.56%	0.83
CART	86.67%	0.33	94.44%	1.00	90.18%	0.67	88.28%	0.43	84.37%	0.43	88.79%	0.57
LightGBM	92.22%	0.80	92.67%	0.67	92.19%	0.60	92.41%	0.67	85.99%	0.40	91.09%	0.63
XGBoost	91.11%	0.67	93.89%	0.43	92.19%	0.43	91.63%	0.67	86.66%	0.57	91.09%	0.55
NSKSVM	78.89%	0.27	81.29%	0.20	85.31%	0.20	84.70%	0.20	80.97%	0.27	87.97%	0.23
TVARF	92.22%	0.53	94.26%	0.60	94.19%	0.73	91.10%	0.60	87.42%	0.67	91.84%	0.63
AE	88.14%	0.56	95.55%	0.44	98.65%	0.48	99.44%	0.48	99.66%	0.26	96.28%	0.44

LCNN	94.44%	0.22	98.88%	0.26	99.79%	0.37	99.88%	0.30	100.00%	0.59	98.59%	0.34
ArcNet	96.66%	0.33	99.07%	0.44	99.47%	0.44	99.55%	0.15	99.60%	0.26	98.78%	0.32
ArcNN	83.33%	0.67	94.63%	0.11	98.28%	0.44	99.33%	0.59	99.49%	0.56	95.01%	0.47
IFWA-1DCNN	95.92%	0.59	98.67%	0.26	100.00%	0.44	100.00%	0.33	99.94%	0.33	98.91%	0.39

Table 6.3 The test accuracy and soft score of arc fault diagnosis using dataset 1 with different SNR

SNR	-5		-3		-1		1		3		5		Average	
	Acc	Score	Acc	Score	Acc	Score	Acc	Score	Acc	Score	Acc	Score	Acc	Score
SVM	56.88%	0.14	57.03%	0.14	55.95%	0.14	44.27%	0.14	46.99%	0.14	47.75%	0.14	51.47%	0.14
L2/L1 norm	81.54%	1.00	81.21%	0.89	83.29%	0.78	85.12%	0.78	88.50%	0.89	91.89%	0.45	85.25%	0.80
KNN	73.36%	0.30	72.54%	0.18	72.66%	0.27	73.74%	0.29	75.52%	0.30	76.46%	0.17	74.05%	0.25
SEmodel	81.21%	1.00	82.69%	1.00	82.78%	0.89	83.82%	1.00	86.90%	1.00	91.52%	0.67	84.82%	0.93
CART	76.93%	0.78	78.49%	0.78	78.50%	0.56	80.92%	0.59	85.04%	0.70	88.28%	0.43	81.36%	0.64
LightGBM	80.21%	0.67	80.43%	0.78	83.29%	0.69	83.78%	0.67	87.94%	0.89	92.41%	0.67	84.68%	0.73
XGBoost	80.35%	0.78	80.91%	0.67	83.30%	0.67	84.15%	0.59	88.20%	0.59	91.63%	0.67	84.75%	0.66
NSKSVM	73.10%	0.20	75.78%	0.20	76.63%	0.20	78.09%	0.20	80.76%	0.20	84.70%	0.20	78.18%	0.20
TVARF	79.53%	0.60	81.44%	0.53	83.07%	0.60	85.53%	0.73	88.06%	0.60	91.10%	0.60	84.79%	0.61
AE	92.34%	0.33	96.17%	0.63	96.35%	0.33	98.14%	0.44	98.70%	0.41	99.44%	0.48	96.86%	0.44
LCNN	94.43%	0.26	98.21%	0.30	99.47%	0.30	99.85%	0.44	99.88%	0.44	99.88%	0.30	99.39%	0.34
ArcNet	96.84%	0.26	98.77%	0.44	99.50%	0.30	99.52%	0.48	99.54%	0.22	99.55%	0.15	98.95%	0.31
ArcNN	93.94%	0.48	97.32%	0.59	98.36%	0.52	98.44%	0.56	98.88%	0.41	99.33%	0.59	97.71%	0.53
IFWA-1DCNN	95.61%	0.26	97.99%	0.48	99.40%	0.33	99.52%	0.30	99.89%	0.44	100.00%	0.33	98.74%	0.36

For deep learning models, the test accuracy is normally higher than ML models, indicating that the automatic feature extraction from raw data might be better than building an artificial feature pool. Different from ML models, as the sampling time increases (limited increase), the test accuracy of deep learning models improves, since they do not need a very small sample time to ensure the precision of detailed features. The same phenomenon is that high test accuracy does not guarantee high interpretability. The AE and ArcNN have lower average accuracy but higher scores than LCNN,ArcNet, and IFWA-1DCNN, which also occurs in each sub-experiment with different sampling times. It is also noticed that the test accuracy of IFWA-1DCNN quickly reaches 100% as the sampling time becomes 1×10^{-1} and 5×10^{-2} and then drops by 0.06% slightly when the sampling time is 2.5×10^{-2}.

This may be due to the large kernel size of the max-pooling layer, which is automatically searched by the fireworks algorithm. It prompts us to think about a problem: does a small kernel size in max-pooling conform to the characteristics of arc faults? Therefore, based on this rethinking, a lightweight balance neural network is proposed in Section 6.4. Notably, the comparison between ML models and deep learning models is not fair, so this article does not mention it.

Another interesting thing in Table 6.2 and Table 6.4 is that the models with higher soft scores all show a rapid decay in test accuracy when the sampling time cannot meet the requirements of feature extraction, such as SEmodel (1×10^{-1}), LightGBM (1×10^{-1}), AE (5×10^{-3}), and ArcNNs (5×10^{-3}). From this perspective, over-emphasizing generalization does not seem to be a good choice for task-driven AI models, as this will make the model focus on general features rather than task-based features. On the contrary, as long as the accuracy is within an acceptable range, a rapid drop in test accuracy is a sign that the model has found the key features and the model is more trustworthy.

Figure 6.3 visualizes four soft feature extraction score experiments as examples. For the L2/L1 norm model, Integral, RMS, Variance, and Entropy have similar SHAP values, which means that the importance of the four features is similar as well. The Range is the last choice of the L2/L1 norm. The performance of XGBoost mainly relies on the Entropy instead of other features, which explains why XGBoost is less interpretable than L2/L1 norm. The SHAP values of the second and third important features are only half of the Entropy. For deep learning models, the visualization results are clearer, that is, ArcNN finds more necessary features than ArcNet. The original data and noisy data are presented at the bottom and middle of the sub-figures. Although finding one arc fault feature is enough to identify the fault type, more features mean higher confidence and accuracy in other similar arc signals.

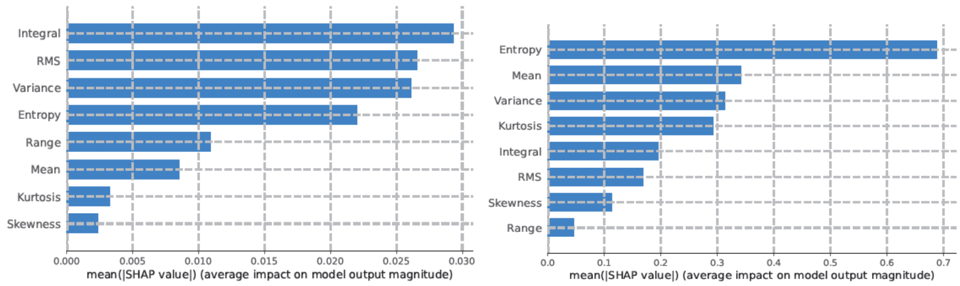

(a) SHAP value of L2/L1 norm model (1×10^{-2}ms) (b) SHAP value of XGBoost (1×10^{-2}ms)

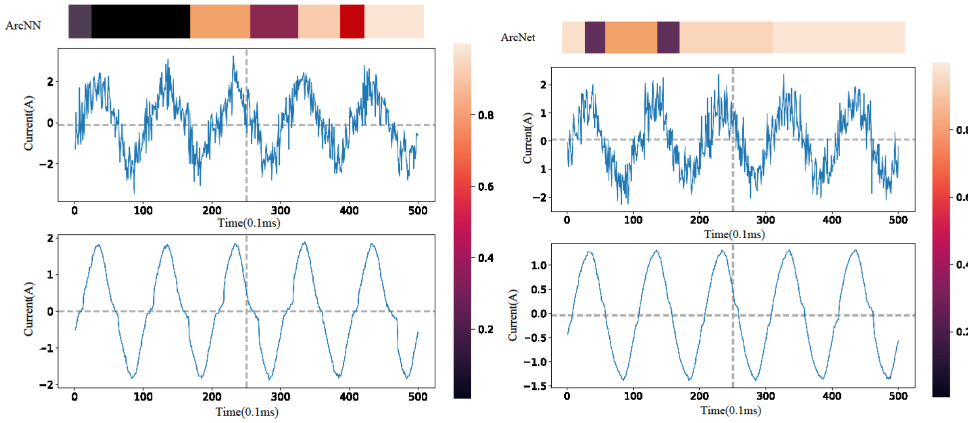

(b) Occlusion experiment of ArcNN(1×10^{-1}ms) (d) Occlusion experiment of ArcNet(1×10^{-1}ms)

Figure 6.3 Visualization examples of soft feature extraction scores using datasets with different sample times.

2) Results using datasets with multiple SNR: Noise is unavoidable in the real-life dataset, which is different from the experimental dataset. The level of noise will directly affect the classification performance of the models. The additional noise is added to the dataset, setting the SNR to -5, -3, -1, 1, 3, 5, respectively. The sample time is 5×10^{-2}ms to ensure model performance distinction.

Table 6.4 The test accuracy and soft score of arc fault diagnosis using dataset 2 with different sample times

Sample Time	5×10^{-3}ms		1×10^{-2}ms		2.5×10^{-2}ms		5×10^{-2}ms		1×10^{-1}ms		Average	
	Acc	Score	Acc	Score	Acc	Score	Acc	Score	Acc	Score	Acc	Score
SVM	66.35%	0.14	69.22%	0.14	74.20%	0.20	88.39%	0.20	88.47%	0.20	77.33%	0.18
L2/L1 norm	97.01%	0.57	99.51%	0.80	99.47%	0.80	99.45%	0.43	96.78%	0.56	98.44%	0.63
KNN	85.12%	0.13	92.85%	0.33	92.74%	0.40	92.56%	0.17	84.44%	0.33	89.56%	0.27
SEmodel	98.75%	0.85	99.38%	1.00	99.27 %	1.00	99.30%	0.66	94.47%	0.66	98.23%	0.83
CART	96.31%	0.80	98.69%	0.46	98.61%	0.60	98.57%	0.40	95.01%	0.43	97.44%	0.54
LightGBM	96.45%	0.80	99.22%	0.58	99.15%	0.67	99.12%	0.50	92.31%	0.40	97.25%	0.59
XGBoost	98.01%	0.65	99.27%	0.43	99.17%	0.43	99.11%	0.67	93.10%	0.57	97.73%	0.55
NSKSVM	86.49%	0.20	91.70%	0.20	92.31%	0.20	92.46%	0.20	92.39%	0.20	91.07%	0.20
TVARF	97.71%	0.53	99.47%	0.47	99.36%	0.60	99.25%	0.47	97.01%	0.43	98.45%	0.50
AE	96.45%	0.67	97.77%	0.59	99.49%	0.48	100.00%	0.52	100.00%	0.36	98.74%	0.52
LCNN	98.60%	0.26	99.40%	0.30	99.82%	0.33	100.00%	0.44	100.00%	0.22	99.56%	0.21
ArcNet	98.71%	0.33	99.41%	0.44	99.74%	0.26	100.00%	0.59	100.00%	0.33	99.57%	0.39
ArcNN	95.12%	0.59	97.10%	0.26	99.36%	0.56	100.00%	0.48	100.00%	0.67	98.33%	0.51
IFWA-1DCNN	98.64%	0.44	99.40%	0.33	100.00%	0.48	100.00%	0.33	100.00%	0.27	99.60%	0.37

Table 6.3 and Table 6.5 show the test accuracy and soft score of arc fault diagnosis using a dataset with different SNRs. For ML models, the performance of the tree models and the ensemble model is superior to that of other models under different SNR conditions, including NSKSVM and KNN, which is the same as in Table 6.2 and Table 6.4. The sparse Kernel in NSKSVM does not make the model more interpretable, except for providing higher test accuracy. The SEmodel still has the best average soft feature extraction score among all models, although its average test accuracy is not the highest in all experiments. Meanwhile, comprehensively considering all tables, the L2/L1 norm can have both high test accuracy and competitive soft scores, achieving a balance between performance and explainability. Although LightGBM, XGBoost, and TVARF achieve acceptable performance in Table 6.3 and Table 6.5, their performance on soft feature extraction scores in Table 6.2 and Table 6.4 is not good enough as L2/L1 norm and SEmodel. Therefore, in the arc fault diagnosis task, for experts who want to ensure the interpretability of the model, SEmodel is a better choice. However, if the tradeoff is pursued between classification accuracy and interpretability, the L2/L1 norm may be more suitable.

Table 6.5 The test accuracy and soft score of arc fault diagnosis using dataset 2 with different SNR

SNR	-5		-3		-1		1		3		5		Average	
	Acc	Score	Acc	Score	Acc	Score	Acc	Score	Acc	Score	Acc	Score	Acc	Score
SVM	88.62%	0.14	88.22%	0.20	87.67%	0.20	88.11%	0.20	88.24%	0.20	88.39%	0.20	88.20%	0.19
L2/L1 norm	98.54%	0.80	98.43%	0.80	98.53%	0.78	98.98%	0.78	99.36%	0.89	99.45%	0.43	98.88%	0.75
KNN	92.08%	0.20	91.91%	0.20	92.32%	0.33	92.45%	0.33	92.54%	0.29	92.56%	0.17	92.31%	0.25
SEmodel	97.55%	0.93	98.42%	1.00	98.50%	0.89	98.52%	0.88	99.17%	1.00	99.30%	0.66	98.58%	0.89
CART	96.06%	0.60	96.55%	0.66	97.04%	0.56	97.24%	0.56	98.68%	0.73	98.57%	0.40	97.36%	0.59
LightGBM	97.32%	0.67	97.44%	0.78	97.45%	0.68	98.01%	0.68	99.04%	0.89	99.12%	0.50	98.06%	0.70
XGBoost	97.45%	0.80	97.53%	0.66	97.56%	0.68	98.10%	0.68	99.06%	0.50	99.11%	0.67	98.14%	0.67
NSKSVM	91.21%	0.14	91.41%	0.20	91.52%	0.20	92.03%	0.20	92.18%	0.20	92.46%	0.20	91.80%	0.19
TVARF	97.15%	0.67	97.46%	0.47	97.51%	0.73	98.07%	0.43	98.97%	0.73	99.25%	0.47	98.07%	0.58
AE	97.89%	0.33	99.01%	0.56	99.25%	0.63	99.96%	0.44	100.00%	0.59	100.00%	0.52	99.35%	0.52
LCNN	99.45%	0.26	99.93%	0.26	99.95%	0.37	99.95%	0.26	100.00%	0.33	100.00%	0.44	99.88%	0.32
ArcNet	99.51%	0.22	99.89%	0.30	99.96%	0.48	99.96%	0.22	100.00%	0.48	100.00%	0.59	99.89%	0.38
ArcNN	98.26%	0.37	99.15%	0.48	99.92%	0.52	99.91%	0.59	100.00%	0.41	100.00%	0.48	99.54%	0.48
IFWA-1DCNN	99.24%	0.16	99.36%	0.33	99.40%	0.48	99.94%	0.44	100.00%	0.44	100.00%	0.33	99.67%	0.36

For deep learning, different from test accuracy and score with different sample times, in which the larger the sampling time, the higher the accuracy, the noise in

Table 6.3 and Table 6.5 can mask the arc fault signal, resulting in a decrease in the test accuracy. AE and ArcNN achieve better average soft feature extraction scores than LCNN, ArcNet, and IFWA-1DCNN despite the lower test accuracy, which is the same as in Table 6.2 and Table 6.4. Comprehensively considering test accuracy and score with different sample times and different SNRs, IFWA-1DCNN seems to strike a balance between test accuracy and scores with moderate performance, which shows the potential of large kernel sizes in the max-pooling layers. In general, deep learning is a better choice for arc fault diagnosis when considering classification accuracy, model interpretability, and visualization of fault location.

Another reason to choose deep learning over ML for arc fault diagnosis is that the fast drop in test accuracy is not obvious or too early in ML experiments, including SEmodel and L2/L1 norm models. There is a 3% drop in test accuracy when the SNR is changed from 3 to 1. For a model that accurately locates a real arc fault, the test accuracy should drop significantly when the noise is sufficient to interfere with the model. Contrary to ML models, there is a 4% drop in test accuracy when AE and ArcNN are used in SNR=-5 and SNR=-3, which is totally different from the performance of LCNN and ArcNet. During the process, the test accuracy drop of IFWA-1DCNN is not obvious enough. This phenomenon can explain why AE and ArcNN can achieve high soft feature extraction scores as well.

Figure 6.4 shows four different soft feature extraction score experiments as examples. The shape values of SEmodel and L2/L1 norm explain why SEmodel performs better than L2/L1 norm in soft feature extraction scores. As depicted in Figure 6.4a and Figure 6.4b, SEmodel relies on four main features to classify the arc faults, while L2/L1 norm focuses more on 'Entropy'. Although other main features are considered as the top-5 features as well in Figure 6.4b, their importance is far less than 'Entropy', which is opposite to SEmodel in Figure 6.4a. The occlusion experiments verify that AE can locate the arc faults better than LCNN, especially in the presence of obvious noise. The two models both find two arc faults as the main features for fault diagnosis, which is colored as 'black'. Whereas, the difference in the interpretability of the two models comes from the identification of other fault signals. In Figure 6.4c, near half arc faults in the signal are detected and identified as important components for arc fault diagnosis, which is different from LCNN in Figure 6.4d. The darker the color, the greater the impact of the fault on arc fault diagnosis.

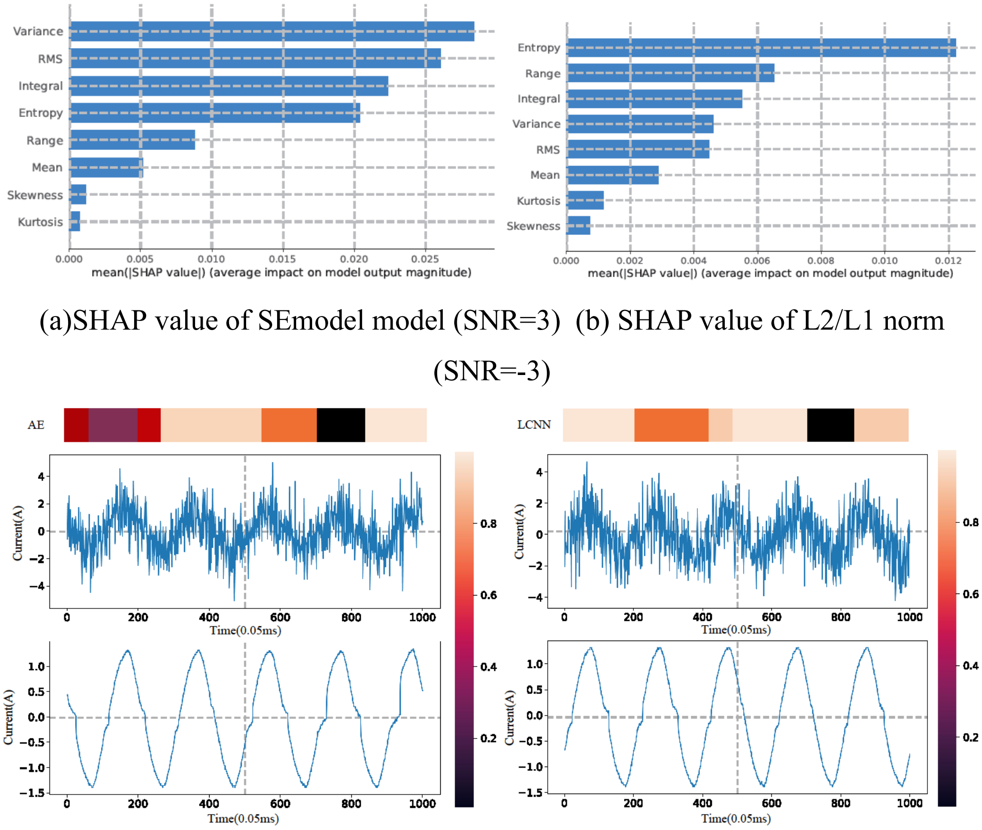

(a)SHAP value of SEmodel model (SNR=3) (b) SHAP value of L2/L1 norm (SNR=-3)

(c) Occlusion experiment of AE(SNR=-3) (d) Occlusion experiment of LCNN (SNR=3)

Figure 6.4 Visualization examples of soft feature extraction scores using datasets with different SNRs.

6.4 Lightweight Balance Neural Network

6.4.1 Architecture of Lightweight Balance Neural Network

Inspired by the good performance of IFWA-1DCNN in balancing the average test accuracy and the soft feature extraction score, another lightweight balance neural network for arc fault diagnosis is proposed. The arc fault features are usually a small area of distortion rather than an instantaneous mutation, which means that the small kernel size in max-pooling may be contrary to the arc fault characteristics. Meanwhile, the larger kernel size of the max-pooling layer in IFWA-1DCNN can help models improve the test accuracy in Table 6.6, which confirms the above idea. It is obvious that the model does not need to be complex to achieve good results, for example, IFWA-1DCNN. Therefore, average pooling should be more practical than max pooling or multiple convolution layers.

Table 6.6 The test accuracy and soft score of ArcNet and IFWA-1DCNN using average-pooling

Sample Time	5×10^{-3}ms		1×10^{-2}ms		2.5×10^{-2}ms		5×10^{-2}ms		1×10^{-1}ms		Average	
	Acc	Score	Acc	Score	Acc	Score	Acc	Score	Acc	Score	Acc	Score
ArcNet	94.44%	0.44	100.00%	0.48	99.93%	0.41	99.96%	0.26	99.96%	0.33	98.86%	0.38
IFWA-1DCNN	94.07%	0.63	99.26%	0.52	100.00%	0.56	100.00%	0.33	99.98%	0.44	98.66%	0.50
SNR	-5		-3		-1		1		3		Average	
	Acc	Score	Acc	Score	Acc	Score	Acc	Score	Acc	Score	Acc	Score
ArcNet	98.88%	0.22	99.14%	0.48	99.81%	0.46	99.88%	0.33	100.00%	0.19	99.72%	0.34
IFWA-1DCNN	98.99%	0.44	99.42%	0.44	99.51%	0.37	99.70 %	0.41	100.00%	0.56	99.52%	0.44

Table 6.7 shows the utilized architecture of the lightweight balance neural network. Table 6.8 shows the parameters of all deep learning-based arc fault diagnosis models. Except for AE, all other models are lightweight, especially ArcNN, in which dilated convolution layers are used.

Table 6.7 Lightweight balance neural network

Layer	Parameters	Activation
Convolution (5 × 1)	Filter size = 6, Padding = 2	ReLU
AvgPooling	Kernel size = 2, Stride = 2	–
Convolution (3 × 1)	Filter size = 16, Padding = 2	ReLU
AvgPooling	Kernel size = 2, Stride = 2	–
Flatten layer		
Fully connected	Size = 256	ReLU
Fully connected	Size = 16	Softmax

Table 6.8 The PRM of deep learning methods. #PRM denotes the number of parameters

Models	AE[65]	LCNN	ArcNet
#PRM	32.75M	1.04M	4.23M
Models	ArcNN	IFWA-1DCNN	LBNN
#PRM	0.53M	1.94M	1.02M

The LBNN is tested using a dataset with different sample times with SNR = -3 and multiple SNRs with sample time = 5×10^{-2} ms to demonstrate the effectiveness of the model. To ensure model performance distinction, the SNR = -3 instead of 5 when the sample time is different. As can be seen in Table 6.9, the LBNN can guarantee the comparative test accuracy and soft scores among all experiments. The fast drop, which is observed in tables about the test accuracy and score with different sample times and different SNRs, appears as well in Table 6.9.

When different SNRs are used, the drop occurs when SNR=-9, which is not included in the table.

Table 6.9 The test accuracy and soft scores of LBNN

Sample time	Indicator		SNR	Indicator	
	Acc	Score		Acc	Score
5×10^{-3}ms	85.56%	0.44	-5	98.03%	0.30
1×10^{-2}ms	93.33%	0.56	-3	99.22%	0.56
2.5×10^{-2}ms	95.36%	0.36	-1	99.40%	0.41
5×10^{-2}ms	99.22%	0.56	1	99.67%	0.41
1×10^{-1}ms	99.28%	0.39	3	99.93%	0.48
Average	94.55%	0.46	Average	99.25%	0.43

6.4.2 Influence of Average-pooling

According to the discovery, to explore the influence of the average-pooling layers and avoid the huge change in model size, two deep learning models (ArcNet and IFWA-1DCNN) are modified using average-pooling to replace max-pooling, since there are pooling layers in the original structures.

The comparisons can be divided into two aspects. First, for data with little noise and different sample times, the average-pooling layer helps the models find the real arc faults at the expense of a slight decrease in average accuracy. Specifically, this decrease is caused by the rapid drop in test accuracy at sampling time 5×10^{-3}ms. This phenomenon remains consistent across other models with high soft feature extraction scores, indicating the effectiveness of our proposed XSEI. Second, for noisy data with certain sample times, the average-pooling layer helps the models improve the test accuracy and the soft feature extraction scores, locating the real faults. The improvement of test accuracy benefits from the shift of the rapid drop phenomenon. It changes from SNR=-5 and a 2.5% accuracy drop to SNR=-9 and a 4% accuracy drop, which is not included in Table 6.6. However, the improvement in soft feature extraction scores is sufficient to reflect the model's feature extraction ability.

6.5 Conclusion

ML and deep learning models have achieved outstanding performance in arc fault diagnosis. Whereas, the inherent problem is how to determine whether these models really focus on the real arc fault. In this light, this chapter summarizes the novel ML and deep learning fault diagnosis models in recent years and proposes an explainable assessment scheme to evaluate the AI-based models. A lightweight balanced neural network is proposed to guarantee competitive classification accuracy and soft score. To demonstrate the effectiveness of the assessment scheme, an arc fault experiment is performed using a standard arc fault test platform. The experiments across seven traditional machine learning methods and four deep learning methods using an arc fault dataset with different sample times and noise levels are conducted as well. The results show that (i) high test accuracy does not guarantee high model interpretability. (ii) An easy way to find a model with good interpretability is to find the fast drop in accuracy when using data of different precisions. (iii) For arc fault diagnosis, the average pooling layer is a more efficient choice than the max pooling layer. It is necessary to highlight that the proposed XAS is not in conflict with accuracy. Instead, it can be regarded as a supplement to the single accuracy-based arc fault assessment scheme, especially when the model achieves acceptable classification accuracy. The main limitation of this method is the multiple combinations of classifiers and XAI techniques, which require a lot of expertise.

7 Conclusions and Future Work

7.1 Conclusions

This thesis presents a comprehensive investigation into the challenges and potential advancements in arc fault detection for AC low-voltage systems. In response to growing safety concerns in residential and commercial electrical infrastructures, it tackles the limitations of arc fault detection devices (AFDDs) and the inadequacies of existing evaluation standards through the development of an experimental platform and novel algorithmic approaches.

A robust and modular arc fault feature extraction platform is developed to simulate realistic electrical environments and assess AFDD performance under various load, impedance, and unwanted tripping conditions. Standard tests, as well as customized masking and unwanted tripping scenarios, are applied to market-available AFDDs. These tests revealed significant shortcomings: many devices failed under low-current and long-cable masking conditions, suffered from unwanted tripping with common appliances such as hair dryers, or were incapable of detecting serial arc faults consistently. Although arc fault detection standards have served well over the past decade, evolving residential electrical environments have revealed their shortcomings. The rise of diverse, modern appliances and increasingly complex usage scenarios has exposed limitations in load coverage, operating level diversity, and test realism. To bridge these gaps, this study introduces some improvements to address key limitations of existing standards, enhancing the realism and reliability of AFDD testing. They support the refinement of IEC62606 and GB/T 31143, contributing to safer electrical systems and the advancement of arc fault detection technologies.

To address the issue of low arc fault identification accuracy in complex scenarios, two novel arc fault detection methods are proposed. The first is a lightweight algorithm that utilizes event-based load classification and transient feature extraction. By incorporating a sequential floating forward selection mechanism, the method ensures both interpretability and real-time efficiency, which is critical for embedded deployment in AFDDs. Loads are categorized based on their turn-on behaviors into resistive, inductive, and switchable types. Tailored feature sets are selected for each category using Sequential Floating Forward Feature Selection. During detection, the system first classifies the load type and then applies a specific detection model accordingly. The approach performs well under complex multi-load conditions, requires low sampling rates and computational resources, and achieves high accuracy. Experiments confirm its superior performance over traditional and deep learning methods. Notably, the study also finds that using more features doesn't always improve detection results.

Arc-fault signals in residential low-voltage systems are often weakened by long cables, limiting the effectiveness of commercial arc fault detection products despite high algorithmic accuracy. Existing standards address only basic cable scenarios, leaving performance under longer distances and complex loads largely untested. To address the gap, the second approach introduces a multi-band feature fusion framework paired with CatBoost, aimed specifically at overcoming the detection challenges posed by cable masking effects and complex load interference. An experimental platform with up to 100 m cables is built. Results show that signal attenuation from longer cables significantly reduces detection accuracy and stability. To counter this, startup power changes are analyzed for load classification, and Recursive Feature Elimination is used to select 10 key features across three frequency bands. CatBoost is employed for classification due to its strong generalization. The model achieves 97% accuracy even when trained solely on data from 0 m cable length.

Experimental results demonstrated that both approaches outperform traditional methods and several deep learning models, particularly in terms of robustness to noise, load diversity, and false trip immunity.

Recent advancements in machine learning (ML) and deep learning have significantly improved arc fault diagnosis. However, a major challenge remains ensuring that these models genuinely focus on the relevant arc fault features rather than overfitting to irrelevant patterns. To address this, the thesis reviews recent AI-based diagnostic methods and introduces an explainable assessment scheme as a supplement to traditional accuracy metrics. Additionally, a lightweight balanced neural network is proposed to maintain strong classification performance while improving interpretability. Experimental validation is conducted using a standard arc fault test platform across seven ML models and four deep learning models under varying noise levels and sampling resolutions. The scheme enhances evaluation depth and provides a practical way to assess model reliability beyond accuracy alone.

Overall, this research bridges a critical gap between theory and practice in arc fault detection. It not only offers effective arc fault detection algorithms in complex scenarios but also contributes to future standardization efforts through improved testing methodologies and model evaluation frameworks.

7.2 Perspectives on Future Work

While the previous work primarily focuses on advancing arc fault detection in AC low-voltage residential systems, future work can be enhanced in the following ways:

1) Exploration of diverse and unpredictable load scenarios

Although this thesis has examined arc-fault signal masking in multi-branch circuits under complex load conditions, the diversity and unpredictability of real-world electrical environments continue to pose significant challenges.

With respect to increasing load complexity, future studies should focus on load interactions based on their internal components, which dominate the features of the arc-fault signals. It is impossible to list all the loads and circuit configurations. By analyzing correlations among load characteristics, such as nonlinearity, switching behavior, and spectral overlap, representative and high-impact features can be analyzed and identified, enabling more efficient testing and improved detection robustness.

With the rapid emergence of new electrical appliances, particularly those based on power electronics and intelligent control, arc-fault signal characteristics are becoming increasingly diverse and dynamic. Future work should focus on developing arc-fault detection methods that can effectively recognize features associated with previously unseen appliances. This may involve leveraging adaptive learning detections, comprehensive datasets, and transfer learning techniques to improve generalization across evolving load types. In addition, incorporating a continual data collection and model updating system online will be essential for maintaining reliable detection performance as new appliances are introduced into real-world electrical systems.

2) Development of an automatic arc-fault labeling system based on optical signals

Existing arc detection methods mainly rely on current signals and manual data labeling, which are often time-consuming and prone to subjective errors. For current signals with a strong masking effect, it is difficult to label the arc-fault event with the naked eye. To address these limitations, this work plans to integrate optoelectronic sensing, edge computing, and neural networks to enable real-time and automatic labeling, as shown in Figure 7.1.

This system is based on the non-stationary optical radiation characteristics generated during arc-fault events. An optocoupler module is used to acquire optical signals with high temporal resolution, while a Raspberry Pi platform constructs real-time optical intensity time series. A trained LSTM neural network is then employed to analyze the temporal features of the optical signal, enabling automatic identification of arc initiation and extinction, as shown in Figure 7.2. By replacing manual labeling, the proposed system is expected to achieve automatic arc-fault labeling with high temporal resolution, greatly providing high-quality labeled datasets for subsequent model training and evaluation. Future work may explore the adoption of different algorithms to further improve label accuracy and system adaptability.

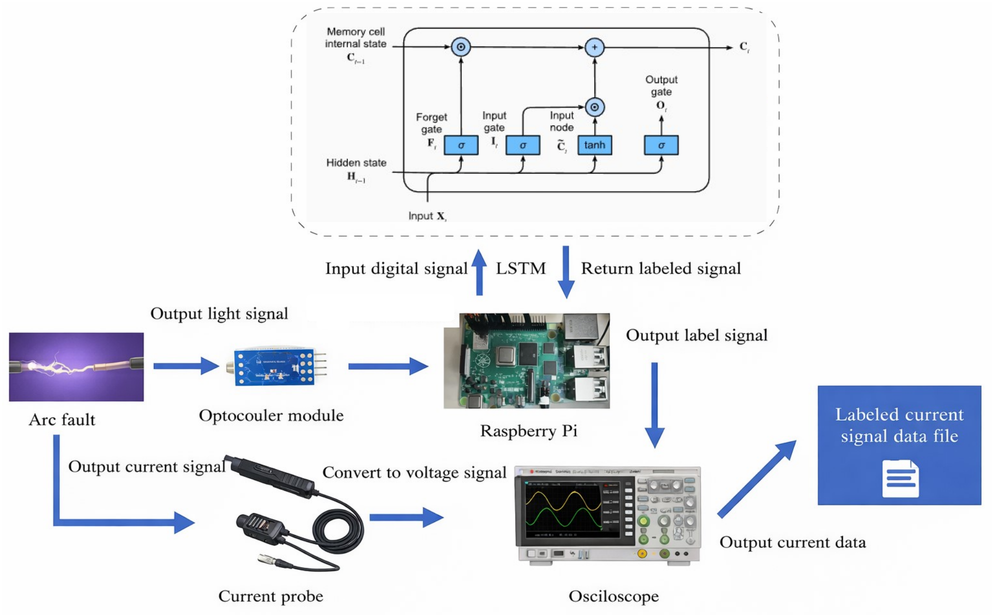

Figure 7.1 The schematic diagram of an automatic arc-fault labeling system.

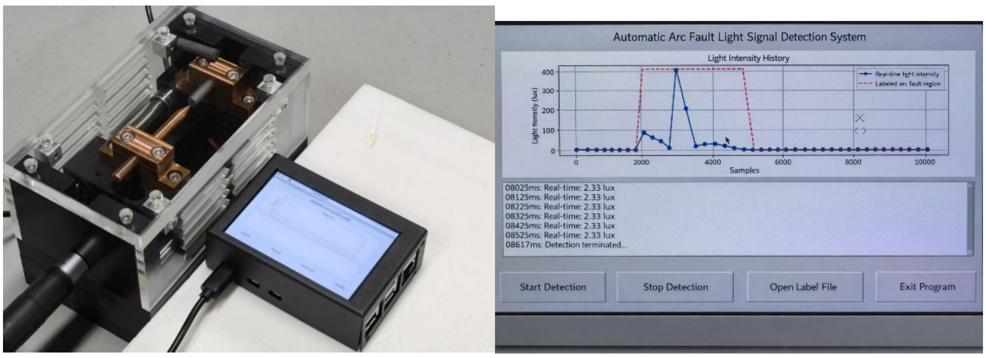

(a) (b)

Figure 7.2 (a) The prototype of the automatic arc-fault labeling system (b) The user interface.

3) Practical deployment and system integration

Although many papers propose highly accurate algorithms for arc-fault detection, such results are typically obtained under experimental conditions. Whether these algorithms can maintain comparable performance in real-world environments remains largely unexplored. This gap highlights the importance of practical deployment and evaluation of arc-fault detection algorithms. Implementing detection models directly on edge devices enables real-time signal processing under realistic operating conditions and exposes the algorithms to practical disturbances, thereby providing a more reliable assessment of their robustness and applicability.

The deployment of arc-fault detection algorithms is critical for bridging the gap between theoretical algorithm performance and practical applications. While many algorithms demonstrate high accuracy in laboratory settings, deployment in real systems exposes them to realistic operating conditions, including complex load dynamics, noise, hardware constraints, and environmental interferences. Implementing arc-fault algorithms in practical devices enables real-time monitoring and early detection of arc faults.

To address the challenge of edge-based arc-fault detection, a portable and low-cost edge detection device is designed as shown in Figure 7.3(a). The device acquires raw current signals from a current transformer and performs high-precision real-time sampling at 65 MHz using an AD9226 analog-to-digital converter (ADC) module. A Field-Programmable Gate Array (FPGA) is employed for batch signal processing. The downsampled signals are segmented and transmitted at the sampling rate of 10 kHz to a Raspberry Pi 4 Model B, ensuring both real-time performance and signal fidelity, as shown in Figure7.3(b). On the Raspberry Pi, a deep learning model is deployed for real-time monitoring and arc fault detection.

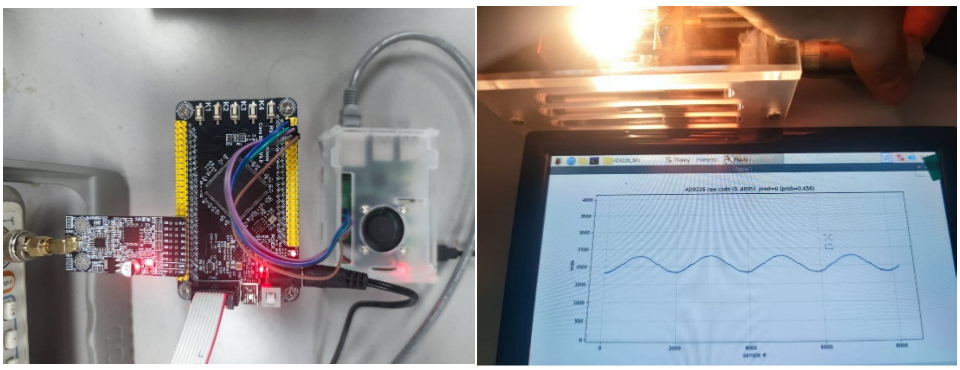

(a) (b)

Figure 7.3 (a) The hardware of an edge detection device. (b) The user interface.

Future efforts should integrate arc fault detection algorithms into real-time embedded hardware devices. Beyond detection accuracy, algorithm design should consider computational complexity, sampling requirements, and memory usage. Deployment in actual environments will enable dynamic and long-term monitoring, supporting the development of reliable, cost-effective, and field-ready arc-fault detection solutions.

4) Enhanced explainability and evaluation techniques

The proposed explainable assessment scheme in this thesis lays the foundation for transparent model assessment for arc fault detection algorithms. However, the selection of ground truth features currently lacks strong support from underlying physical principles. Future work should aim to address this gap by grounding feature selection in the fundamental mechanisms of arc generation. By analyzing the physical characteristics of arc initiation, more direct and representative features can be identified, thereby enhancing both the reliability and interpretability of arc fault detection models. In addition, data augmentation and expansion by introducing noise levels, sampling rates, and different fault durations can improve model robustness and generalizability.

5) Cybersecurity, standardization, and industry collaboration

As AFDDs/AFDs are applied to the Internet of Things and cloud-based infrastructures for centralized monitoring and remote updates, cybersecurity must be embedded by design. Secure communication protocols, adversarial robustness, and user privacy protections should be integral components of future systems. Simultaneously, collaboration with industry partners and standardization committees is essential to translate research findings into practical standards like IEC 62606 and GB/T 31143, ensuring wider adoption and impact.

These research directions aim to further enhance the reliability, transparency, and practical applicability of arc-fault detection systems, ultimately contributing to the reduction of electrical fire risks and the protection of human life and property.

Reference

[1] U. S. F. Administration. "Residential Building Electrical Malfunction Fire Trends (2014-2023)." https://www.usfa.fema.gov/statistics/residential-fires/electrical.html (accessed.

[2] E. F. S. ALLIANCE. "White Paper Residential Electrical Safety." https://www.europeanfiresafetyalliance.org/publications/white-paper-residential-electrical-safety/ (accessed.

[3] A. Borghetti, C. A. Nucci, and M. Paolone, "An Improved Procedure for the Assessment of Overhead Line Indirect Lightning Performance and Its Comparison with the IEEE Std. 1410 Method," *IEEE Transactions on Power Delivery,* vol. 22, no. 1, pp. 684-692, 2007, doi: 10.1109/tpwrd.2006.881463.

[4] M. Rabla, E. Tisserand, P. Schweitzer, and J. Lezama, "Arc fault analysis and localisation by cross-correlation in 270 V DC," in *2013 IEEE 59th Holm Conference on Electrical Contacts (Holm 2013)*, 2013: IEEE, pp. 1-6.

[5] R. H. Lee, "The other electrical hazard: Electric arc blast burns," *IEEE Transactions on Industry Applications,* no. 3, pp. 246-251, 2008.

[6] S. Huang, L. Yu, F. Zhang, W. Zhu, and Q. Guo, "Cluster Analysis Based Arc Detection in Pantograph-Catenary System," *Journal of Advanced Transportation,* vol. 2018, pp. 1-12, 2018, doi: 10.1155/2018/1329265.

[7] G. Crotti *et al.*, "Pantograph-to-OHL Arc: Conducted Effects in DC Railway Supply System," *IEEE Transactions on Instrumentation and Measurement,* vol. 68, no. 10, pp. 3861-3870, 2019, doi: 10.1109/tim.2019.2902805.

[8] S. Huang, Y. Zhai, M. Zhang, and X. Hou, "Arc detection and recognition in pantograph–catenary system based on convolutional neural network," *Information Sciences,* vol. 501, pp. 363-376, 2019, doi: 10.1016/j.ins.2019.06.006.

[9] Z. Wang, McConnell, S., Balog, R. S., & Johnson, J., "Arc Fault Signal Detection - Fourier Transformation vs. Wavelet Decomposition Techniques using Synthesized Data," *2014 IEEE 40th Photovoltaic Specialist Conference (PVSC)* pp. 3239-3244, 2014.

[10] C. S. P. Meckler, "Arc faults in photovoltaic systems," *2010 Proceedings of the 56th IEEE Holm Conference on Electrical Contacts. IEEE, 2010: 1-7.,* conference 2010.

[11] N. L. Georgijevic, M. V. Jankovic, S. Srdic, and Z. Radakovic, "The Detection of Series Arc Fault in Photovoltaic Systems Based on the Arc Current Entropy," *IEEE T Power Electr,* vol. 31, no. 8, pp. 5917-5930, 2016, doi: 10.1109/tpel.2015.2489759.

[12] Y. Gao, Zhang, J., Lin, Y., & Sun, Y, "An innovative photovoltaic DC arc fault detection method through multiple criteria algorithm based on a new arc initiation method," *2014 IEEE 40th Photovoltaic Specialist Conference (PVSC),* 2014.

[13] M. Ahmadi, H. Samet, and T. Ghanbari, "A New Method for Detecting Series Arc Fault in Photovoltaic Systems Based on the Blind-Source Separation," *IEEE Transactions on Industrial Electronics,* vol. 67, no. 6, pp. 5041-5049, 2020, doi: 10.1109/tie.2019.2922926.

[14] N. L. Georgijevic, D. Stojic, and Z. Radakovic, "Series arc fault detection in photovoltaic system by small-signal impedance and noise monitoring," *International Transactions on Electrical Energy Systems,* vol. 30, no. 2, 2019, doi: 10.1002/2050-7038.12234.

[15] M. Ahmadi, H. Samet, and T. Ghanbari, "Series Arc Fault Detection in Photovoltaic Systems Based on Signal-to-Noise Ratio Characteristics Using Cross-Correlation Function," *IEEE Transactions on Industrial Informatics,* vol. 16, no. 5, pp. 3198-3209, 2020, doi: 10.1109/tii.2019.2909753.

[16] F. M. Uriarte *et al.*, "A DC Arc Model for Series Faults in Low Voltage Microgrids," *IEEE Transactions on Smart Grid,* vol. 3, no. 4, pp. 2063-2070, 2012, doi: 10.1109/tsg.2012.2201757.

[17] A. Shekhar, L. Ramirez-Elizondo, S. Bandyopadhyay, L. Mackay, and P. Bauera, "Detection of Series Arcs Using Load Side Voltage Drop for Protection of Low Voltage DC Systems," *IEEE Transactions on Smart Grid,* vol. 9, no. 6, pp. 6288-6297, 2018, doi: 10.1109/tsg.2017.2707438.

[18] D. Yaping, T. C. Cheng, and A. S. Farag, "Principles of power-frequency magnetic field shielding with flat sheets in a source of long conductors," *IEEE T Electromagn C,* vol. 38, no. 3, pp. 450-459, 1996, doi: 10.1109/15.536075.

[19] V. Le, X. Yao, B.-H. Tsao, and C. Miller, "Series DC Arc Fault Detection Based On Ensemble Machine Learning," *IEEE T Power Electr,* pp. 1-1, 2020, doi: 10.1109/tpel.2020.2969561.

[20] "STANDARD FOR SAFETY Arc-Fault Circuit-Interrupters," UL 1699, 2019.

[21] "IEC 62606: General requirements for arc fault detection devices," International Electrotechnical Commission, IEC 62606:2017, 2017.

[22] "General requirements for arc fault detection devices （AFDD)," GB/T 31143-2014, 2014.

[23] A. Cassie, "Theorie Nouvelle des Arcs de Rupture et de la Rigidité des Circuits," *Cigre, Report,* vol. 102, pp. 588-608, 1939.

[24] O. Mayr, "Beiträge zur Theorie des statischen und des dynamischen Lichtbogens," *Archiv für Elektrotechnik,* vol. 37, no. 12, pp. 588-608, 1943.

[25] P. H. Schavemaker and L. Van der Slui, "An improved Mayr-type arc model based on current-zero measurements [circuit breakers]," *IEEE Transactions on Power delivery,* vol. 15, no. 2, pp. 580-584, 2002.

[26] J. Guardado, S. Maximov, E. Melgoza, J. Naredo, and P. Moreno, "An improved arc model before current zero based on the combined Mayr and Cassie arc models," *IEEE Transactions on Power Delivery,* vol. 20, no. 1, pp. 138-142, 2005.

[27] A. Khakpour, S. Franke, S. Gortschakow, D. Uhrlandt, R. Methling, and K.-D. Weltmann, "An improved arc model based on the arc diameter," *IEEE transactions on power delivery,* vol. 31, no. 3, pp. 1335-1341, 2015.

[28] S. Ghavami, A. A. Razi-Kazemi, and K. Niayesh, "Estimation of the arc model parameters using heuristic optimization methods," in *2021 29th Iranian Conference on Electrical Engineering (ICEE)*, 2021: IEEE, pp. 296-301.

[29] Y. Gao, L. Wang, Y. Zhang, and K. Zeng, "Research on the calculation method for the parameters of the simplified Schavemaker AC arc model," in *2018 Prognostics and System Health Management Conference (PHM-Chongqing)*, 2018: IEEE, pp. 150-156.

[30] M. Wei *et al.*, "High impedance arc fault detection based on the harmonic randomness and waveform distortion in the distribution system," *IEEE transactions on power delivery,* vol. 35, no. 2, pp. 837-850, 2019.

[31] Y. Wang, Y. Liu, X. Ning, D. Sheng, and T. Lan, "Research on the Randomness of Low-Voltage AC Series Arc Faults Based on the Improved Cassie Model," *Energies,* vol. 18, no. 3, p. 538, 2025.

[32] J. Slepian and R. Mason, "The Experimental Validity of Paschen's Law and of a Similar Relation for the Reignition Potential of an Alternating Current Arc," *Journal of Applied Physics,* vol. 8, no. 9, pp. 619-621, 1937.

[33] L. Kumpulainen, G. A. Hussain, M. Rival, M. Lehtonen, and K. Kauhaniemi, "Aspects of arc-flash protection and prediction," *Electric power systems research,* vol. 116, pp. 77-86, 2014.

[34] Y. Kayano, H. Miura, K. Miyanaga, and H. Inoue, "The relationship between voltage and duration of short-time arc generated by slowly breaking silver contact," *IEICE transactions on electronics,* vol. 91, no. 8, pp. 1230-1232, 2008.

[35] H. Inoue, H. Miura, Y. Kayano, and K. Miyanaga, "Current noise up to GHz band generated by slowly breaking silver-compound contacts with external DC magnetic field," *The European Physical Journal-Applied Physics,* vol. 49, no. 2, p. 22908, 2010.

[36] C. J. Kim, "Electromagnetic radiation behavior of low-voltage arcing fault," *IEEE transactions on power delivery,* vol. 24, no. 1, pp. 416-423, 2008.

[37] Q. Gong, Q. Gao, K. Peng, Y. Liu, and Y. Jiang, "Low-voltage AC series arc fault identification method based on the randomness of differential voltage at double-ended monitoring points," *IEEE Transactions on Instrumentation and Measurement,* 2025.

[38] J. Jiang *et al.*, "Series arc detection and complex load recognition based on principal component analysis and support vector machine," *IEEE Access,* vol. 7, pp. 47221-47229, 2019.

[39] Y. Wang, F. Zhang, X. Zhang, and S. Zhang, "Series AC Arc Fault Detection Method Based on Hybrid Time and Frequency Analysis and Fully Connected Neural Network," *IEEE Transactions on Industrial Informatics,* vol. 15, no. 12, pp. 6210-6219, 2019, doi: 10.1109/tii.2018.2885945.

[40] J. Jiang, W. Li, Z. Wen, Y. Bie, H. Schwarz, and C. Zhang, "Series Arc Fault Detection Based on Random Forest and Deep Neural Network," *IEEE Sensors Journal,* vol. 21, no. 15, pp. 17171-17179, 2021, doi: 10.1109/jsen.2021.3082294.

[41] M. Jalil, H. Samet, T. Ghanbari, and M. Tajdinian, "An enhanced Cassie–Mayr-based approach for DC series arc modeling in PV systems," *IEEE Transactions on Instrumentation and Measurement,* vol. 70, pp. 1-10, 2021.

[42] R. Jiang and Y. Zheng, "Series Arc Fault Detection Using Regular Signals and Time-Series Reconstruction," *IEEE Transactions on Industrial Electronics,* vol. 70, no. 2, pp. 2026-2036, 2023, doi: 10.1109/tie.2022.3165260.

[43] F. A. Borges, R. A. Fernandes, I. N. Silva, and C. B. Silva, "Feature extraction and power quality disturbances classification using smart meters signals," *IEEE Transactions on Industrial Informatics,* vol. 12, no. 2, pp. 824-833, 2015.

[44] C. E. Restrepo, "Arc fault detection and discrimination methods," in *Electrical Contacts-2007 Proceedings of the 53rd IEEE Holm Conference on Electrical Contacts*, 2007: IEEE, pp. 115-122.

[45] N. Hadziefendic, M. Kostic, and Z. Radakovic, "Detection of series arcing in low-voltage electrical installations," *European Transactions on Electrical Power,* vol. 19, no. 3, pp. 423-432, 2009, doi: 10.1002/etep.229.

[46] Y.-W. Liu, C.-J. Wu, and Y.-C. Wang, "Detection of serial arc fault on low-voltage indoor power lines by using radial basis function neural network," *International Journal of Electrical Power & Energy Systems,* vol. 83, pp. 149-157, 2016, doi: 10.1016/j.ijepes.2016.04.013.

[47] P. Qi, S. Jovanovic, J. Lezama, and P. Schweitzer, "Discrete wavelet transform optimal parameters estimation for arc fault detection in low-voltage residential power networks," *Electric Power Systems Research,* vol. 143, pp. 130-139, 2017, doi: 10.1016/j.epsr.2016.10.008.

[48] Z. Yin, L. Wang, B. Zhang, L. Meng, and Y. Zhang, "An integrated DC series arc fault detection method for different operating conditions," *IEEE Transactions on Industrial Electronics,* vol. 68, no. 12, pp. 12720-12729, 2020.

[49] G. Artale, A. Cataliotti, V. Cosentino, D. Di Cara, S. Nuccio, and G. Tine, "Arc fault detection method based on CZT low-frequency harmonic current analysis," *IEEE Transactions on Instrumentation and Measurement,* vol. 66, no. 5, pp. 888-896, 2017.

[50] M. K. Khafidli, E. Prasetyono, D. O. Anggriawan, A. Tjahjono, and M. H. R. A. Syafii, "Implementation AC series arc fault recognition using mikrokontroller based on fast Fourier transform," in *2018 International Electronics Symposium on Engineering Technology and Applications (IES-ETA)*, 2018: IEEE, pp. 31-36.

[51] N. Qu, J. Zuo, J. Chen, and Z. Li, "Series Arc Fault Detection of Indoor Power Distribution System Based on LVQ-NN and PSO-SVM," *IEEE Access,* vol. 7, pp. 184020-184028, 2019, doi: 10.1109/access.2019.2960512.

[52] C. Han, Z. Wang, A. Tang, H. Gao, and F. Guo, "Recognition method of AC series arc fault characteristics under complicated harmonic conditions," *IEEE Transactions on Instrumentation and Measurement,* pp. 1-1, 2021, doi: 10.1109/tim.2021.3051669.

[53] Y. Wu, Z. Song, and X. Li, "A method for arc fault detection based on the analysis of signal's characteristic frequency band with wavelet transform," in *2013 2nd International Conference on Electric Power Equipment-Switching Technology (ICEPE-ST)*, 2013: IEEE, pp. 1-4.

[54] P. Duan, L. Xu, X. Ding, C. Ning, and C. Duan, "An arc fault diagnostic method for low voltage lines using the difference of wavelet coefficients," in *2014 9th IEEE Conference on Industrial Electronics and Applications*, 2014: IEEE, pp. 401-405.

[55] E. Saeed, K. Abdulhassan, and O. Khudair, "Series And Parallel Arc Fault Detection Based on Discrete Wavelet VS. FFT Techniques," *Iraqi Journal for Electrical and Electronic Engineering,* vol. 18, no. 1, pp. 38-47, 2021, doi: 10.37917/ijeee.18.1.5.

[56] G. S. Da Rocha, L. T. C. Pulz, and D. S. Gazzana, "Serial Arc Fault Detection Through Wavelet Transform and Support Vector Machine," presented at the 2021 IEEE International Conference on Environment and Electrical Engineering and 2021 IEEE Industrial and Commercial Power Systems Europe (EEEIC / I&CPS Europe), 2021.

[57] Q. Lu, T. Wang, B. He, T. Ru, and D. Chen, "A new series arc fault identification method based on wavelet transform," in *IECON 2017-43rd Annual Conference of the IEEE Industrial Electronics Society*, 2017: IEEE, pp. 4817-4822.

[58] Y. Wang, F. Zhang, and S. Zhang, "A New Methodology for Identifying Arc Fault by Sparse Representation and Neural Network," *IEEE Transactions on Instrumentation and Measurement,* vol. 67, no. 11, pp. 2526-2537, 2018, doi: 10.1109/tim.2018.2826878.

[59] N. Qu, J. Wang, and J. Liu, "An Arc Fault Detection Method Based on Current Amplitude Spectrum and Sparse Representation," *IEEE Transactions on Instrumentation and Measurement,* vol. 68, no. 10, pp. 3785-3792, 2019, doi: 10.1109/tim.2018.2880939.

[60] Y. Wang, L. Hou, K. C. Paul, Y. Ban, C. Chen, and T. Zhao, "ArcNet: Series AC Arc Fault Detection Based on Raw Current and Convolutional Neural Network," *IEEE Transactions on Industrial Informatics,* vol. 18, no. 1, pp. 77-86, 2022, doi: 10.1109/tii.2021.3069849.

[61] K. Yang, R. Zhang, J. Yang, C. Liu, S. Chen, and F. Zhang, "A Novel Arc Fault Detector for Early Detection of Electrical Fires," *Sensors,* vol. 16, no. 4, p. 500, 2016, doi: 10.3390/s16040500.

[62] J.-h. Yang, H.-y. Fang, R.-c. Zhang, and K. Yang, "An arc fault diagnosis algorithm using multiinformation fusion and support vector machines," *Royal Society Open Science,* vol. 5, no. 9, p. 180160, 2018, doi: 10.1098/rsos.180160.

[63] J. E. Siegel, S. Pratt, Y. Sun, and S. E. Sarma, "Real-time Deep Neural Networks for internet-enabled arc-fault detection," *Engineering*

Applications of Artificial Intelligence, vol. 74, pp. 35-42, 2018, doi: 10.1016/j.engappai.2018.05.009.

[64] C.-J. Park, H.-L. Dang, S. Kwak, and S. Choi, "Deep learning-based series AC arc detection algorithms," *Journal of Power Electronics,* vol. 21, no. 10, pp. 1621-1631, 2021.

[65] G. Zhou *et al.*, "Intever Public Database for Arcing Event Detection: Feature Analysis, Benchmark Test, and Multi-Scale CNN Application," *IEEE Transactions on Instrumentation and Measurement,* vol. 70, pp. 1-15, 2021, doi: 10.1109/tim.2021.3082998.

[66] Z. Wang, S. Tian, H. Gao, C. Han, and F. Guo, "An on-line detection method and device of series arc fault based on lightweight CNN," *IEEE Transactions on Industrial Informatics,* vol. 19, no. 10, pp. 9991-10003, 2023.

[67] J. Yan, Q. Li, and S. Duan, "A simplified current feature extraction and deployment method for DC series arc fault detection," *IEEE Transactions on Industrial Electronics,* vol. 71, no. 1, pp. 625-634, 2023.

[68] Y.-L. Shen and R.-J. Wai, "Wavelet-analysis-based singular-value-decomposition algorithm for weak arc fault detection via current amplitude normalization," *IEEE Access,* vol. 9, pp. 71535-71552, 2021.

[69] E. Tisserand, J. Lezama, P. Schweitzer, and Y. Berviller, "Series arcing detection by algebraic derivative of the current," *Electric Power Systems Research,* vol. 119, pp. 91-99, 2015, doi: 10.1016/j.epsr.2014.09.011.

[70] C. J. Kim and B. D. Russell, "Classification of faults and switching events by inductive reasoning and expert system methodology," *IEEE Transactions on Power Delivery,* vol. 4, no. 3, pp. 1631-1637, 1989.

[71] M. J. Rust, M. Bates, and X. Zhuang, "Sub-diffraction-limit imaging by stochastic optical reconstruction microscopy (STORM)," *Nat Methods,* vol. 3, no. 10, pp. 793-5, Oct 2006, doi: 10.1038/nmeth929.

[72] J. Lezama, P. Schweitzer, E. Tisserand, J.-B. Humbert, S. Weber, and P. Joyeux, "An embedded system for AC series arc detection by inter-period correlations of current," *Electric Power Systems Research,* vol. 129, pp. 227-234, 2015, doi: 10.1016/j.epsr.2015.08.005.

[73] R. Jiang, G. Bao, Q. Hong, and C. D. Booth, "A coupling method for identifying arc faults based on short-observation-window SVDR," *IEEE Transactions on Instrumentation and Measurement,* vol. 70, pp. 1-10, 2021.

[74] S. Zhang, F. Zhang, P. Liu, and Z. Han, "Identification of Low Voltage AC Series Arc Faults by using Kalman Filtering Algorithm," *Elektronika ir Elektrotechnika,* vol. 20, no. 5, 2014, doi: 10.5755/j01.eee.20.5.4294.

[75] E. Calderon-Mendoza, P. Schweitzer, and S. Weber, "Kalman filter and a fuzzy logic processor for series arcing fault detection in a home electrical network," *International Journal of Electrical Power & Energy Systems,* vol. 107, pp. 251-263, 2019, doi: 10.1016/j.ijepes.2018.11.002.

[76] K. J. Lippert and T. A. Domitrovich, "AFCIs—From a Standards Perspective," *IEEE Transactions on Industry Applications,* vol. 50, no. 2, pp. 1478-1482, 2014, doi: 10.1109/tia.2013.2272670.

[77] "Electrical fire monitoring system-Part 4 : Arcing fault detectors," GB 14287.4-2014, 2014.

[78] W.-S. Moon, J.-C. Kim, A. Jo, S.-B. Bang, and W.-S. Koh, "Ignition characteristics of residential series arc faults in 220-V HIV wires," *IEEE Transactions on Industry Applications,* vol. 51, no. 3, pp. 2054-2059, 2014.

[79] W. Su and C. Wu, "The assessment of introduction of the arc fault circuit interrupters," *Report prepared for Institute of Occupational Safety and Health Taipei, Taiwan,* 2010.

[80] B. Liu and X. Zeng, "AC Series Arc Fault Modeling for Power Supply Systems Based on Electric-to-Thermal Energy Conversion," *IEEE Transactions on Industrial Electronics,* vol. 70, no. 4, pp. 4167-4174, 2023, doi: 10.1109/tie.2022.3181372.

[81] W. Miao, Z. Wang, F. Wang, K. H. Lam, and P. W. Pong, "Multicharacteristics arc model and autocorrelation-algorithm based arc fault detector for DC microgrid," *IEEE Transactions on Industrial Electronics,* vol. 70, no. 5, pp. 4875-4886, 2022.

[82] H. D. Vu, E. Calderon, P. Schweitzer, S. Weber, and N. Britsch, "Multi criteria series arc fault detection based on supervised feature selection," *International Journal of Electrical Power & Energy Systems,* vol. 113, pp. 23-34, 2019, doi: 10.1016/j.ijepes.2019.05.012.

[83] T. Kari *et al.*, "An integrated method of ANFIS and Dempster-Shafer theory for fault diagnosis of power transformer," *IEEE Transactions on Dielectrics and Electrical Insulation,* vol. 25, no. 1, pp. 360-371, 2018.

[84] M. Dong, P. C. Meira, W. Xu, and C. Chung, "Non-intrusive signature extraction for major residential loads," *IEEE Transactions on Smart Grid,* vol. 4, no. 3, pp. 1421-1430, 2013.

[85] B. Najafi, S. Moaveninejad, and F. Rinaldi, "Data analytics for energy disaggregation: Methods and applications," in *Big data application in power systems*: Elsevier, 2018, pp. 377-408.

[86] L. Farinaccio and R. Zmeureanu, "Using a pattern recognition approach to disaggregate the total electricity consumption in a house into the major end-uses," *Energy and buildings,* vol. 30, no. 3, pp. 245-259, 1999.

[87] L. Pereira, "Developing and evaluating a probabilistic event detector for non-intrusive load monitoring," in *2017 Sustainable Internet and ICT for Sustainability (SustainIT)*, 2017: IEEE, pp. 1-10.

[88] R. Jiang, Y. Wang, X. Gao, G. Bao, Q. Hong, and C. D. Booth, "AC Series Arc Fault Detection Based on RLC Arc Model and Convolutional Neural Network," *IEEE Sensors Journal,* vol. 23, no. 13, pp. 14618-14627, 2023, doi: 10.1109/jsen.2023.3280009.

[89] I. Guyon, S. Gunn, M. Nikravesh, and L. A. Zadeh, *Feature extraction: foundations and applications*. Springer, 2008.

[90] Q. Gong, Q. Gao, X. Qu, K. Peng, L. Feng, and C. Xiao, "Low-voltage AC series arc fault location method based on RBF neural network," *Electric Power Systems Research,* vol. 229, p. 110176, 2024.

[91] E. Calderon-Mendoza, P. Schweitzer, and S. Weber, "A double ended AC series arc fault location algorithm for a low-voltage indoor power line using impedance parameters and a neural network," *Electric Power Systems Research,* vol. 165, pp. 84-93, 2018.

[92] E. Calderon, P. Schweitzer, and S. Weber, "A series arc fault location algorithm based on an impedance method for a domestic AC system," in *2017 IEEE Holm conference on electrical contacts*, 2017: IEEE, pp. 312-316.

[93] Q. Gong, K. Peng, Q. Gao, L. Feng, and C. Xiao, "Series arc fault identification method based on wavelet transform and feature values decomposition fusion DNN," *Electric Power Systems Research,* vol. 221, 2023, doi: 10.1016/j.epsr.2023.109391.

[94] S. Zhang, N. Qu, T. Zheng, and C. Hu, "Series Arc Fault Detection Based on Wavelet Compression Reconstruction Data Enhancement and Deep Residual Network," *IEEE Transactions on Instrumentation and Measurement,* vol. 71, pp. 1-9, 2022, doi: 10.1109/tim.2022.3158990.

[95] C. Hu, N. Qu, and S. Zhang, "Series arc fault detection based on continuous wavelet transform and DRSN-CW with limited source data," *Scientific Reports,* vol. 12, no. 1, 2022, doi: 10.1038/s41598-022-17235-7.

[96] Q. Yu, Y. Hu, and Y. Yang, "Identification Method for Series Arc Faults Based on Wavelet Transform and Deep Neural Network," *Energies,* vol. 13, no. 1, 2019, doi: 10.3390/en13010142.

[97] C. Jia *et al.*, "Serial Arc-Fault Restriction Survey with Standard-listed Products in the Chinese Market," *IEEE Transactions on Industry Applications,* 2023.

[98] K. C. Paul, C. Chen, Y. Wang, and T. Zhao, "LArcNet: Lightweight Neural Network for Real-Time Series AC Arc Fault Detection," *IEEE Open Journal of Industry Applications,* 2024.

[99] Y. Zhang *et al.*, "Lightweight AC Arc Fault Detection Method by Integration of Event-Based Load Classification," *IEEE Transactions on Industrial Electronics,* vol. 71, no. 4, pp. 4130-4140, 2024, doi: 10.1109/tie.2023.3277125.

[100] F. Pedregosa *et al.*, "Scikit-learn: machine learning in python, journal of machine learning research. vol 12 (Oct)," 2011.

[101] L. Prokhorenkova, G. Gusev, A. Vorobev, A. V. Dorogush, and A. Gulin, "CatBoost: unbiased boosting with categorical features," *Advances in neural information processing systems,* vol. 31, 2018.

[102] J.-C. Gu, D.-S. Lai, J.-M. Wang, J.-J. Huang, and M.-T. Yang, "Design of a DC series arc fault detector for photovoltaic system protection," *IEEE Transactions on Industry Applications,* vol. 55, no. 3, pp. 2464-2471, 2019.

[103] J.-B. Ahn, H.-B. Jo, and H.-J. Ryoo, "Real-time DC series arc fault detection based on noise pattern analysis in photovoltaic system," *IEEE*

Transactions on Industrial Electronics, vol. 70, no. 10, pp. 10680-10689, 2022.

[104] S. Ali *et al.*, "Explainable Artificial Intelligence (XAI): What we know and what is left to attain Trustworthy Artificial Intelligence," *Information fusion,* vol. 99, p. 101805, 2023.

[105] C. Van Zyl, X. Ye, and R. Naidoo, "Harnessing eXplainable artificial intelligence for feature selection in time series energy forecasting: A comparative analysis of Grad-CAM and SHAP," *Applied Energy,* vol. 353, p. 122079, 2024.

[106] Z. Chen, F. Xiao, F. Guo, and J. Yan, "Interpretable machine learning for building energy management: A state-of-the-art review," *Advances in Applied Energy,* vol. 9, p. 100123, 2023.

[107] D. Batic, V. Stankovic, and L. Stankovic, "Toward transparent load disaggregation—a framework for quantitative evaluation of explainability using explainable ai," *IEEE Transactions on Consumer Electronics,* vol. 70, no. 1, pp. 4345-4356, 2023.

[108] K. Zhu, Z. Teng, W. Qiu, A. Mingotti, Q. Tang, and W. Yao, "Aiming to complex power quality disturbances: a novel decomposition and detection framework," *IEEE Transactions on Industrial Informatics,* vol. 20, no. 3, pp. 4317-4326, 2023.

[109] S. M. Lundberg and S.-I. Lee, "A unified approach to interpreting model predictions," *Advances in neural information processing systems,* vol. 30, 2017.

[110] H. Chen, I. C. Covert, S. M. Lundberg, and S.-I. Lee, "Algorithms to estimate Shapley value feature attributions," *Nature Machine Intelligence,* vol. 5, no. 6, pp. 590-601, 2023.

[111] M. D. Zeiler and R. Fergus, "Visualizing and understanding convolutional networks," in *European conference on computer vision*, 2014: Springer, pp. 818-833.

[112] M. Sundararajan and A. Najmi, "The many Shapley values for model explanation," in *International conference on machine learning*, 2020: PMLR, pp. 9269-9278.

[113] P. H. Valois, K. Niinuma, and K. Fukui, "Occlusion sensitivity analysis with augmentation subspace perturbation in deep feature space," in *Proceedings of the IEEE/CVF Winter Conference on Applications of Computer Vision*, 2024, pp. 4829-4838.

[114] W. Dai, X. Zhou, Z. Sun, Q. Miao, and G. Zhai, "Series AC Arc Fault Detection Method Based on L2/L1 Norm and Classification Algorithm," *IEEE Sensors Journal,* vol. 24, no. 10, pp. 16661-16672, 2024, doi: 10.1109/jsen.2024.3386694.

[115] G. Ke *et al.*, "Lightgbm: A highly efficient gradient boosting decision tree," *Advances in neural information processing systems,* vol. 30, 2017.

[116] T. Chen and C. Guestrin, "Xgboost: A scalable tree boosting system," in *Proceedings of the 22nd acm sigkdd international conference on knowledge discovery and data mining*, 2016, pp. 785-794.

[117] H. Hua, D. Fang, and M. Guo, "Series Arc Fault Identification Based on a Novel Newton-optimized Sparse Kernel Support Vector Machine," *IEEE Transactions on Instrumentation and Measurement,* 2025.

[118] H. Tong, X. Zeng, K. Yu, J. Mu, C. Luo, and B. Liu, "Research on the identification method of series arc fault based on the feature sensitivity analysis and the TVA coefficient optimized random forest," *IEEE Transactions on Power Delivery,* vol. 39, no. 2, pp. 751-762, 2023.